Characterization of CdbS, a PilZ domain protein involved in chromosome organization and segregation during heat shock stress in *Myxococcus xanthus*

Dissertation

zur Erlangung des akademischen Grades des

Doktors der Naturwissenschaften

(Dr. rer. nat.)

dem Fachbereich Biologie

der Philipps-Universität Marburg

vorgelegt von

Michael Seidel

aus Mering

Marburg (Lahn), März 2023

Die Untersuchungen zur vorliegenden Arbeit wurden von März 2019 bis März 2023 am Max-Planck-Institut für terrestrische Mikrobiologie unter der Leitung von Prof. Dr. MD Lotte Søgaard-Andersen durchgeführt.

Vom Fachbereich Biologie der Philipps-Universität Marburg als Dissertation angenommen am:

20 . 04 . 2023

Erstgutachterin: Prof. Dr. MD Lotte Søgaard-Andersen

Zweitgutachter: Prof. Dr. Martin Thanbichler

Weitere Mitglieder der Prüfungskommission:

Prof. Dr. Hans-Ulrich Mösch

Prof. Dr. Victor Sourjik

Tag der mündlichen Prüfung: 07.07.2023

Everyone deserves

the chance to fly

- Wicked The Musical

Table of Contents

Abbreviations 8

Zusammenfassung 10

1 Introduction 12

1.1 Nucleotide-based second messengers 12

1.2 The second messenger c-di-GMP 13

1.2.1 c-di-GMP metabolism 13

1.2.2 c-di-GMP effectors 15

1.2.3 The PilZ domain as a c-di-GMP binding effector 17

1.2.4 Specificity of c-di-GMP signaling 19

1.3 The DnaK-DnaJ-GrpE chaperone system 20

1.3.1 Hsp70 protein are is the core chaperone of the KJE system 22

1.3.2 The Hsp40 J-domain co-chaperone 24

1.3.3 The nucleotide exchange factor GrpE 25

1.4 The model organism *Myxococcus xanthus* 25

1.4.1 Development 26

1.4.2 Chromosome organization and segregation in *M. xanthus* 27

1.4.3 Regulation of cell division site placement in *M. xanthus* 30

1.4.4 KJE proteins in *M. xanthus* 31

1.4.5 c-di-GMP in Myxococcus xanthus 32

1.4.6 c-di-GMP is important during the life cycle of *M. xanthus* 32

1.4.7 Characterized c-di-GMP receptors in *M. xanthus* 33

1.4.8 CdbA represents a novel type of c-di-GMP effector and is essential for viability 34

1.5 Scope of the study....37
2 Results....38
2.1 *cdbS* encodes a stand-alone PilZ domain protein and is conserved in closely related species....38
2.2 CdbS binds c-di-GMP....41
2.3 The essentiality of CdbA depends on the presence of CdbS....42
2.4 CdbA-depletion causes increased CdbS accumulation....46
2.5 A strain with an elevated CdbS level phenocopies a CdbA-depletion mutant....48
2.6 CdbS does not affect the accumulation and localization of CdbA....50
2.7 CdbS activity is independent of c-di-GMP binding....51
2.8 Identification of interaction candidates of CdbS and their bioinformatical analyses 52
2.9 Investigation of the putative PilZ-KJE protein folding machinery and its clients 61
2.10 CsdK1 and CsdK2 act during CdbA-depletion....64
2.11 CsdK1 and CsdK2 are important for the increased CdbS accumulation during CdbA-depletion 65
2.12 CdbA-depletion induces increased *csdK1* and *csdK2* transcription and accumulation 69
2.13 CdbS overaccumulating cells have no defect in DNA replication....71
2.14 The CdbS level increases during heat stress....73
2.15 CdbS accelerates cell death during heat stress....78
3 Discussion....80
3.1 Model of the CdbA/CdbS system....80
3.2 The role of CdbS in chromosome biology....84
3.3 CdbA is a NAP that also influences gene expression....85

3.4 CdbA and CdbS share characteristics of toxin-antitoxin systems 86
3.5 The putative role of c-di-GMP in heat shock response 88
4 Material & Methods 91
4.1 Reagents, kits and equipment 91
4.2 Media 93
4.3 Microbiological methods 94
4.3.1 *E. coli* strains 94
4.3.2 M. xanthus strains.....94
4.3.3 Bacterial cultivation methods 96
4.3.4 Development assay under submerged conditions to test CdbS-FLAG accumulation 96
4.3.5 Stress conditions to test CdbS-FLAG accumulation.....96
4.3.6 BACTH assay 97
4.3.7 Fluorescence microscopy and image analysis 97
4.4 Molecular methods 98
4.4.1 Plasmids and oligonucleotides.....98
4.4.2 Plasmid construction.....104
4.4.3 Construction of in-frame deletion and insertion strains.....107
4.4.4 DNA isolation.....108
4.4.5 Polymerase chain reaction (PCR).....108
4.4.6 Agarose gel electrophoresis 109
4.4.7 Restriction enzyme digest of DNA and ligation 110
4.4.8 Preparation and transformation of chemically competent *E. coli* 110
4.4.9 Electroporation of *M. xanthus* 111

4.4.10 RNA isolation and cDNA synthesis 111

4.4.11 RT-qPCR and *ori*/*ter* measurements 112

4.5 Biochemical methods 112

4.5.1 SDS polyacrylamide gel electrophoresis (SDS-PAGE) 112

4.5.2 Immunoblot analysis 113

4.5.3 Protein purification 114

4.5.4 Bio-layer interferometry 114

4.5.5 Co-Immunoprecipitation and label-free mass spectrometry-based quantitative proteomics 115

4.6 Bioinformatic analyses 116

5 References 117

Acknowledgements 127

Curriculum vitae 130

List of publications 131

Erklärung 132

Einverständniserklärung 133

Abbreviations

ATP/ADP/AMP	adenosine tri-/di-/monophosphate
BACTH	bacterial adenylate cyclase-based two-hybrid
bp	base pair
c-di-AMP	cyclic di-3′,5′-adenosine monophosphate
c-di-GMP	cyclic di-3’,5’-guanosine monophosphate
cDNA	single-stranded complementary DNA
cAMP	adenosine 3’,5′-cyclic monophosphate
cGAMP	cyclic guanosine monophosphate-adenosine monophosphate
CRP	cAMP-receptor protein
C-terminus	carboxyl-terminus
CTP	cytidine triphosphate
CTT	casitone tris medium
DAPI	4′,6-diamidino-2-phenylindole
DGC	diguanylate cyclase
DNA	deoxyribonucleic acid
DTT	dithiothreitol
EDTA	ethylenediaminetetraacetic acid
EPS	exopolysaccharide
(sf)GFP	(superfolded) green fluorescent protein
GTP/GDP/GMP	guanosine tri-/di-/monophosphate
h	hour
HA	hemagglutinin tag
Hsp	heat shock protein
IPTG	isopropyl β-D-1-thiogalactopyranoside
kDa	kilodalton
kV	kilovolt
l	litre
LC/MS	liquid chromatography-mass spectrometry
m-	milli-
M	molarity
mCh/mCherry	monomeric Cherry
min	minute
mV/mVenus	monomeric Venus
OD	optical density
PDE	phosphodiesertase
pGpG	5'-phosphoguanylyl- (3' −> 5')- guanosine
(p)ppGpp	guanosine 3'-diphosphate 5'-triphosphate
RNA	ribonucleic acid
rpm	rounds per minute
s	seconds
SDS-PAGE	sodium dodecyl sulfate polyacrylamide gel electrophoresis
T4P	type IV pili
TEMED	N,N,N′,N′-Tetramethylethane-1,2-diamine
Tris	2-amino-2-hydroxymethyl-propane-1,3-diol
V	volt
v/v	volume per volume
w/v	weight per volume
WT	wild type
X-gal	5-brom-4-chlor-3-indoxyl-β-D-galactopyranosid
(e)YFP	(enhanced) yellow fluorescent protein
µ-	micro-

Abstract

The second messenger c-di-GMP regulates a wide variety of processes in bacteria that are often related to changes in lifestyle. Unexpectedly, we recently reported a link between c-di-GMP and chromosome organization. Specifically, the DNA-binding protein CdbA binds c-di-GMP, is essential for viability, and important for chromosome organization and segregation in *Myxococcus xanthus*. CdbA is highly abundant and binds >500 sites on the chromosome but its depletion causes no or only modest changes in transcription. Based on these findings, we proposed that CdbA is a nucleoid-associated protein whose activity is modulated by c-di-GMP.

Most nucleoid-associated proteins are not essential. Therefore, to explore the CdbA essentiality, suppressor mutants that were viable in the absence of CdbA were isolated. Among eight suppressors, seven had mutations in *mxan_4328* that encodes a stand-alone PilZ domain protein, henceforth CdbS. The inactivation of *cdbS* completely suppressed the lethal CdbA depletion phenotype, and *cdbS* in otherwise wild-type cells was dispensable for viability. Notably, CdbA depletion, without affecting transcription of *cdbS*, resulted in a four-fold increased CdbS level. Moreover, overexpression of *cdbS* phenocopied the CdbA depletion phenotype. These observations support that the defects caused by CdbA depletion are the result of CdbS over-accumulation. *In vitro*, purified CdbS binds c-di-GMP, but the function of CdbS is independent of c-di-GMP binding *in vivo*. In *in vivo* pull-down experiments with an active CdbS-FLAG protein, significantly enriched proteins included five chaperones and co-chaperones including two PilZ-Hsp70 proteins, henceforth CsdK1 and CsdK2, a DnaJ homolog and a GrpE homolog. *csdK1* as well as *csdK2* were transcriptionally upregulated in response to CdbA depletion, and the resulting increased CsdK1 and CsdK2 accumulation lead to an elevated CdbS level. Searching for a physiological function of this system, we found that CdbS accumulation increased in response to high temperature stress at 37°C in a CsdK1- and CsdK2-dependent manner and caused accelerated cell death at this temperature.

In total, our data support that increased CdbS accumulation caused by either CdbA depletion or high temperature stress, by an unknown mechanism, results in chromosome segregation and organization defects, thereby causing cell division inhibition and cell death. We speculate that the CdbA/CsdK1/CsdK2/CdbS system could be linked to c-di-GMP signaling and that altered cellular levels of c-di-GMP level modulate DNA binding by CdbA and, ultimately, the cellular level of CdbS. Finally, we speculate that if this system is aberrantly or excessively activated it has detrimental effects on cell viability.

Zusammenfassung

Der weitverbreitete sekundäre Botenstoff c-di-GMP reguliert eine große Vielfalt an zellulären Prozessen in Bakterien, die typischerweise mit Veränderungen im Lebensstil einhergehen. Kürzlich identifizierten wir das DNS-bindende Protein CdbA als Verbindung zwischen c-di-GMP und der Organisation und Segregation des Chromosoms in *Myxococcus xanthus*. CdbA ist essenziell und bindet entweder DNS oder c-di-GMP. Zusätzlich zeigten wir, dass CdbA an über 500 Stellen des *M. xanthus* Chromosomes bindet, aber nur wenig Einfluss auf die transkriptionelle Genregulation hat. Anhand dieser Beobachtungen charakterisierten wir CdbA als Nukleoid-assoziiertes Protein (NAP), dessen Aktivität durch c-di-GMP reguliert wird.

Die meisten NAPs sind nicht essenziell und um die Unentbehrlichkeit von CdbA zu verstehen, haben wir Suppressor-Mutanten isoliert. Von acht Suppressor-Mutanten zeigten sieben eine Mutation in einem Genlokus, der für ein PilZ Domäne Protein codiert, welches wir CdbS genannt haben. Weitere Ergebnisse zeigen, dass der Funktionsverlust von *cdbS* den CdbA Depletionsphänotypen unterdrückt. Der Verlust von CdbS in der Anwesenheit von CdbA führte zu keinem wahrnehmbaren Defekt, während der Verlust von CdbA zu einem erhöhten Proteinlevel an CdbS führte, was aber nicht auf erhöhter Transkription basierte. Die *cdbS* Überexpression führte zu demselben Phänotyp wie der Mangel an CdbA. Diese Beobachtungen befürworten, dass der Effekt der CdbA Depletion auf der Überproduktion von CdbS beruht. *In vitro* bindet CdbS c-di-GMP, aber die Aktivität von CdbS *in vivo* ist davon unabhängig. Um die Funktion von CdbS zu verstehen, haben wir ein *Pull-down* Experiment durchgeführt, um potentielle Interaktionspartner von CdbS zu identifizieren. Fünf der signifikant angereicherten Protein sind mit der Proteinfaltung assoziiert, darunter Csdk1 und Csdk2, zwei PilZ-Hsp70 Proteine, und Homologe von DnaJ und GrpE. Wir zeigen hier, dass Csdk1 und Csdk2 in der Abwesenheit von CdbA hochreguliert werden und dadruch CdbS auf einem erhöhtem Level akkumuliert. Zuletzt zeigen wir, dass CdbS in Abhängigkeit von CsdK1 und CsdK2 während des Hitzestresses wirkt und den Zelltod beschleunigt.

Zusammenfassend unterstützen unsere Daten ein Model, in dem CdbS durch die Depletion von CdbA oder durch Hitzestress auf einem erhöhten Level akkumuliert, um die

Störung der Organisation und Segregation des Chromosoms zu befördern. Dies führt zur Inhibierung der Zellteilung und verursacht den Zelltod.

Wir spekulieren, dass das CdbA/CsdK1/CsdK2/CdbS System durch ein c-di-GMP Signal reguliert sein könnte. Der Botenstoff könnte die DNS-Bindung von CdbA verändern und dadurch das zelluläre CdbS Level steuern. Zuletzt diskutieren wir, dass dieses System, wenn es fehlerhaft oder übermäßig aktiviert wird, einen schädlichen Effekt die die Lebensfähigkeit hat.

1 Introduction

1.1 Nucleotide-based second messengers

Bacteria sense and respond to changes in their surroundings to optimize their survival. Exposure to various external stimuli activates different stress sensors and specific response pathways within the bacterial cell. One of the strategies that bacteria use to respond to environmental changes is based on second messenger systems (Pesavento and Hengge, 2009). In these systems, the sensing of an extracellular signal results in the production of a small cytoplasmic molecule, i.e. the second messenger. This compound then triggers intracellular signal transduction cascades, which generate the appropriate output response (Newton *et al.*, 2016).

Bacterial second messengers include a diverse group of nucleotides including the linear nucleotide guanosine 3'-diphosphate 5'-tri/diphosphate ((p)ppGpp), the cyclic nucleotides adenosine 3',5′-cyclic monophosphate (cAMP), and guanosine 3',5'-cyclic monophosphate (cGMP) as well as the cyclic dinucleotides cyclic di-3′,5′-adenosine monophosphate (c-di-AMP), cyclic di-3',5'-guanosine monophosphate (c-di-GMP), and cyclic GMP-AMP (cGAMP), Some of these second messengers regulate the same cellular processes, indicating that they are part of the same, complex signaling cascade (Hengge, 2021a). Among the most extensively studied bacterial second messengers are (p)ppGpp, cAMP, c-di-AMP and c-di-GMP (He *et al.*, 2020, Pesavento and Hengge, 2009).

Upon nutrient limitation, bacteria initiate the stringent response, which is mediated by the production of (p)ppGpp. This second messenger is synthesized via transfer of pyrophosphate from ATP to GTP or GDP, while it is degraded by the removal of the pyrophosphate. These processes are performed by proteins of the RelA/SpoT homolog superfamily that have either the synthetase or the hydrolysis domain (Steinchen and Bange, 2016). Proteins of the RelA/SpoT homolog superfamily can be found in most bacteria and also in chloroplasts (Atkinson *et al.*, 2011). Once (p)ppGpp accumulates in the cell, it shifts the transcription of genes involved in metabolism to genes for nutrient transporters and amino acid synthesis (Irving *et al.*, 2021). In *Escherichia coli*, (p)ppGpp regulates transcription by directly interacting with the RNA polymerase (Srivatsan and Wang, 2008). Furthermore, the second messenger also modulates the purine nucleotide pools, DNA replication and antibiotic resistance (Irving *et al.*, 2021, Liu *et al.*, 2015).

cAMP was the first identified second messenger and modulates various cellular processes dependent on the availability of carbon sources. cAMP is synthesized from ATP by adenylate cyclases and degraded to AMP by phosphodiesterases (PDEs) (Görke and Stülke, 2008). By binding to and allosterically activating the transcription factor cAMP-receptor protein (CRP), this signaling molecule regulates the carbon catabolite repression (Gomelsky, 2011, McDonough and Rodriguez, 2011).

c-di-AMP has been mostly studied in Gram-positive bacteria, but has also been identified in some Gram-negative species (Fahmi *et al.*, 2017). In contrast to most other second messengers, c-di-AMP is essential for growth in many bacteria, as it regulates a variety of cellular processes such as potassium transport, cell wall maintenance, and DNA damage repair (Corrigan and Gründling, 2013). C-di-AMP is synthesized from two ATP molecules by diadenylate cyclases and degraded to 5'-phosphadenylyl adenosine by PDEs (Fahmi *et al.*, 2017). While the c-di-AMP binding effectors are poorly understood, most of the currently known effectors are potassium transporters, but c-di-AMP binding transcription factors, sensor kinases, as well as riboswitches have been identified. (Stülke and Krüger, 2020)

1.2 The second messenger c-di-GMP

The second messenger c-di-GMP has been studied for decades and is recognized as a widespread global regulator of various cellular processes in bacteria (Jenal *et al.*, 2017). It is best known for having a key function in transitioning between motile and sessile bacterial lifestyles. Typically, low levels of c-di-GMP are associated with free-living, motile cells while high levels promote adhesion and biofilm formation as well as inhibition of motility (Boyd and O'Toole, 2012, Hengge, 2009, Krasteva *et al.*, 2012, Römling *et al.*, 2013). However, c-di-GMP also regulates a great variety of other cellular processes including cell cycle progression, virulence, and multicellular development (Jenal *et al.*, 2017, Römling *et al.*, 2013).

1.2.1 c-di-GMP metabolism

Cyclic di-GMP is synthesized from two molecules of GTP by diguanylate cyclases (DGCs) (Figure 1). These enzymes are characterized by the GGDEF domain (Römling *et al.*, 2013). DGCs are thought to form homodimers in which each GGDEF domain binds one GTP molecule that are

organized in an antiparallel manner in the dimer. During catalysis, two phosphodiester bonds between the two GTP molecules are generated (Schirmer, 2016). The enzymatic activity of most DGCs is regulated via the RxxD motif, which is N-terminal to the catalytic GGDEF motif and is referred to as the inhibitory I-site. DGC activity is allosterically inhibited by binding of c-di-GMP to this site (Sondermann *et al.*, 2012).

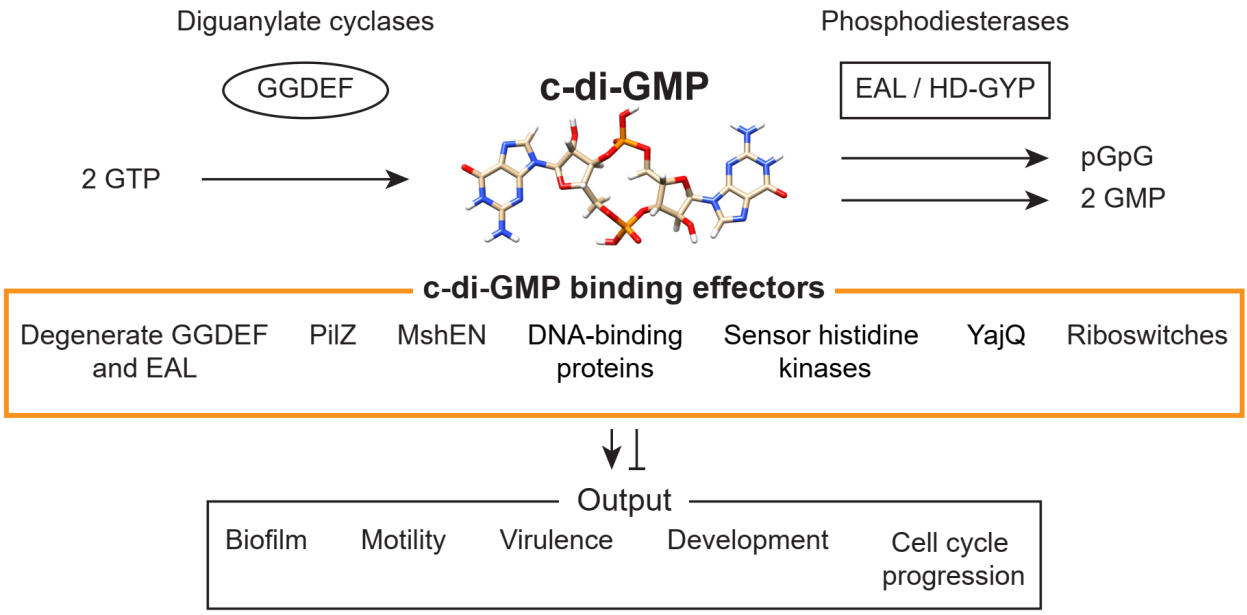

Figure 1: Overview of the c-di-GMP metabolism. The signaling molecule is synthesized from two molecules of GTP by DGCs and degraded by PDEs. By binding to different receptors, c-di-GMP regulates various cellular processes. The figure was modified from Sondermann *et al.*, 2012

C-di-GMP is hydrolyzed by PDEs containing either an EAL or HD-GYP domain (Figure 1). Enzymes featuring the EAL domain commonly linearize c-di-GMP to 5'-phosphoguanylyl-(3',5')-guanosine (pGpG), which is then further degraded to two molecules of GMP by other enzymes (Orr *et al.*, 2015). Proteins featuring the HD-GYP domain typically degrade c-di-GMP directly into two monomers of GMP (Hengge, 2009, Römling *et al.*, 2013). Multidomain proteins have also been identified that have both a GGDEF and an EAL or a HD-GYP domain. However, only a few of these proteins have bifunctional activity, as in most cases one of the two domains is enzymatically inactive (Römling *et al.*, 2013).

The environmental signals that ultimately regulate the level of c-di-GMP vary greatly between bacterial species. In *E. coli*, the global cellular level of c-di-GMP is growth phase dependent and increases during the exponential growth phase with a peak at the transition to the stationary growth phase, when its level starts to decrease slightly (Spangler *et al.*, 2010). In *Caulobacter crescentus*, the global cellular c-di-GMP level oscillates during the cell cycle, being low in non-dividing swarmer cells, increasing during the differentiation to stalked cells and at an intermediate level in pre-divisional cells (Lori *et al.*, 2015). On the other hand, in *Myxococcus xanthus*, the global cellular c-di-GMP level does not vary significantly in different growth phases, but increases significantly upon nutrient starvation and this elevated level is important for multicellular development (Skotnicka *et al.*, 2016a, Skotnicka *et al.*, 2016b). In contrast in Streptomycetes, a high c-di-GMP level promotes growth while a drop in its level initiates the differentiation into spores (Bush *et al.*, 2015).

Many DGCs and PDEs contain additional domains in addition to the enzymatically active domains including receiver, a Per-Arnt-Sim (PAS) domain and GAF domains (Römling *et al.*, 2013). It has been hypothesized that these domains sense different signals such as oxygen and light, and then modulate the enzyme activities of the associated GGDEF, HD-GYP or EAL domains (Tamayo *et al.*, 2007).

1.2.2 c-di-GMP effectors

c-di-GMP binds to various receptors to generate a cellular response (Figure 1) (Hengge, 2009). Together, these effectors are highly versatile, allowing c-di-GMP to act at the transcriptional, post-transcriptional, translational, and post-translational level (Römling *et al.*, 2013, Sondermann *et al.*, 2012). While the c-di-GMP metabolizing enzymes can be identified via their characteristic domains and signature motifs, the c-di-GMP binding receptors are highly diverse. They include proteins with diverse domains as well as riboswitches and use different motifs and mechanisms to bind c-di-GMP (Chou and Galperin, 2016, Römling *et al.*, 2013). Here, we provide an overview of the currently identified types of c-di-GMP receptors and will discuss the PilZ domain in detail in the following chapter 1.2.3 (Figure 1).

Early c-di-GMP effector candidates were proteins with a degenerate GGDEF or EAL domain that do not have enzymatic activity. Degenerate GGDEF domains can still bind c-di-GMP via the I-site, which then modulates the activity of the protein (Jenal *et al.*, 2017, Römling *et al.*, 2013). While degenerate EAL domains are not active, they can still bind the second messenger via the eponymous motif (Chou and Galperin, 2016). For instance, PopA protein of *C. cresenctus* binds c-di-GMP via its degenerate GGDEF domain to direct the replication initiation inhibitor CtrA to ClpXP for degradation, allowing the cell cycle to progress (Ozaki *et al.*, 2014). CdgA of *Bdellovibrio bacteriovorus* also has an enzymatically inactive GGDEF domain, but binds c-di-GMP to allow fast prey cell invasion (Hobley *et al.*, 2012). FimX of *Pseudomonas aeruginosa* is a degenerate GGDEF-EAL protein that binds c-di-GMP via its EAL domain and is vital for twitching motility and biofilm formation (Kazmierczak *et al.*, 2006, Navarro *et al.*, 2009). LapD of *P. fluorescens* has an enzymatically inactive GGDEF domain as well as a degenerate EAL domain, the latter of which binds c-di-GMP (Newell *et al.*, 2009).

A large group of diverse of c-di-GMP effectors include DNA-binding proteins of different families. The transcription factor BldD in *Streptomyces* regulates development and was identified to bind tetrameric c-di-GMP (Tschowri *et al.*, 2014). Clp from *Xanthomonas campestris* is a CRP-like protein that binds both DNA and c-di-GMP in a competitive manner to regulate the expression of virulence genes (Chin *et al.*, 2010). CuxR of *Sinorhizobium meliloti* is an AraC-like transcriptional regulator that binds the second messenger with a mechanism similar to the PilZ domain and controls the production of expopolysaccharides (EPS) (Schäper *et al.*, 2017). CdbA of *M. xanthus* is a ribbon-helix helix protein and was characterized as a nucleoid-associated protein and not as a transcriptional regulator (Skotnicka *et al.*, 2020), and will be discussed in detail in chapter 1.4.8. FleQ of *P. aeruginosa* and VpsR of *Vibrio cholerae* are both transcriptional regulators of the NtrC family that bind c-di-GMP via their AAA+ ATPase domains to regulate gene expression (Hickman and Harwood, 2008, Srivastava *et al.*, 2011).

Some ATPases also bind c-di-GMP (Jenal *et al.*, 2017). In *P. fluorescens*, the flagellar export ATPase FliI and its homologs HrcN from a type III secretion system and ClpB2 from a type VI secretion system were reported to bind the second messenger (Trampari *et al.*, 2015). In addition, the ATPase activity of the ribosomal modification protein RimK in *Pseudomonas* species is regulated by c-di-GMP (Little *et al.*, 2016).

The MshEN domain has the most extended c-di-GMP binding motif reported so far and consists of two 24-residue long tandem sequences that are separated by a short linker (Wang *et al.*, 2016). This domain was first identified in the N-terminal part of the MshE ATPase in *V. cholerae*, and binds c-di-GMP via this domain to regulate its ATPase activity (Wang *et al.*, 2016). Another characterized MshEN domain protein is NfrB of *E. coli*, which binds the second messenger and modulates the accumulation of EPS (Junkermeier and Hengge, 2021).

The YajQ family of proteins is associated with binding to nucleotides and tRNAs, and XC_3703 from *X. campestris* and PA4395 of *P. aeruginosa* were shown to bind c-di-GMP (An *et al.*, 2014). XC_3703 interact with a LysR-like transcription factor to regulate virulence gene expression depending on c-di-GMP (An *et al.*, 2014). A similar system was discovered in *Lysobacter enzymogenes*, where the YajQ protein CdgL interacts with LysR to modulate the production of an antifungal component (Han *et al.*, 2020).

Some sensor histidine protein kinases of two-component systems have also been shown to bind c-di-GMP. Upon binding of c-di-GMP, the bifunctional sensor histidine kinase CckA in *C. crescentus* shifts from kinase to phosphatase activity to inactivate CtrA, which allows the initiation of replication and cell cycle progression (Lori *et al.*, 2015). Recently, the histidine protein kinase, ShkA, was reported to modulate *C. crescentus* cell cycle progression by binding c-di-GMP via its pseudo-receiver domain (Kaczmarczyk *et al.*, 2020). Another sensor histidine kinase that binds c-di-GMP is PdtaS in *Mycobacterium smegmatis*. This kinase autophosphorylates upon binding of c-di-GMP thereby regulating signaling by the PdtaR-PdtaS two-component system, which is important for metabolic adaptation and nutrient sensing (Hariharan *et al.*, 2021).

Riboswitches represent the so far only non-proteinaceous c-di-GMP receptors. These RNA aptamers bind c-di-GMP with nanomolar affinity, and the resulting change in secondary structure regulates transcription or processing of the mRNA (Römling *et al.*, 2013).

1.2.3 The PilZ domain as a c-di-GMP binding effector

Amikam and Galperin were the first to hypothesize that the PilZ domain could bind c-di-GMP (Amikam and Galperin, 2006). Experimental evidence for binding was later confirmed for various PilZ domain proteins including YcgR in *E. coli,* Alg44 in *P. aeruginosa,* as well as PlzC and PlzD in *V. cholerae* (Merighi *et al.*, 2007, Pratt *et al.*, 2007, Ryjenkov *et al.*, 2006). The

canonical PilZ domain consists of a six-stranded β-barrel and a C-terminal α–helix (Figure 2). PilZ domains lacking the C-terminal α–helix have also been identified and are referred to as xPilZ domains (Galperin and Chou, 2020).

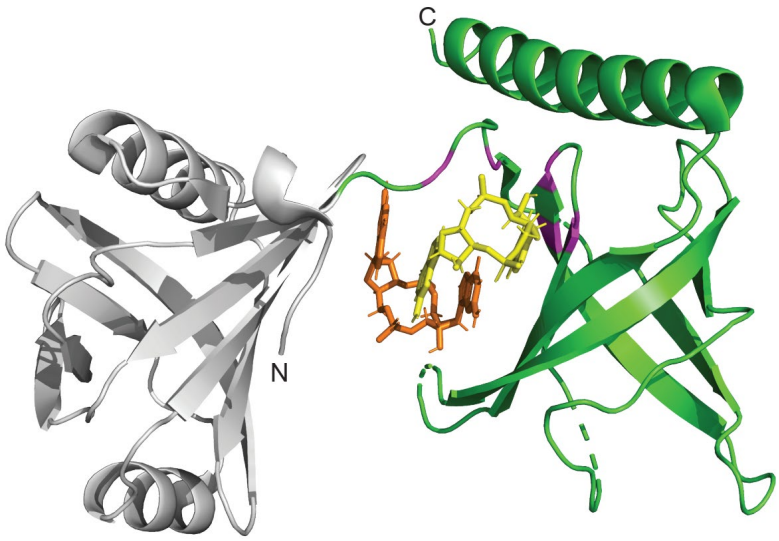

Figure 2: Crystal structure of YcgR in complex with c-di-GMP. YcgR binds a c-di-GMP dimer (orange and yellow). The PilZ domain with the six-stranded β-barrel and the C-terminal α–helix is highlighted in green, with the residues involved in c-di-GMP binding in pink. In white, the YcgR-N domain is marked. The image is modified from Hou *et al.,* 2020, using entry ID 5Y6F of the protein data bank and PyMOL.

The only conserved sequence of the PilZ domain is the bipartite c-di-GMP binding motif RxxxRx$^{20\text{-}30}$[D/N]hSxxG in which h refers to a hydrophobic residue and x to any amino acid (Galperin and Chou, 2020). The c-di-GMP binding motif is located at the N-terminus of the PilZ domain (Figure 2) (Ryjenkov *et al.*, 2006). Upon binding of c-di-GMP, the PilZ domain undergoes a small conformational change that typically activates the protein enabling it to interact with downstream targets (Hengge, 2009). The PilZ domain is capable of binding monomeric as well as dimeric c-di-GMP, where the guanine bases of the second messenger are stacked (Chou and Galperin, 2016). It was suggested that PilZ domains with the LRxxxR motif bind monomeric and PilZ domains with the (Q/E)(R/K)RxxxR motif bind dimeric c-di-GMP; however, experimental evidence remains inconclusive (Chou and Galperin, 2016). Intriguingly, many bacteria encode PilZ domain proteins that lack the RxxxR sequence but contain the [D/N]hSxxG motif, and such proteins are not able to bind c-di-GMP (Chou and Galperin, 2016). Paradoxically, the domain was

named after the PilZ protein in *P. aeruginosa*, which does not bind c-di-GMP (Alm *et al.*, 1996, Merighi *et al.*, 2007).

The PilZ domain can be the single domain of a protein or can occur in multi-domain proteins (Galperin and Chou, 2020, Sondermann *et al.*, 2012). Stand-alone PilZ proteins transduce the signal primarily via protein-protein interactions with downstream targets and mainly act as adaptor proteins, while multi-domain PilZ proteins feature additional domains such as DNA-binding and receiver domains that then act in a c-di-GMP dependent manner (Benach *et al.*, 2007, Habazettl *et al.*, 2011, Mills *et al.*, 2011).

One of the earliest identified and best-studied PilZ domain proteins is YcgR in *E. coli* that consists of a YcgR-N domain at the N-terminus and a C-terminal PilZ domain (Figure 2) (Ryjenkov *et al.*, 2006). YcgR binds c-di-GMP with a K_D of 0.84 µM via the PilZ domain and regulates motility in a c-di-GMP dependent manner (Ryjenkov *et al.*, 2006). YcgR is a flagellar brake that inhibits the flagellar motor by interacting with FliG, FliM, and MotA (Hou *et al.*, 2020, Paul *et al.*, 2010). Another well-studied PilZ protein is Alg44 in *P. aeruginosa*, which regulates the biosynthesis of the polysaccharide alginate in a c-di-GMP-dependent way (Merighi *et al.*, 2007). Interestingly, a PilZ protein of *X. campestris* does not bind c-di-GMP and interacts with FimX, a protein with a degenerate GGDEF and EAL domain, and PilB to initiate T4P biogenesis. However, the interplay between these proteins depends on the presence of c-di-GMP, and the second messenger was described as a molecular glue for this interaction (Chin *et al.*, 2012).

In summary, PilZ domain proteins represent a highly versatile group of c-di-GMP effectors and are involved in a regulating a broad spectrum of cellular processes.

1.2.4 Specificity of c-di-GMP signaling

Most bacteria encode multiple c-di-GMP synthesizing and degrading enzymes as well as receptors (Conner *et al.*, 2017, Ryjenkov *et al.*, 2006). Nevertheless, lack of individual DGCs or PDEs can cause specific defects, demonstrating that not all DGCs or PDEs in a bacterium regulate the same process. These observations bring up the question how the c-di-GMP that is produced or degraded by different DGCs or PDEs can elicit different responses (Dahlstrom and O'Toole, 2017, Hengge, 2016).

The production of some DGCs and/or PDEs is temporally regulated, ensuring that e.g. motility or biofilm formation is modulated according to the growth phase (Hengge, 2009). Nevertheless, some DGCs are expressed at the same time and therefore can influence the global c-di-GMP level. Hence, it was proposed that the specificity in c-di-GMP signaling depends on the affinities of the diverse effectors for the second messenger, as well as the affinity of the I-sites of the DGCs (Hengge, 2021b). In several cases, it has also been found that lack of a DGC or PDE does not affect the global cellular c-di-GMP level. These observations lead to the hypothesis that some DGCs and/or PDEs may contribute to local c-di-GMP pools that are separated or insulated from the global cellular c-di-GMP pool (Hengge, 2021b). Local c-di-GMP pools are suggested to be regulated independently of the global c-di-GMP pool and, therefore, generate specific local outputs with their associated effectors (Hengge, 2021b). Based on mathematical modelling, it was proposed that local pools can exist in a bacterial cell without microcompartments (Richter *et al.*, 2020), allowing local c-di-GMP pools to influence cellular processes in a targeted manner.

1.3 The DnaK-DnaJ-GrpE chaperone system

Changes in the surrounding environment, such as heat or acidity, can put cells under major stress, as they can directly impact the function and stability of the proteome. To perform cellular processes and to survive, every living cell relies on correctly folded proteins (Clerico *et al.*, 2015). Chaperones maintain the cellular protein homeostasis using different mechanisms, i.e. they are involved in *de novo* protein folding, refolding of misfolded and stress-induced unfolded proteins, or target such proteins for degradation (Hartl *et al.*, 2011). Historically, many chaperones are termed heat shock proteins (Hsp), because they were initially discovered as induced in response to heat stress, but chaperones are now known to function in the folding of *de novo* synthesized proteins as well as in response to various stress signals (Voth and Jakob, 2017).

The major molecular chaperones are grouped into five different classes: Hsp60, Hsp70, Hsp90, Hsp100 and the small Hsps (Bascos and Landry, 2019). Most of these chaperone families are well-conserved across all domains of life, further indicating their vital role in all living organisms (Richter *et al.*, 2010). Chaperones of different families can work together in a complex network to

maintain protein homeostasis (Bhattacharya *et al.*, 2020, Schumacher *et al.*, 1996, Zietkiewicz *et al.*, 2004).

Small heat shock proteins such as Hsp20 or Hsp10 were described as the first proteins to respond to increased misfolding events and irreversible protein aggregation. Nevertheless, they rely on other chaperones to refold their client proteins (Haslbeck and Vierling, 2015). Hsp20 chaperones, such as IbpA from *E. coli*, associate promiscuously with proteins in their nonnative state, which are then transferred to other chaperones such as the DnaK-DnaJ-GrpE (KJE) system for refolding (Haslbeck and Vierling, 2015, Haslbeck *et al.*, 2019, Richter *et al.*, 2010).

Hsp60 are also termed chaperonins and are grouped in two classes: class I are present in bacteria and mitochondria, while class II are present in archaea and eukaryotes (Conway de Macario *et al.*, 2019). The most studied bacterial Hsp60 is GroEL from *E. coli*, which, together with the co-chaperonin GroES, forms a complex that folds proteins in an ATP-dependent manner (Lin and Rye, 2006). On the other hand, Hsp90 chaperones are poorly understood, with HtpG of *E. coli* being the most prominent member. However, it has become clear that Hsp90 work together with the KJE system to assist in protein folding (Fauvet *et al.*, 2021, Wickner *et al.*, 2021). Hsp100, such as ClpX from *E. coli*, are AAA+ ATPase chaperones that unfold their aggregated clients and either cooperate with KJE systems to refold these clients or deliver them to proteases such as ClpP for degradation (Kim *et al.*, 2001, Mogk *et al.*, 2015, Schramm *et al.*, 2019).

The proteins DnaK (Hsp70), DnaJ (Hsp40) and GrpE from *E. coli* make up the canonical and well-studied KJE chaperone system (Figure 3). The KJE system generally establishes protein homeostasis and provides protection from various stress conditions by assisting in *de novo* folding and refolding of proteins as well as by disaggregation of aggregated proteins and channeling of proteins to proteases for degradation (Mayer, 2021). The core component of the KJE chaperone system is the Hsp70 protein (also often referred to as DnaK in bacteria). Hsp70 proteins are typically working in concert with two co-chaperones: an Hsp40 protein (often referred to as a DnaJ protein) characterized by the J-domain, and a nucleotide exchange factor (NEF) (often referred to as GrpE) (Genevaux *et al.*, 2007). Together, these proteins assist client proteins in folding via multiple rounds of an ATP-dependent cycle, as explained in detail in the following chapters (Figure 3).

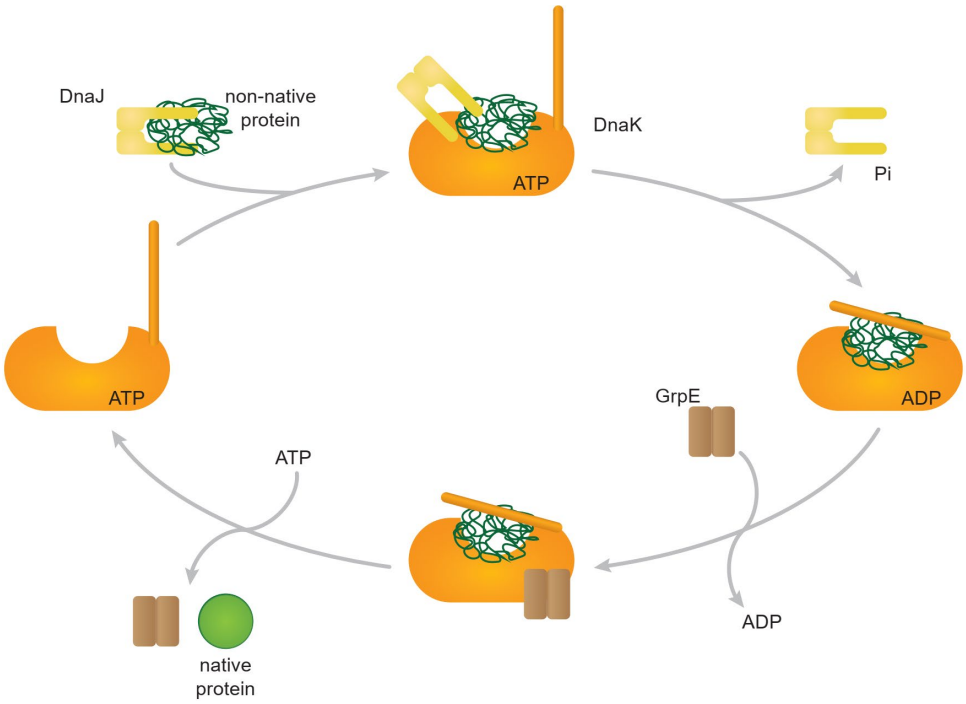

Figure 3: Chaperone cycle of a KJE system. Homodimeric DnaJ transfers the client to DnaK in the ATP-bound state, stimulating its ATPase activity. Upon ATP hydrolysis, DnaK switches into the closed conformation. The GrpE dimer facilitates the nucleotide exchange of DnaK back to ATP, which brings DnaK back into the open conformation. This releases the client protein, which then refolds. The figure was modified from Imamoglu *et al.*, 2020.

1.3.1 Hsp70 protein are is the core chaperone of the KJE system

Typically, Hsp70 proteins function as ATP-dependent chaperones that participate in protein folding of de novo synthesized proteins, protein refolding, disaggregation of aggregated proteins and protein degradation (Genevaux *et al.*, 2007). A canonical Hsp70 protein consists of a nucleotide-binding domain (NBD) with ATPase activity in their N-terminal part, a substrate binding domain (SBD) at their C-terminal part and a linker between these two domains. The NBD forms two lobes and can be further divided into the four subdomains IA, IB, IIA, and IIB. The SBD is characterized by a ß-sandwich subdomain, an α-helical subdomain, and a short disordered region (Genevaux *et al.*, 2007, Kityk *et al.*, 2018, Mayer, 2021). To function, an Hsp70 cycles between an open and closed conformation depending on its ATP- or ADP-bound state (Figure 3). Upon interaction with a J-domain protein that transfers a client protein, the low intrinsic ATPase activity of the Hsp70 protein generally increases more than 1,000-fold, and the bound ATP is

hydrolyzed (Laufen *et al.*, 1999, Mayer, 2021). This results in a switch into the closed conformation of the Hsp70, thereby trapping a client, as Hsp70 has a high affinity for its substrates in the ADP-bound state. A GrpE-like protein facilitates the nucleotide exchange to ATP. During nucleotide exchange, a conformational change occurs in the Hsp70 protein to the open state, allowing substrate release. The client is then either refolded or transferred to another chaperone system (Genevaux *et al.*, 2007, Imamoglu *et al.*, 2020).

How this allosteric cycle of the Hsp70 protein leads to properly folded clients remains elusive. Two different models are described: The Hsp70 chaperone can work as an ”unfoldase” that partially unfolds clients in their misfolded state, followed by spontaneous refolding. In other reports, they act as “holdases” that keep the bound polypeptide in place while the surrounding peptides of the client fold (Mayer and Gierasch, 2019, Richter *et al.*, 2010, Zuiderweg *et al.*, 2013).

Most bacteria encode more than one Hsp70 protein (Genevaux *et al.*, 2007). For instance, *E. coli* encodes three Hsp70 proteins: DnaK, which is studied intensively and serves as the canonical Hsp70 protein; HscA, a specialized chaperone required for the assembly of iron-sulfur clusters (Vickery and Cupp-Vickery, 2007); and, HcsC, which is important for the response to UV radiation and Cd^{2+} ions (Kluck *et al.*, 2002). Strikingly, HscA and HscC lack critical residues to bind GrpE and show some structural alterations compared to DnaK (Brehmer *et al.*, 2001, Mayer, 2021). HscA and HscC homologs are only found in prokaryotes, while DnaK is highly conserved across all three domains of life, underlining the importance of this protein family (Genevaux *et al.*, 2007).

Under laboratory conditions, none of the three *E. coli* Hsp70 chaperones are essential for viability (Bukau and Walker, 1989, Hesterkamp and Bukau, 1998, Kluck *et al.*, 2002). Lack of DnaK results in slower growth, increased sensitivity to lower as well as higher temperatures, cellular filamentation and defects in motility (Bukau and Walker, 1989, Genevaux *et al.*, 2007, Shi *et al.*, 1992). Interestingly, removal of one of the two DnaK homologs in *C. crescentus* induces a lethal cell cycle arrest, as lack of the protein directs DnaA for degradation by the Lon protease (da Silva *et al.*, 2003, Jonas *et al.*, 2013, Susin *et al.*, 2006a). Furthermore, it acts in response to high and low temperatures but not to saline, osmotic or oxidative stress (Susin *et al.*, 2006b).

1.3.2 The Hsp40 J-domain co-chaperone

In KJE systems, Hsp40 proteins recognize the misfolded client proteins and are characterized by the J-domain. This domain consists of ~70 residues and contains a HPD motif, which is essential for interacting with the interdomain linker of an Hsp70. This interaction induces a conformational change in the Hsp70 protein, stimulating its ATPase activity (Kityk *et al.*, 2018).

J-domain proteins are grouped into three classes according to their domain architecture and structural features. However, a new classification scheme according to the phylogenetic relatedness of the domain is currently debated (Ajit Tamadaddi and Sahi, 2016, Kampinga *et al.*, 2019). Based on the current classifications, class I J-domain proteins, to which the prototypical DnaJ from *E. coli* belongs, feature the J-domain at their N-terminal part, followed by a G/F rich region, a central domain with four repeats of the CXXCXGXG motif forming a zinc-finger, and a diverse dimerization domain at the C-terminal end. Class II proteins are similar to class I but lack the central domain. In contrast, class III proteins only contain the J-domain but can feature other domains (Ajit Tamadaddi and Sahi, 2016).

Class I J-domain proteins form homodimers that recognize hydrophobic polypeptides of a client protein via multiple binding sites to establish a stable chaperone-client interaction. This multivalent and dynamic interaction allows J-domain proteins to distinguish between native and non-native proteins and to effectively transfer the clients to an Hsp70 protein (Jiang *et al.*, 2019, Mayer, 2021). Typically, bacteria and other organisms encode more J-domain co-chaperones than Hsp70 proteins, suggesting that Hsp70 proteins function together with more than one J-domain protein (Kampinga and Craig, 2010).

E. coli encodes six and *C. crescentus* five J-domain proteins (Genevaux *et al.*, 2007, Schroeder and Jonas, 2021). Lack of DnaJ in *E. coli* leads to filamentation and affects the assembly of the flagellum (Sell *et al.*, 1990, Shi *et al.*, 1992). In *C. crescentus*, the DnaJ homolog is involved in responding to high and low temperatures. Additionally, it also has a vital role in cell cycle progression (Susin *et al.*, 2006b).

1.3.3 The nucleotide exchange factor GrpE

To exchange ADP for ATP, most Hsp70 proteins rely on a NEF. So far, four different classes of NEFs for Hsp70 have been identified, of which three are only found in eukaryotes (Bracher and Verghese, 2015).

In bacteria, homologs of the *E. coli* protein GrpE facilitate the nucleotide exchange by Hsp70 proteins. These proteins consist of a long α-helical dimerization domain and a ß-sheet domain. Homodimeric GrpE-like proteins interact with an Hsp70 protein via the ß-sheet domain, which interacts with IIB of the NBD to induce a conformational shift (Harrison *et al.*, 1997). This rotates the NBD into an open state that releases the bound ADP, thus allowing the Hsp70 to bind ATP, restarting the chaperone cycle (Bracher and Verghese, 2015, Harrison *et al.*, 1997). *E. coli* and *C. crescentus* each encode one GrpE-domain protein according to the KEGG database (https://www.kegg.jp/dbget-bin/www_bfind_sub?mode=bfind&max_hit=1000&dbkey=eco&keywords=GrpE; https://www.kegg.jp/dbget-bin/www_bfind_sub?mode=bfind&max_hit=1000&dbkey=ccs&keywords=GrpE; accessed on 21st Feb 2023).

1.4 The model organism *Myxococcus xanthus*

Due to its large genome, complex multicellular life cycle and coordinated predation, *M. xanthus* is a model organism for chromosome biology, motility, and social behavior. The Gram-negative, rod-shaped bacterium belongs to the phylum *Myxococcota* and its biphasic life cycle depends on the availability of nutrients (Figure 4) (Konovalova *et al.*, 2010, Muñoz-Dorado *et al.*, 2016, Oren and Garrity, 2021). In the presence of nutrients, *M. xanthus* cells grow, divide and spread coordinately using type IV pili (T4P)-dependent and gliding motility to encounter and feed on prey (Muñoz-Dorado *et al.*, 2016). Upon nutrient depletion, *M. xanthus* cells initiate a developmental program that culminates in the formation of spore-filled fruiting bodies (Treuner-Lange and Søgaard-Andersen, 2020, Zusman *et al.*, 2007).

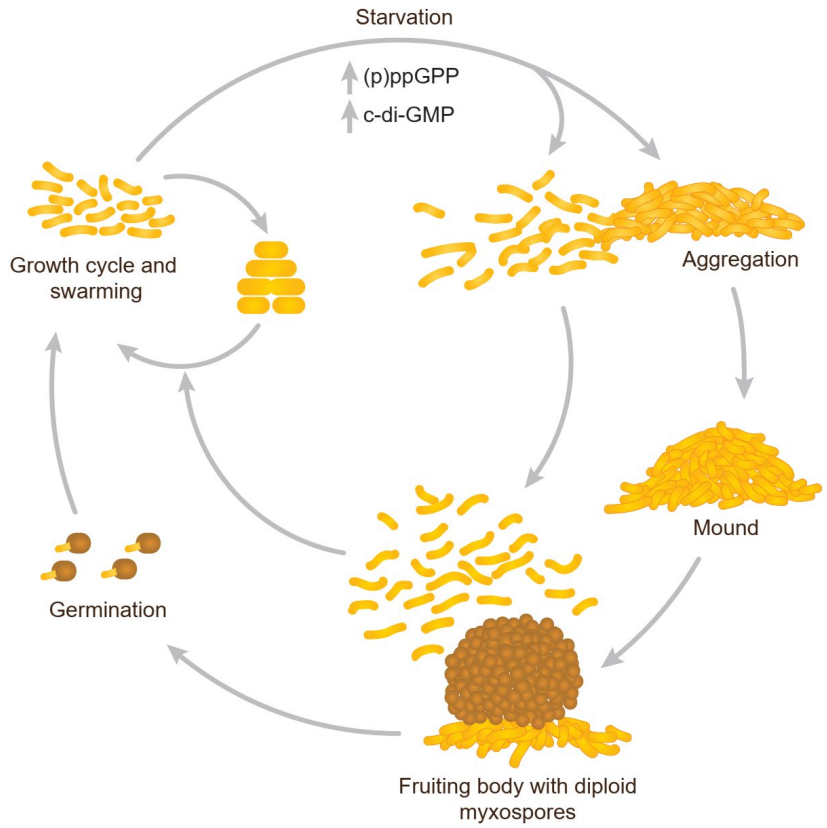

Figure 4: Life cycle of *M. xanthus*. In the presence of nutrients, cells grow, divide and swarm to feed on prey cells. In the absence of nutrients, the cells initiate a developmental program that culminates in the formation of fruiting bodies filled with myxospores. Once environmental conditions become favorable again, the spores germinate. The figure was modified from Zusman *et al.*, 2007 and Treuner-Lange and Søgaard-Andersen, 2020.

1.4.1 Development

When nutrients become limiting, the alarmone (p)ppGpp accumulates in *M. xanthus* cells at elevated levels (Singer and Kaiser, 1995). This molecule triggers the expression of genes involved in the developmental program (Harris *et al.*, 1998, Singer and Kaiser, 1995). Additionally, the level of the second messenger c-di-GMP increases during development and will be discussed in more detail in chapter 1.4.6. Within the first six hours of starvation, the cells aggregate into translucent mounds. At 24 h, fruiting body formation has been completed (Konovalova *et al.*, 2010). Inside these multicellular mounds, cells differentiate into diploid spores, while up to 30% of all cells remain outside the fruiting bodies and differentiate into peripheral rods (O'Connor and Zusman, 1991, Tzeng and Singer, 2005). The remaining cells undergo cell lysis (Rosenbluh *et*

al., 1989). Spore maturation is completed at ~72 h. Once the environmental conditions become favorable, the mature spores germinate (Konovalova *et al.*, 2010).

1.4.2 Chromosome organization and segregation in *M. xanthus*

Similar to *E. coli* (Åkerlund *et al.*, 1995), the number of chromosomes per cell is dependent on the growth phase in *M. xanthus*. Specifically, exponentially growing cells contain one to two chromosomes and cells in stationary phase contain one chromosome (Tzeng and Singer, 2005). Furthermore, myxospores were found to contain two complete chromosomes (Tzeng and Singer, 2005).

The 9.14 Mb large genome of *M. xanthus* is arranged in a circular chromosome that is replicated once per cell cycle, and DNA replication starts early after cell division (Harms *et al.*, 2013). The chromosome is placed along the longitudinal axis of the rod-shaped cell: In newborn cells, the origin of replication (*ori)* is positioned in the subpolar region of the old cell pole, while the terminus region (*ter*) localizes in the subpolar region of the new cell pole with the bulk of the chromosome in between (Harms *et al.*, 2013). During chromosome segregation, one *ori* remains stationary while the second is segregated to the opposite cell pole. During this process, the *ter* moves towards mid-cell where it is eventually replicated (Harms *et al.*, 2013). As DNA replication and chromosome segregation occur simultaneously in bacteria, these cellular processes must be precisely regulated (Badrinarayanan *et al.*, 2015). In *M. xanthus*, three systems have been identified so far to be important for chromosome organization and segregation: the ParAB*S* system as an essential machinery for chromosome segregation, and the BacNOP/PadC and the Smc/ScpAB systems with distinct yet redundant roles (Figure 5).

The ParAB*S* system is widespread among bacteria and is essential in *M. xanthus* (Harms *et al.*, 2013, Iniesta, 2014). It consists of the ATPase ParA and the DNA-binding protein ParB, which binds to specific *parS* sites on the chromosome close to the *ori* (Harms et al., 2013). In its ATP-bound state, ParA is dimeric and binds the chromosome nonspecifically (Badrinarayanan *et al.*, 2015). Upon interaction with the ParB:*parS* segregation complex, ParB stimulates the ATPase activity of dimeric ParA, leading to the disassembly of ParA dimers to monomers that do not bind DNA (Jalal and Le, 2020). Locally stimulated ATP hydrolysis by ParA allows the ParB:*parS* segregation complex to translocate to the opposite cell pole along the DNA-bound ParA-ATP

(Badrinarayanan *et al.*, 2015, Harms *et al.*, 2013, Iniesta, 2014, Ptacin *et al.*, 2010). ParB also binds and hydrolyzes CTP, thereby regulating the affinity of ParB for *parS* sites (Osorio-Valeriano *et al.*, 2019). Furthermore, CTP modulates a cycle of conformational changes in ParB that are relevant to the dynamics of the segregation complex (Osorio-Valeriano *et al.*, 2021). In addition to chromosome segregation, ParB was demonstrated to be involved in different other cellular processes like chromosome organization and initiation of DNA replication in various bacteria (Jalal and Le, 2020).

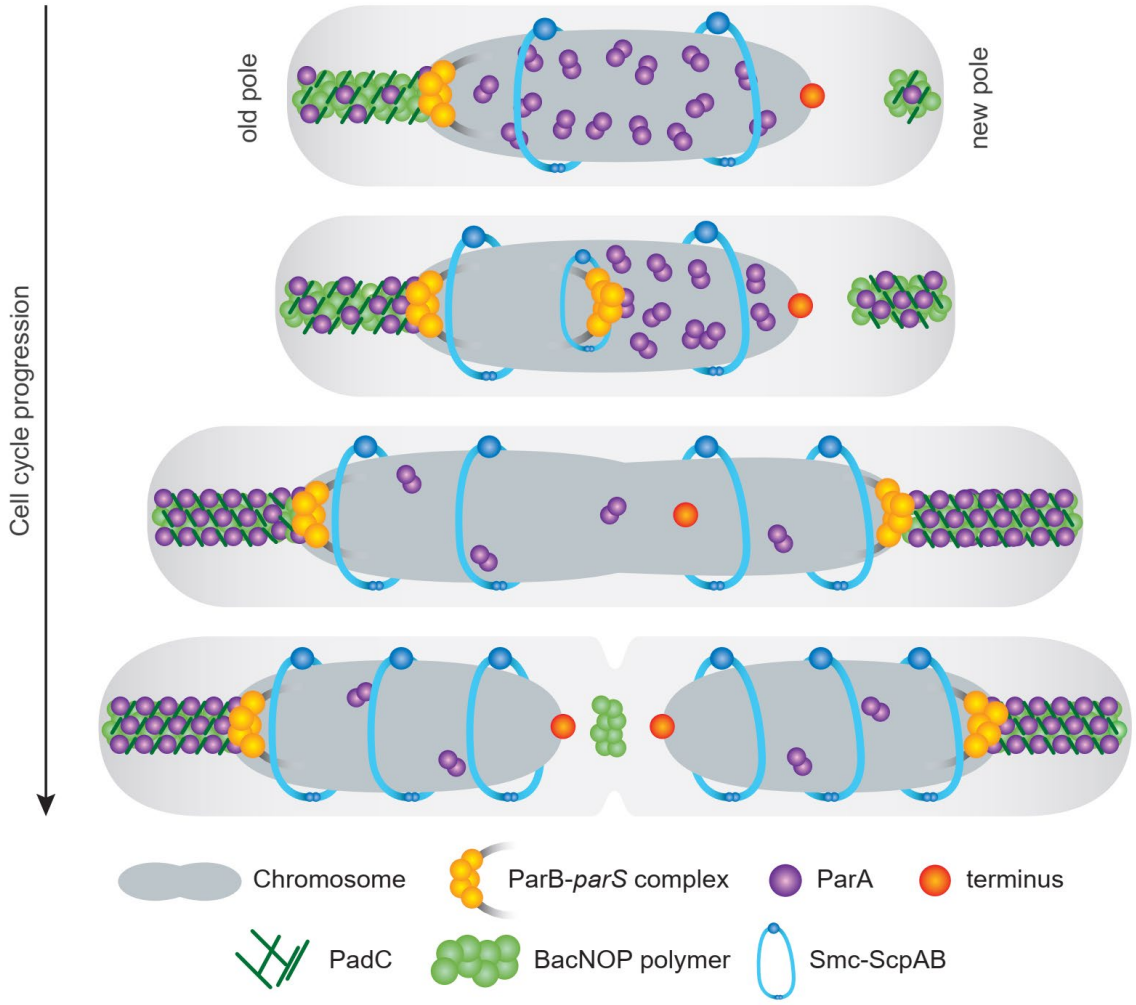

Figure 5: Chromosome organization and segregation in *M. xanthus*. The ParAB*S* system functions as the main machinery to segregate the chromosomes. A scaffold of PadC and the bactofilins BacNOP anchor the chromosome via the ParB:*parS* complexes and captures monomeric ParA. Based on observations in other species, Smc/ScpAB are suggested to be loaded on the nucleoid via the ParB:*parS* complexes to individualize the replicated chromosomes. The figure was adapted and modified from Lin *et al.*, 2017.

The ParB:*parS* complex of *M. xanthus* is anchored in the subpolar regions of the cell by interaction with a scaffold consisting of the three bactofilins BacNOP and the adapter protein PadC (Lin *et al.*, 2017). BacNOP were suggested to form a heteropolymer, with BacP at its core, BacO as an important component for proper assembly of the polymer, and BacN with a yet unknown function (Lin *et al.*, 2017). Newborn cells generally have asymmetrically bipolar localization of the BacNOP/PadC scaffold at the cell poles, with a large complex at the old cell pole and a smaller at the new cell pole. During the cell cycle, the scaffold at the new cell pole gradually grows and a new complex forms at midcell before cell division (Lin *et al.*, 2017). The ParB-like protein PadC is recruited by BacP and colocalizes with the BacNOP polymer (Lin *et al.*, 2017). PadC is a ParB-like protein that recruits monomeric ParA to the BacNOP/PadC scaffold. Like ParB, PadC binds CTP, which was suggested to induce a conformational change that allows PadC to bind monomeric ParA, but unlike ParB, no CTPase activity of PadC was observed (Osorio-Valeriano *et al.*, 2019). Mutant cells lacking BacNOP or PadC have disrupted localization and erratic motion of the ParB:*parS* segregation complex as well as a more condensed nucleoid (Anand *et al.*, 2020, Lin *et al.*, 2017).

The condensin-like structural maintenance of chromosomes complex (SMC) in *M. xanthus* consists of the Smc and the ScpAB subunits and is involved in individualizing the replicated chromosomes (Anand *et al.*, 2020). Generally, the Smc protein has an ATPase head formed by the N- and C-termini, two extended coiled-coil domains, and a hinge domain, which modulates dimerization. ScpA and ScpB interact with each other and promote ring formation by Smc. (Nolivos and Sherratt, 2014, Yatskevich *et al.*, 2019). In several bacterial species, SMC is loaded onto the nucleoid via the ParB:*parS* complex and encircles individual replichores. By moving along the replichores towards the *ter*, the two daughter chromosomes are kept separated (Böhm *et al.*, 2020, Dame *et al.*, 2020). However, for *M. xanthus*, this has not been demonstrated yet (Anand *et al.*, 2020). Smc forms numerous dynamic foci on the *M. xanthus* nucleoid, and Smc/ScpAB were suggested to have a redundant but distinct role compared to BacNOP/PadC, as mutants lacking one or the other system are viable, but lack of both systems is synthetic lethal (Anand *et al.*, 2020). Of note, mutants lacking one or more of the Smc/ScpAB proteins have a temperature-dependent growth defect and only survive at 25°C but not at 32°C (Anand *et al.*, 2020).

1.4.3 Regulation of cell division site placement in *M. xanthus*

A crucial step in cell division in most bacteria is the formation of the FtsZ-ring at the division site (Barrows and Goley, 2021). FtsZ subsequently directly or indirectly recruits all the proteins import for executing cytokinesis resulting in the physical separation of the two daughter cells (Xiao and Goley, 2016). *M. xanthus* cells divide at mid-cell and use the PomXYZ complex to promote FtsZ-ring formation at this position (Figure 6) (Schumacher and Søgaard-Andersen, 2017).

The PomXYZ complex consists of the ParA/MinD ATPase PomZ and its two ATPase-activating proteins PomX and PomY (Schumacher *et al.*, 2017, Schumacher *et al.*, 2021, Treuner-Lange *et al.*, 2013). All three proteins interact with each other and form a single complex in the cell that dynamically localizes on the nucleoid. During the cell cycle, the complex moves in a biased random walk from an off-center position close to the new pole to midnucleoid, which coincides with midcell. At midcell, the complex displays constrained motion and stimulates FtsZ-ring formation (Schumacher *et al.*, 2017). During cell division, the PomXYZ complex likely splits, resulting in each daughter cell containing a complex close to the new cell pole (Figure 6) (Schumacher *et al.*, 2017).

PomX forms filaments that serves as a scaffold to recruit PomY to form a complex containing both proteins (Schumacher *et al.*, 2021). PomZ in its ATP-bound state forms dimers that dynamically and nonspecifically bind to the nucleoid and tether the PomXY complex to the nucleoid (Schumacher *et al.*, 2017). PomX as well as PomY stimulate the ATPase activity of dimeric, DNA-bound PomZ, resulting in the formation of PomZ monomers that localize diffusively in the cell. It was suggested that the PomXY complex moves in the direction of the highest PomZ concentration, which eventually restricts the movement of the complex around midcell (Bergeler and Frey, 2018). While all three proteins are important for FtsZ-ring formation, only PomY and PomZ directly interact with FtsZ (Schumacher *et al.*, 2017).

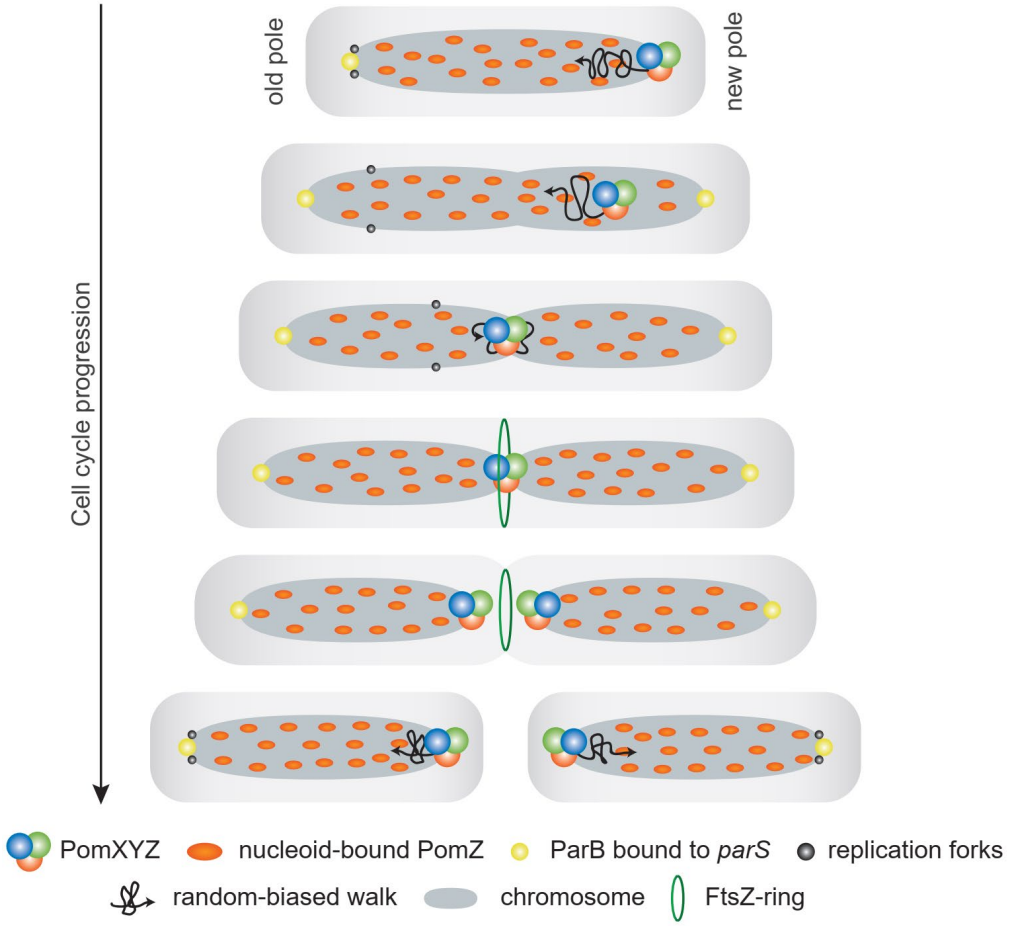

Figure 6: Cell division site placement by the PomXYZ complex**.** During the cell cycle, the PomXYZ cluster moves to midcell in a random-biased walk facilitated by the concentration of PomZ on the nucleoid. At midcell, the complex stimulates the formation of the FtsZ-ring that physically separates the cells, while the PomXYZ complex is split and distributed to the daughter cells. The figure was adapted and modified from Schumacher *et al.*, 2017.

1.4.4 KJE proteins in *M. xanthus*

The *M. xanthus* genome encodes 15 Hsp70 proteins, 16 J-domain proteins, and two GrpE domain proteins. Only a few of these proteins have been analyzed.

The first studied Hsp70 protein in *M. xanthus* was SglK (Mxan_6671), which is encoded in an operon with the GrpE homolog referred to as GrpS (Mxan_6672) (Weimer *et al.*, 1998). Lack of SglK abolishes EPS synthesis, T4P-dependent motility and development, while deletion of *grpS* does not affect these processes (Weimer *et al.*, 1998). A recent study analyzed *sglK* and five additional genes encoding Hsp70 proteins (*mxan_2747*, *mxan_3016*, *mxan_3192*, *mxan_5323,*

and *mxan_7025*) for their expression in responses to different stresses, revealing high transcriptional divergence of these genes in response to heat shock and oxidative stress (Pan *et al.*, 2021). This study also revealed *mxan_3192* as essential, and both Mxan_3192 and SglK can functionally replace DnaK in *E. coli* (Pan *et al.*, 2021). Another characterized Hsp70 protein is StkA (Mxan_3474), which acts as a negative regulator of exopolysaccharide synthesis and has been suggested to function between the T4P machine and the chemosensory Dif system, which regulates EPS synthesis (Moak *et al.*, 2015). In addition to GrpS, *M. xanthus* encodes a second GrpE domain protein, Mxan_4331, which has not been studied as of now.

Among the J-domain proteins, the two proteins Mxan_0750 and Mxan_3292 are class I J-domain proteins and are potential homologs of DnaJ. So far, the only investigated J-domain protein in *M. xanthus* is Mxan_6013, which encodes a class III J-domain protein that also contains a PilZ domain. Lack of this protein neither affects T4P-dependent nor gliding motility; it is also dispensable for exopolysaccharide synthesis and development (Kuzmich *et al.*, 2021).

1.4.5 c-di-GMP in Myxococcus xanthus

In total, the *M. xanthus* genome is predicted to encode 18 GGDEF domain proteins, two proteins containing an EAL domain, six proteins containing a HD-GYP domain, 25 PilZ domain proteins and 22 MshEN domain proteins. However, no c-di-GMP binding riboswitch has been identified (Römling *et al.*, 2013, Kuzmich *et al.*, 2021, Skotnicka *et al.*, 2016a, Skotnicka *et al.*, 2016b, Wang *et al.*, 2016, https://www.genome.jp/dbget-bin/get_linkdb?-t+genes+-p+8+pf:PilZ accessed on 8th Dec 2022). Of these bioinformatically predicted proteins, several have been investigated in detail.

1.4.6 c-di-GMP is important during the life cycle of *M. xanthus*

During growth, *M. xanthus* accumulates a constant c-di-GMP level that does not differ significantly during the exponential and stationary phase (Skotnicka *et al.*, 2016a). The c-di-GMP concentration in vegetative *M. xanthus* cells is ~1.4 ± 0.5 µM (Skotnicka *et al.*, 2020). Manipulation of the global c-di-GMP level in *M. xanthus* by overexpression of a heterologous DGC in otherwise wild type (WT) cells causes a defect in T4P-dependent motility as the transcription of *pilA*, which

codes for the major pilin, is reduced, while gliding motility is unaffected. Similarly, decreasing the global c-di-GMP level by overexpression of a heterologous PDE in otherwise WT cells also causes a defect in T4P-dependent motility but not in gliding motility (Skotnicka *et al.*, 2016a). Further investigations identified the GGDEF domain proteins DmxA, TmoK, and SgmT to be involved in T4P-dependent motility, among which only DmxA has DGC activity. Both DmxA and SgmT bind c-di-GMP using I-sites, while TmoK does not bind c-di-GMP (Skotnicka *et al.*, 2016a).

During starvation, the c-di-GMP level in *M. xanthus* increases more than 10-fold due to the DGC activity of DmxB (Skotnicka *et al.*, 2016b). This increased level is necessary for EPS accumulation during development. A certain threshold of c-di-GMP is necessary to complete the developmental program, however, an increase in the c-di-GMP level in vegetative cells is not sufficient to initiate development (Skotnicka *et al.*, 2016a, Skotnicka *et al.*, 2016b).

Thus, in total only two enzymatically active DGCs have been identified in *M. xanthus* to have a role in T4P-dependent motility and development. The expression of *dmxA* is downregulated during development, while the expression of *dmxB* is increased. MrpC serves as the master regulator of development in *M. xanthus* and modulates the expression of *dmxB*, but not *dmxA* (Kroos, 2017, Kuzmich *et al.*, 2022). This transcription factor also promotes the expression of *pmxA* during development, which encodes an enzymatically active PDE of the HD-GYP type and is important for development (Skotnicka *et al.*, 2016b). PmxA is a bifunctional PDE that degrades c-di-GMP and cGAMP *in vitro* (Skotnicka *et al.*, 2016b, Wright *et al.*, 2020). Interestingly, cells lacking PmxA accumulate c-di-GMP as WT cells during development but the level of cGAMP is increased (Kuzmich *et al.*, 2022). The function of cGAMP in *M. xanthus* remains unexplored.

1.4.7 Characterized c-di-GMP receptors in *M. xanthus*

The first reported c-di-GMP effector in *M. xanthus* was the histidine protein kinase SgmT (Petters *et al.*, 2012). This kinase features an enzymatically inactive GGDEF domain but binds the second messenger via the I-site. Upon ligand binding, the protein localizes in clusters distributed along the cell body. Together with the DNA-binding response regulator DigR, SgmT regulates T4P-dependent motility and the composition of the extracellular matrix (Overgaard *et al.*, 2006, Petters *et al.*, 2012, Skotnicka *et al.*, 2016a). Another known c-di-GMP effector is the

transcription factor EpsI/Nla24, which was suggested to modulate EPS synthesis during development (Lancero *et al.*, 2004, Skotnicka *et al.*, 2016b).

In-frame deletion mutants of 24 PilZ domain proteins in *M. xanthus* have been analyzed for motility, EPS accumulation, and development (Jakobsen *et al.*, 2004, Kuzmich *et al.*, 2021, Muñoz-Dorado *et al.*, 1991, Pérez-Burgos and Søgaard-Andersen, 2020, Pogue *et al.*, 2018). Among these, only lack of four caused a phenotype. Pkn1 and PlpA were shown to be involved in regulating development and cellular reversals (Muñoz-Dorado *et al.*, 1991, Pogue *et al.*, 2018). The PilZ domain of Pkn1 has not been tested for c-di-GMP binding, while PlpA was reported not to bind c-di-GMP (Muñoz-Dorado *et al.*, 1991, Pogue *et al.*, 2018). PixA and PixB both affect the cellular reversal frequency in the presence of nutrients, and PixB is also important for development (Kuzmich *et al.*, 2021). Although both proteins bind c-di-GMP *in vitro*, c-di-GMP binding was reported not to be important for their role in regulating cellular reversals (Kuzmich *et al.*, 2021). By contrast, c-di-GMP binding by PixB is important for its function in development (Kuzmich *et al.*, 2021).

As the MshEN domain was only relatively recently identified as a c-di-GMP binding domain, none of the MshEN domain containing proteins in *M. xanthus* have been tested for c-di-GMP binding (Wang *et al.*, 2016). Among the 22 MshEN domain proteins in *M. xanthus*, only the T4P assembly ATPase PilB has been studied intensively (Jakovljevic *et al.*, 2008); however, its connection to c-di-GMP remains unresolved.

1.4.8 CdbA represents a novel type of c-di-GMP effector and is essential for viability

Using the unbiased c-di-GMP capture compound approach, the DNA-binding, ribbon-helix-helix proteins CdbA and CdbB were recently identified in *M. xanthus* and shown to represent a novel class of c-di-GMP binding effectors (Skotnicka *et al.*, 2020). CdbA and CdbB are small paralogs (67 and 86 amino acids, respectively) and encoded in an operon. All fully sequenced Myxococcales genomes encode at least one ortholog, and when only one is present, it is CdbA-like based on sequence identity/similarity. CdbA and CdbB bind c-di-GMP, and CdbA binds with a K_D of 83 nM (Skotnicka *et al.*, 2020). Analytical size-exclusion chromatography supports that CdbA is a tetramer (Figure 7) and that c-di-GMP binding does not alter CdbA oligomerization but

modulates the conformation of tetrameric CdbA, resulting in a more open conformation than in the unbound form. The crystal structure of CdbA has been solved in the absence of c-di-GMP and confirmed that CdbA is a tetramer (Skotnicka *et al.*, 2020).

CdbA is essential for viability, and depletion of the protein results in cellular filamentation and eventually cells lyse (Skotnicka *et al.*, 2020). More detailed analysis revealed that lack of CdbA disrupts chromosome organization and segregation, thereby causing a cell division defect and cellular filamentation. By contrast, CdbB is dispensable for viability (Skotnicka *et al.*, 2020). CdbA interacts directly with CdbB, and CdbB can partially substitute CdbA (Skotnicka *et al.*, 2020). CdbA is highly abundant and bound >500 sites on the *M. xanthus* genome in ChiP-seq analysis with moderate sequence specificity, while also bending the DNA (Skotnicka *et al.*, 2020). However, depletion of CdbA causes no or only minor changes in transcription (Skotnicka *et al.*, 2020). Based on these observations, it was suggested that CdbA is a nucleoid-associated protein (NAP). Binding of CdbA to DNA and c-di-GMP is mutually exclusive *in vitro* and involves the same interfaces of the tetramer (Figure 7) (Skotnicka *et al.*, 2020). Nevertheless, altering the c-di-GMP level *in vivo* has no effect on cell length and does not visibly alter chromosome organization and segregation (Skotnicka *et al.*, 2016a). Taken together, it was suggested that CdbA is a ligand-regulated NAP and that c-di-GMP fine-tunes the binding of CdbA to DNA (Skotnicka *et al.*, 2020).

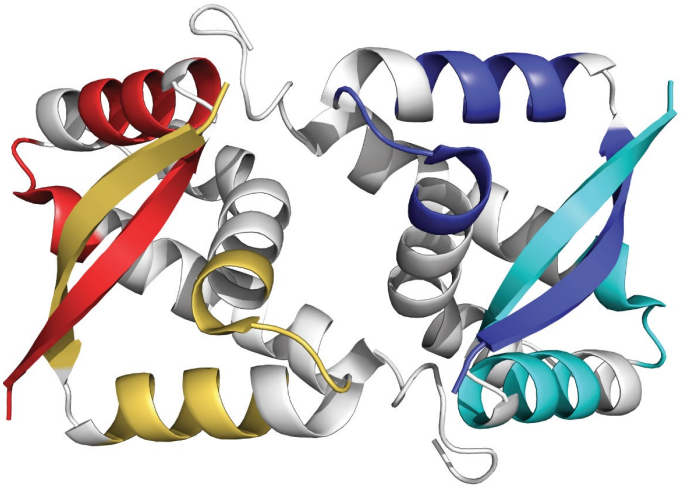

Figure 7: CdbA forms a tetramer. The interfaces of the individual monomers involved in DNA-binding as well as c-di-GMP binding are highlighted in red, yellow, blue and turquoise. Figure was modified from Skotnicka *et al.*, 2020 using entry ID 6SBW of the protein data bank.

In contrast to most NAPs, CdbA is essential for viability. To understand how CdbA is essential, a suppressor screen was performed (D. Skotnicka, unpublished) using a strain containing an in-frame deletion of *cdbA* (Δ*cdbA*) and in which the active fusion *cdbA-mCherry* was expressed from a vanillate-inducible promoter (Skotnicka *et al.*, 2020). This strain grows with a lower growth rate than the wild-type (WT), because, even in the presence of 500 µM vanillate, the cellular level of CdbA-mCh is lower than when expressed from the native site (Skotnicka *et al.*, 2020). After plating cells on growth medium without vanillate, suppressors were isolated that were able to grow in the absence of vanillate. In total, 20 mutants were isolated (D. Skotnicka, unpublished). Sequence analysis demonstrated that six had mutations in the vanillate inducible promoter or in the gene encoding the vanillate repressor. Moreover, by immunoblot analysis, six of the remaining 14 strains accumulated CdbA-mCh even in the absence of vanillate. The remaining eight strains did not accumulate CdbA-mCh in the absence of vanillate and, therefore, were viable in the absence of CdbA-mCh (D. Skotnicka, unpublished). These eight strains were subjected to whole genome sequencing.

The whole genome sequencing revealed that one suppressor strain had a mutation in *cdbB* resulting in a Q22R substitution in CdbB (D. Skotnicka, unpublished). The remaining seven suppressor strains had four different mutations in the locus *mxan_4328* (Table 1) (D. Skotnicka, unpublished). Mxan_4328 encodes a stand-alone PilZ domain protein (Kuzmich *et al.*, 2021).

Table 1: List of identified suppressor mutations for CdbA depletion (Skotnicka, unpublished).

Gene locus	Mutation	Position of mutation	Amino acid change
mxan_4362	A → G	+65 bp upstream of start codon	Q22R
mxan_4328	T → C	-67 bp upstream of start codon	(intergenic region)
mxan_4328	C → T	-60 bp upstream of start codon	(intergenic region)
mxan_4328	A → C	95 bp downstream of start codon	V32G
mxan_4328	G → A	226 bp downstream of start codon	Q76stop

1.5 Scope of the study

The second messenger c-di-GMP is a widespread regulator of various cellular processes in bacteria. Recently, CdbA was identified as an NAP essential for viability in *M. xanthus* that is involved in chromosome organization and segregation and is modulated by c-di-GMP. A suppressor screen using CdbA-depleted cells identified most suppressor mutations in the gene locus *mxan_4328*. Here, the focus is on the characterization of the gene locus *mxan_4328*, from hereon *cdbS* (CdbA essentiality suppressor) and its connection to chromosome biology.

2 Results

2.1 *cdbS* encodes a stand-alone PilZ domain protein and is conserved in closely related species

cdbS encodes a stand-alone PilZ domain protein of 119 amino acids. The PilZ domain encompasses the residues 7-82 (Figure 8a) and contains the two sequence motifs 9RSHLR13 and 35NISARG40, hence having all residues important for c-di-GMP binding (Figure 8a,b).

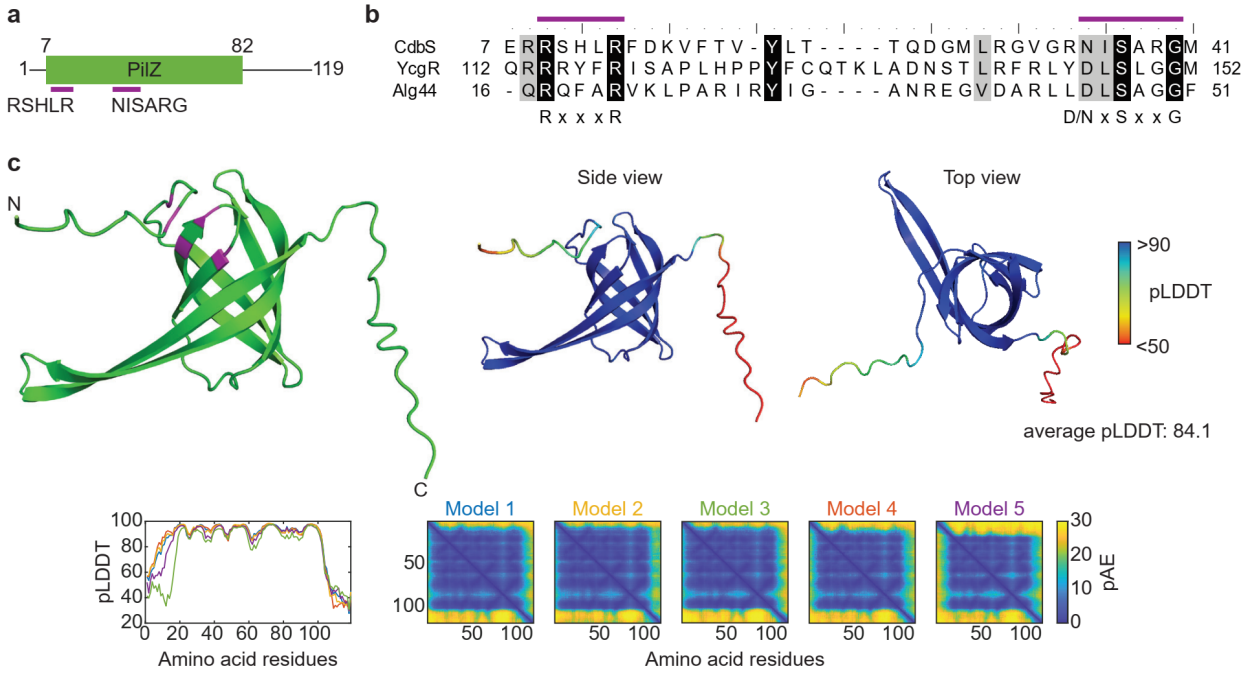

Figure 8: Domain architecture and AlphaFold model of CdbS. (a) CdbS is a stand-alone PilZ domain protein. The domain encompasses the residues 7-82. The residues 9-14 and 34-40 are marked in pink. (b) Alignment of the residues 7-41 of CdbS with the corresponding residues of the well-studied PilZ domain proteins YcgR of *E. coli* and Alg44 of *P. aeruginosa*. The amino acids of the c-di-GMP binding motif are marked in pink. Below the alignment, the consensus sequences of the c-di-GMP binding motifs are included (Ryjenkov *et al.*, 2006). (c) AlphaFold model of CdbS with corresponding pLDDT (predicted local distance difference test) and pAE (predicted alignment error) plots for five models. Model rank 1 is shown with the residues of the c-di-GMP binding motif are marked in pink.

A structural model of CdbS using AlphaFold modeled CdbS as a six-stranded β-barrel, which is typical for the PilZ domain, but the α-helix at the C-terminus characteristic for canonical PilZ domains was not predicted. This classifies CdbS as an xPilZ domain protein (Figure 8c) (Galperin and Chou, 2020). The residues important for c-di-GMP binding are modeled similar to the solved

crystal structures of the xPilZ domain protein PlzA in *Borreliella burgdorferi* (Singh *et al.*, 2021a), forming a pocket that consists of an unstructured region at the N-terminus of the protein and of the loop connecting β2 and β3. Unusually, β5 and β6 of CdbS are predicted to extend beyond the β-barrel, which has not previously been observed for other PilZ domain proteins (Figure 8c).

Based on RNA-seq and cappable-seq analyses (Kuzmich et al., 2022), *cdbS* does not form an operon with its neighbouring genes (Figure 9a). The genetic neighbourhood of *cdbS* encodes two hypothetical proteins, a Thr-tRNA, a glutatamate dehydrogenase, a periplasmic serine protease and a GrpE domain protein. The functions of these proteins do not suggest a direct function in cell division or chromosome biology (Figure 9a).

While *cdbA* is encoded in all fully sequenced Myxococcales (Skotnicka *et al.*, 2020), we found that *cdbS* and its genetic neighbourhood are only conserved in the closely related *Cystobacterineae* and *Nanocystineae*, but not in *Sorangineae* (Figure 9b). Intriguingly, M. xanthus encodes *cdbA* 33 genes downstream of *cdbS*. Similarly, in all Myxococcaceae, Vulgatibacteraceae and in *Stigmatella aurantiaca*, *cdbA* is encoded ~ 30 genes downstream of *cdbS* (Figure 9b). The amino acid sequence of CdbS is highly conserved among homologs in related species (Figure 9b,c), suggesting that the CdbS function is conserved in these species.

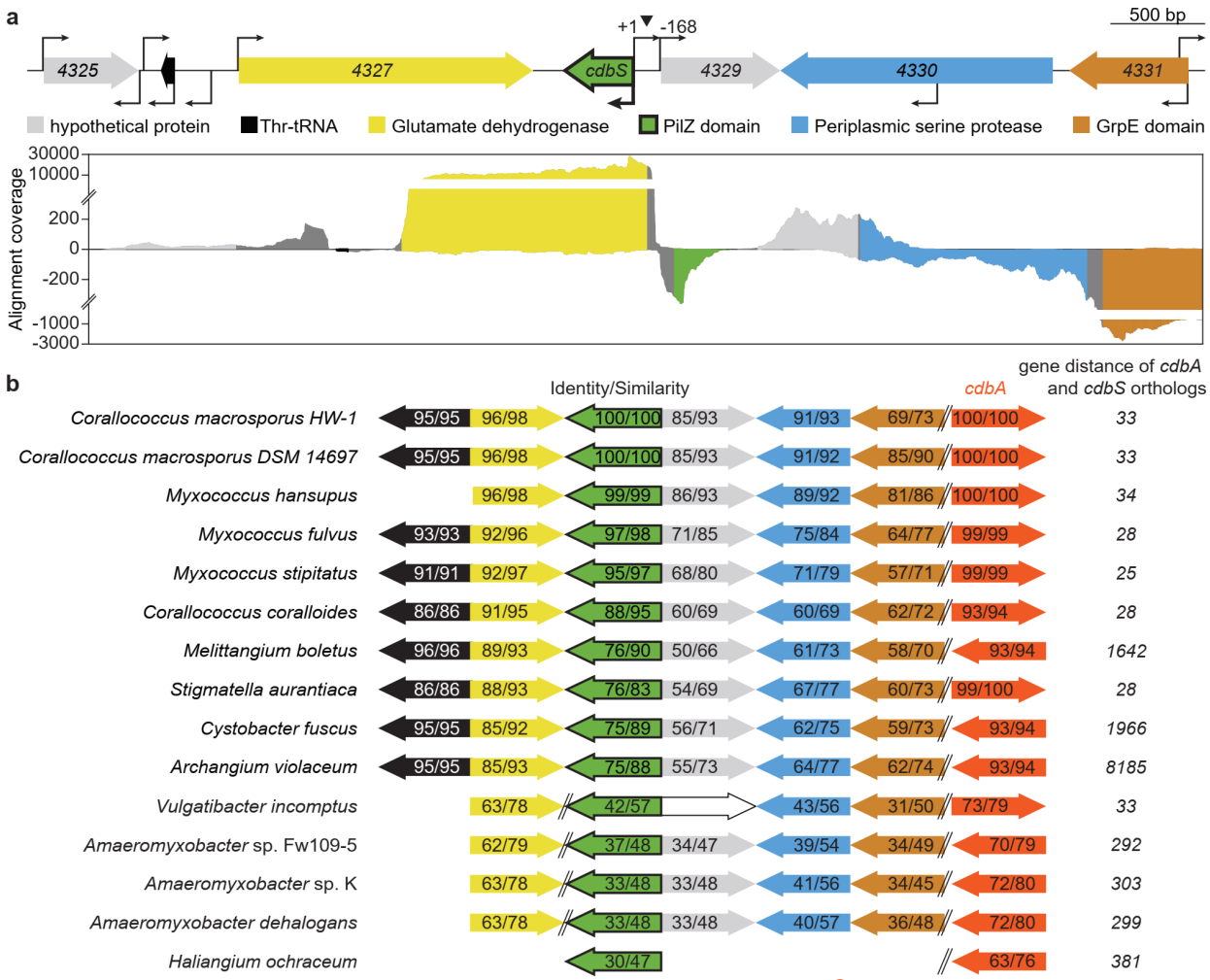
a
500 bp
+1
-168
4325
4327
cdbS
4329
4330
4331
hypothetical protein
Thr-tRNA
Glutamate dehydrogenase
PilZ domain
Periplasmic serine protease
GrpE domain
Alignment coverage
30000
10000
200
0
-200
-1000
-3000
b
Identity/Similarity
cdbA
gene distance of cdbA and cdbS orthologs
Corallococcus macrosporus HW-1
95/95 96/98 100/100 85/93 91/93 69/73 100/100 33
Corallococcus macrosporus DSM 14697
95/95 96/98 100/100 85/93 91/92 85/90 100/100 33
Myxococcus hansupus
96/98 99/99 86/93 89/92 81/86 100/100 34
Myxococcus fulvus
93/93 92/96 97/98 71/85 75/84 64/77 99/99 28
Myxococcus stipitatus
91/91 92/97 95/97 68/80 71/79 57/71 99/99 25
Corallococcus coralloides
86/86 91/95 88/95 60/69 60/69 62/72 93/94 28
Melittangium boletus
96/96 89/93 76/90 50/66 61/73 58/70 93/94 1642
Stigmatella aurantiaca
86/86 88/93 76/83 54/69 67/77 60/73 99/100 28
Cystobacter fuscus
95/95 85/92 75/89 56/71 62/75 59/73 93/94 1966
Archangium violaceum
95/95 85/93 75/88 55/73 64/77 62/74 93/94 8185
Vulgatibacter incomptus
63/78 42/57 43/56 31/50 73/79 33
Amaeromyxobacter sp. Fw109-5
62/79 37/48 34/47 39/54 34/49 70/79 292
Amaeromyxobacter sp. K
63/78 33/48 33/48 41/56 34/45 72/80 303
Amaeromyxobacter dehalogans
63/78 33/48 33/48 40/57 36/48 72/80 299
Haliangium ochraceum
30/47 63/76 381
c
G
CdbS (Mxan_4328)
LILAB_29770
MYMAC_004251
A176_002574
MFUL124B02_26480
MYSTI_04839
COCOR_03571
MEBOL_006151
STAUR_04709
CYFUS_003703
JQX13_45285
AKJ08_1991
Anae109_2048
AnaeK_1071
A2cp1_2163
Hoch_5866
Stop

Figure 9: Conservation of the *cdbS* locus and CdbS protein in Myxococcales**.** (a) Illustration of the genetic neighbourhood of *cdbS* and its expression levels in *M. xanthus*, to scale. Top schematic illustrates the neighbouring genes. +1 indicate the transcription start site of *cdbS*, which overlaps with the first nucleotide of the start codon in *cdbS*. Kinked arrows indicate transcription start sites as detected in Kuzmich *et al.*, 2022. Coordinates indicate bp relative to the transcription start site of *cdbS*. Triangle shows peak summit of CdbA in ChIP-seq analysis from Skotnicka *et al.*, 2020, at -71 bp relative to the transcription start site of *cdbS*. Lower diagram shows RNA-seq data from Kuzmich *et al.*, 2022 in the same colours. Dark grey indicates intergenic regions. (b) Conservation of the genetic neighbourhood of *cdbS* in closely related species. CdbS homologs were identified using reciprocal BLASTP analysis. Arrows indicate the direction of transcription and the numbers in the arrows indicate identity/similarity between CdbS and its homologs calculated using EMBOSS Needle. Double slash indicates more than one gene distance. *Vulgatibacter incomptus* encodes a different hypothetical protein instead of a homolog of *mxan_4329*. (c) Conservation of CdbS and its homologs from related Myxococcales with fully sequenced genomes. Arrows indicate the identified suppressor mutations in the coding region.

2.2 CdbS binds c-di-GMP

Because CdbS contains the conserved c-di-GMP binding motif characteristic for the PilZ domain (Figure 8b), we tested its binding of c-di-GMP. To this end, we first purified a His6-CdbS variant from *E. coli* as well as the His_6-$CdbS^{R9A}$ variant, which contains the Arg9 to Ala substitution that was reported to abolish c-di-GMP binding of the PilZ domain protein YcgR (Ryjenkov *et al.*, 2006). We obtained pure samples of both protein variants (Figure 10a). The purified proteins were used in a biolayer interferometry (BLI) assay, in which 500 nM biotinylated c-di-GMP was immobilized on a streptavidin-coated sensor chip. As expected from the bioinformatics analysis, His_6-CdbS bound c-di-GMP and displayed a stable interaction with a K_D of 1.37 µM (Figure 10b,c), while we did not detect binding by His_6-$CdbS^{R9A}$ to c-di-GMP (Figure 10c). As the K_D for this interaction approximates the estimated c-di-GMP concentration of ~ 1.4 µM in *M. xanthus* (Skotnicka *et al.*, 2020), this suggests that c-di-GMP binding by CdbS could be important *in vivo*.

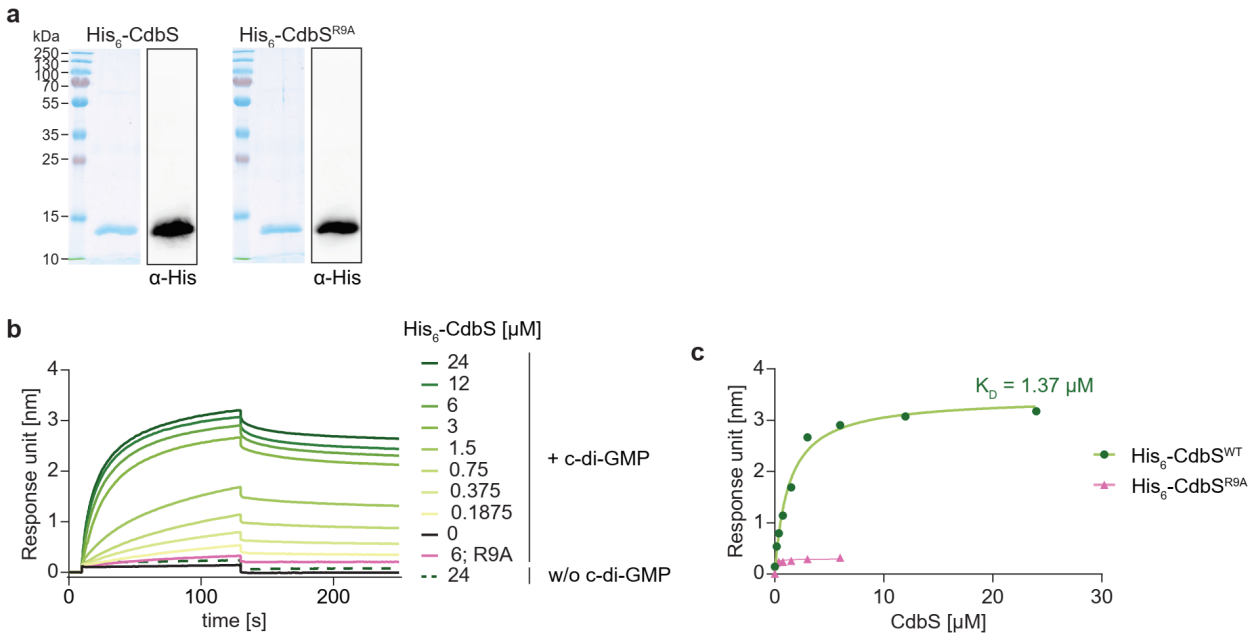

Figure 10: CdbS binds c-di-GMP. (a) InstantBlue-stained SDS-PAGE gel and corresponding immunoblot of purified His_6-CdbS and His_6-$CdbS^{R9A}$. (b) BLI sensogram of His_6-CdbS (shades of green) or His_6-$CdbS^{R9A}$ (pink, 6 µM) and biotinylated c-di-GMP immobilized on a streptavidin coated sensor chip. Unspecific binding of the protein to the sensor was tested in the absence of c-di-GMP and is shown as a dashed line. (c) Saturation curves of His_6-CdbS (green) and His_6-$CdbS^{R9A}$ (pink). The calculated K_D of His_6-CdbS for c-di-GMP is shown.

2.3 The essentiality of CdbA depends on the presence of CdbS

As two of the *cdbS* mutations obtained in the suppressor screen were in the predicted promoter region of *cdbS* and one results a premature stop codon, we hypothesized that the suppressor mutations cause the loss-of-function of CdbS. To test whether the loss-of-function of CdbS suppresses the CdbA-depletion phenotype, we generated an in-frame deletion in *cdbS* (Δ*cdbS*) in a Δ*cdbA* strain in which *cdbA-mCh* is expressed from the vanillate-inducible promoter in a single copy from the *mxan_18/19* locus. To follow chromosome organization and segregation, we analyzed strains that ectopically synthesized ParB-YFP from the native promoter from a plasmid integrated in a single copy at the MxB *attB* site (the genotype is *parB*$^+$/*attB::Pnat parB-eyfp*, from here on *parB-YFP*). Subsequently, we tested these strains for growth, viability as well as chromosome organization and segregation in the presence and absence of 500 µM vanillate.

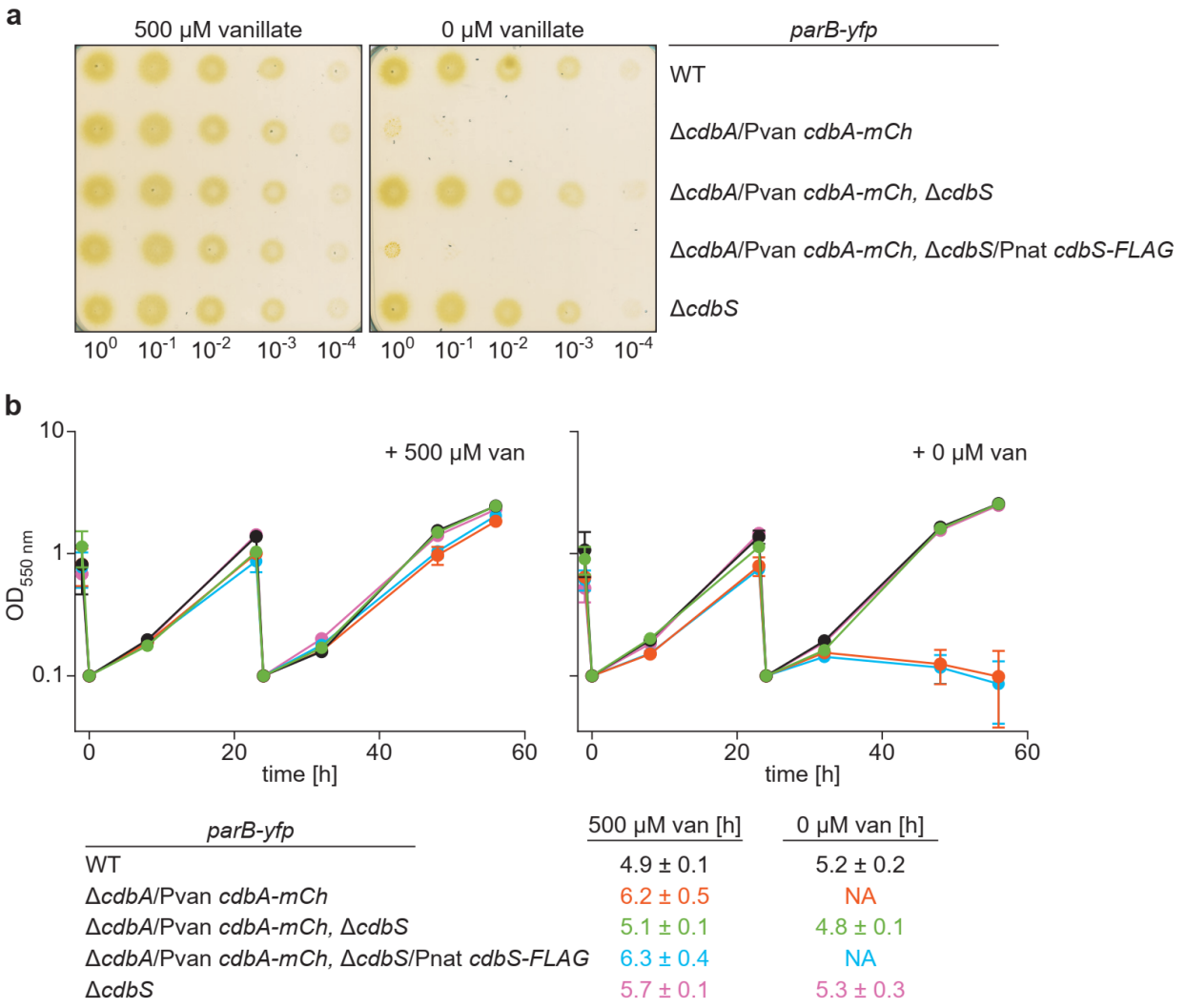

parB-yfp	500 µM van [h]	0 µM van [h]
WT	4.9 ± 0.1	5.2 ± 0.2
Δ*cdbA*/Pvan *cdbA-mCh*	6.2 ± 0.5	NA
Δ*cdbA*/Pvan *cdbA-mCh,* Δ*cdbS*	5.1 ± 0.1	4.8 ± 0.1
Δ*cdbA*/Pvan *cdbA-mCh,* Δ*cdbS*/Pnat *cdbS-FLAG*	6.3 ± 0.4	NA
Δ*cdbS*	5.7 ± 0.1	5.3 ± 0.3

Figure 11: Lack of CdbS suppresses the essentiality of CdbA**.** (a) Both plates contain 1.5% agar supplemented with 1% CTT growth medium, the plate shown on the left additionally contains 500 µM vanillate. Cells of the respective strains were concentrated as indicated. After spotting, the plates were incubated for 96 h. (b) Growth curves of indicated strains in suspension supplemented with 500 µM or 0 µM vanillate. In the right diagram, vanillate was removed at t = 0 h. Table indicates generation times. Mean ± standard deviation (STDEV) are shown from three biological replicates. NA = not applicable.

In agreement with previous reports (Skotnicka *et al.*, 2020), 500 µM vanillate had no effect on growth and viability of WT. Similarly, the CdbA-mCh depletion strain only grew when supplemented with vanillate, and at a slower rate than WT, while growth ceased after 24 h in the absence of vanillate (Figure 11a,b) (Skotnicka *et al.*, 2020). Importantly, the Δ*cdbS* mutation in the CdbA-mCh depletion strain rendered the cells viable in the absence of vanillate and with a growth rate similar to that of WT (Figure 11a,b), indicating that lack of CdbS suppresses the

essentiality of CdbA. Next, we ectopically expressed a *cdbS-FLAG* allele as well as *parB-YFP* under the control of the respective putative native promoters from a plasmid integrated in a single copy at the Mx8 *attB* site in the Δ*cdbS* CdbA-mCh depletion strain. Upon removal of vanillate, this strain phenocopied the *cdbS*$^{+}$ CdbA-mCh depletion strain. The Δ*cdbS* mutation in otherwise WT cells did not affect growth or viability (Figure 11a,b). We conclude that the essentiality of CdbA depends on the presence of CdbS, while lack of CdbS by itself does not affect viability or growth.

CdbA-depletion causes disrupted chromosome organization and segregation resulting in the formation of cellular filaments, and ultimately cell lysis (Skotnicka *et al.*, 2020). Because cells lacking both CdbA and CdbS are viable, we investigated this mutant strain for cell length and chromosome biology (Figure 12). As previously reported (Skotnicka *et al.*, 2020), the CdbA-mCh depletion strain supplemented with 500 µM vanillate had a slightly increased cell length compared to WT, while depleting the cells of CdbA-mCh for 24 h resulted in cellular filamentation (Figure 12a) In contrast, ∆*cdbS* cells depleted of CdbA-mCh had a cell length similar to that of WT. Upon ectopic expression of *cdbS-FLAG* from its native promoter in this strain, cells again became filamentous in the absence of vanillate. Finally, the ∆*cdbS* mutation in otherwise WT cells did not affect cell length (Figure 12a).

To investigate chromosome organization in these strains, we stained the cells with 4′,6-diamidino-2-phenylindole (DAPI), which is a fluorescent dye that binds to adenine-thymine rich DNA sequences (Kapuscinski, 1995). To follow chromosome segregation, we used the localization of ParB-YFP as a readout for the number and localization of the *ori* (Harms *et al.*, 2013). In agreement with published results (Harms *et al.*, 2013), short WT cells had one DAPI signal reflecting one nucleoid centered around midcell, while longer cells had two separated DAPI signals centered around the quarter cell lengths positions, and with ParB-YFP localizing to the outer edges of the segregated nucleoids (Figure 12b). The same pattern was observed for the CdbA-mCh depletion strain in the presence of vanillate; however, cells depleted of CdbA-mCh had an irregular distribution of the nucleoids along the cell length, and ParB-YFP localizing accordingly (Figure 12b) (Skotnicka *et al.*, 2020). Importantly, cells lacking both CdbA-mCh and CdbS showed WT-like chromosome organization and segregation. Moreover, ectopic expression of *cdbS-FLAG* from its putative native promoter in these cells resulted in irregular distribution of the nucleoids along the cell length, and ParB-YFP localizing accordingly. Cells lacking only CdbS

did not have a defect in chromosome organization and segregation, as expected from the lack of a growth defect (Figure 12b, Figure 11a). Taken together, these results show that CdbA is only essential in the presence of CdbS, and provide evidence that CdbS is a key player during CdbA-depletion that causes disruption of chromosome organization and segregation.

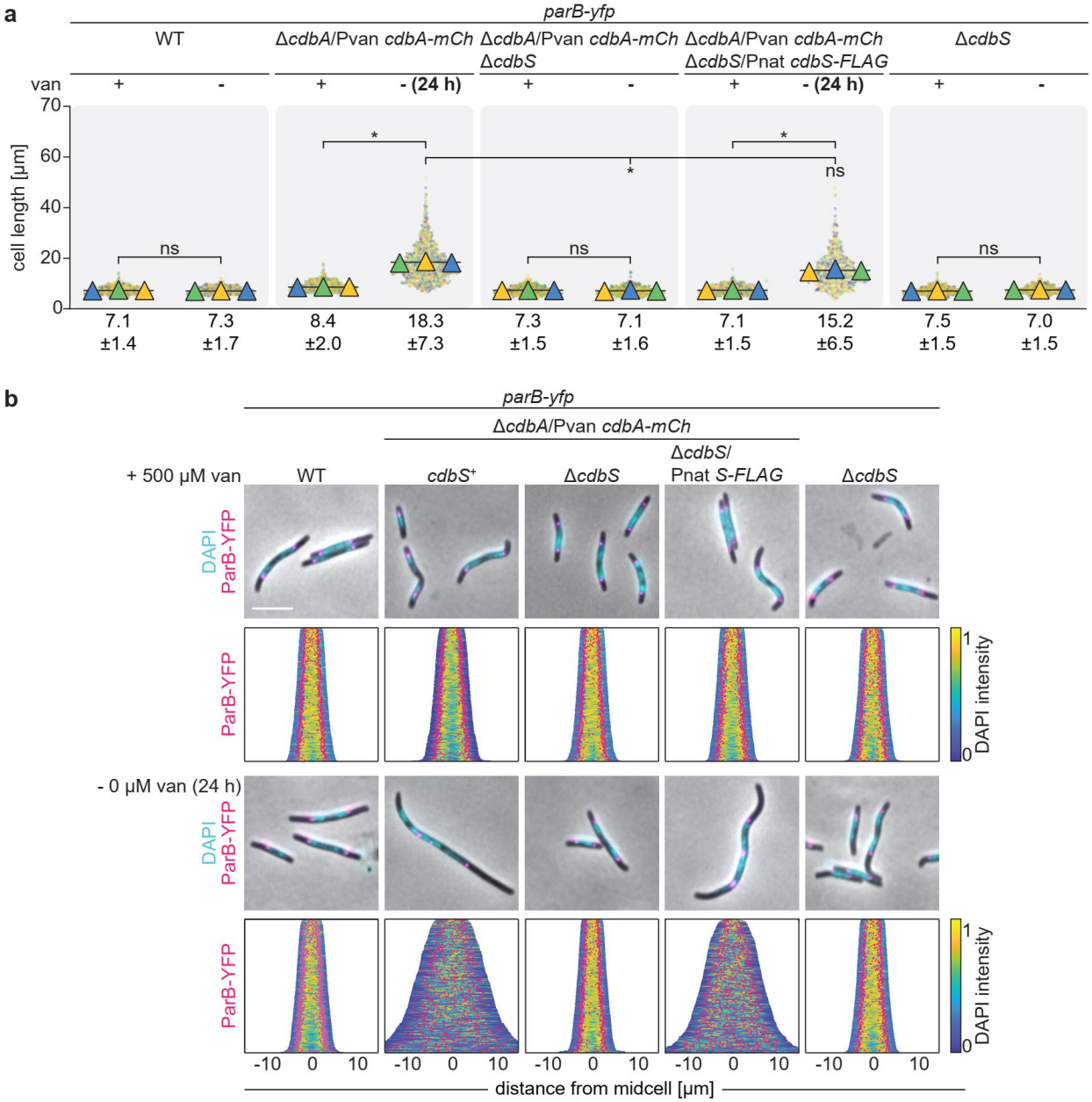

Figure 12: Lack of CdbS suppresses the CdbA-depletion phenotype. (a) Cell length analyses of indicated strains supplemented with or without 500 µM vanillate for 24 h. Measurements of three independent experiments are shown in different coloured dots with the respective means as triangles. Numbers above indicate mean ± STDEV in µm. * , $p < 0.0001$, ns, not significant in 2way ANOVA multiple comparisons test. (b) Fluorescence microscopy of cells stained

with DAPI and synthesizing ParB-YFP. In the demographs, cells are sorted by cell length, DAPI signals are shown according to the intensity scale, and ParB-YFP signals in pink. Scale bar, 5 µm. N = 400 cells for all strains.

2.4 CdbA-depletion causes increased CdbS accumulation

Next, we sought to understand the connection between CdbA and CdbS. Because CdbA is a DNA-binding protein, we asked whether it binds in the promotor region of *cdbS* using published ChIP-seq data (Skotnicka *et al.*, 2020). CdbA binds in the putative promoter region of *cdbS* with a ChIP-seq peak centered at position -71 bp relative to the transcriptional start site of *cdbS* at +1 bp (Figure 13a).

To test whether CdbA regulates the expression of *cdbS*, we determined its transcription in the CdbA-depletion strain in the presence and absence of vanillate. We observed that in the presence of CdbA-mCh, i.e. when the cells were supplemented with vanillate, *cdbS* was expressed at a level similar to *cdbS* in WT, which expressed native *cdbA* (*cdbA*$^{+}$). In cells depleted of CdbA-mCh, *cdbS* was also expressed as in WT (Figure 13b).

Next, we investigated the accumulation of CdbS-FLAG during CdbA-mCh depletion by immunoblot analysis. In the presence of CdbA-mCh, the CdbA-mCh depletion strain accumulated CdbS-FLAG at a level similar to that of WT expressing *cdbS-FLAG* from the native site. However, upon depletion of CdbA-mCh, the CdbS-FLAG level increased ~4-fold (Figure 13c).

Because lack of CdbA does not cause increased *cdbS* transcription, these observations suggest that the elevated CdbS level is either the result of increased *cdbS* translation or increased CdbS stability.

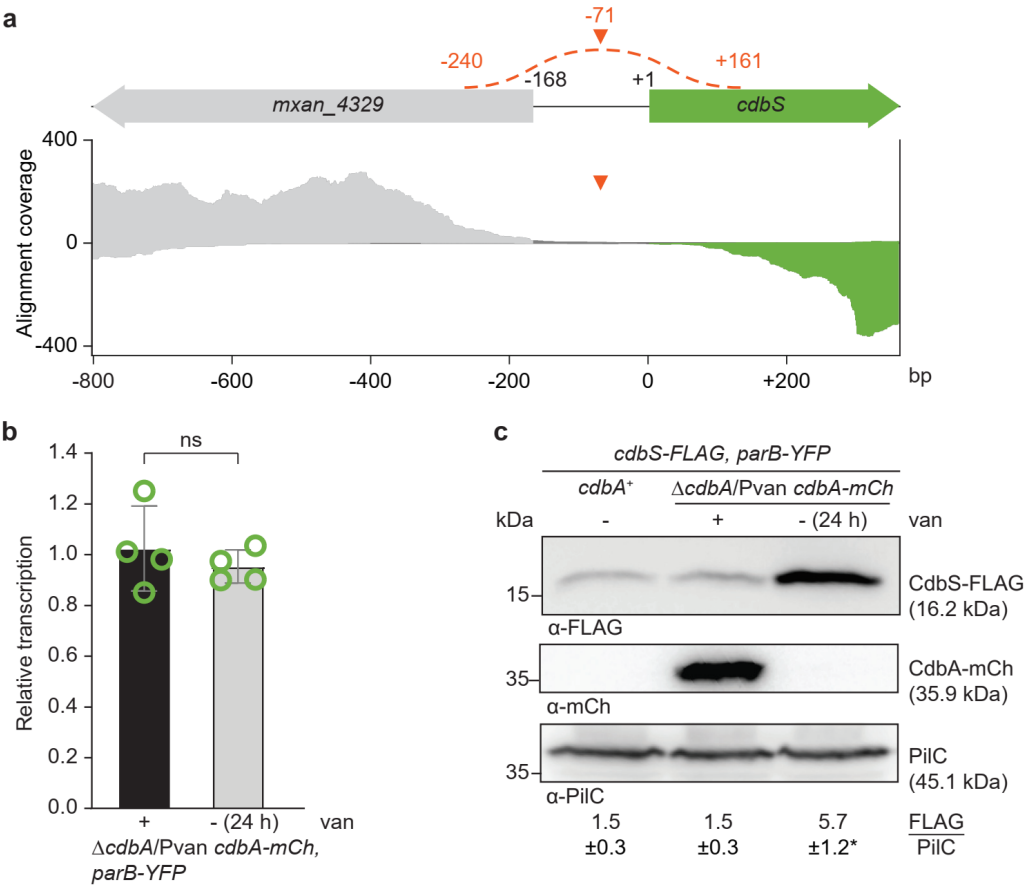

Figure 13: Lack of CdbA stabilizes CdbS. (a) Visualization of the CdbA binding site in ChIP-seq analysis relative to the transcription start site of *cdbS*. Upper schematic illustrates *cdbS* and its neighbouring gene to scale. Dotted red line indicates the CdbA peak in ChIP-seq anaylsis from Skotnicka *et al.*, 2020, with the peak coordinates in red, and its summit as a red triangle at -71 bp. Coordinates indicate bp relative to transcriptional start site of *cdbS* at +1 bp. Lower graph shows RNA-seq data from Kuzmich *et al.*, 2022 in the same colours as the genes. Dark grey indicates intergenic region. (b) RT-qPCR analysis of *cdbS* transcript levels in the CdbA-mCh depletion strain supplemented with vanillate or grown without 500 µM vanillate for 24 h normalized to the *cdbS* transcript level in WT. Transcript levels are shown as mean ± STDEV from four biological replicates with three technical replicates each. Individual data points are shown in green. ns, no significant difference in two-sided Student's t-test. (c) Immunoblot analysis of CdbS-FLAG accumulation in the CdbA-mCh depletion strain compared to otherwise WT expressing *cdbS-FLAG* from the native site. Cells were grown in the presence or absence of 500 µM vanillate for 24 h before sample preparation. Cell lysate from the same number of cells was loaded per lane. PilC was used as a loading control. Numbers below show the mean level of CdbS-FLAG normalized by the PilC level ± STDEV in the indicated strains calculated from three independent experiments. *, $p < 0.05$ in Student's t test in which samples were compared to WT.

2.5 A strain with an elevated CdbS level phenocopies a CdbA-depletion mutant

In order to study the cellular response to the increased CdbS-FLAG level, we generated a Δ*cdbS* strain that ectopically expresses *cdbS-FLAG* under the control of the vanillate inducible promoter. In the absence of vanillate, CdbS-FLAG was not detectable in this conditional overexpression strain in immunoblots with α-FLAG antibodies. In the presence of 500 µM vanillate for 24 h, CdbS-FLAG accumulated at a ~4-fold higher level relative to the strain expressing *cdbS-FLAG* from the native site (Figure 14a).

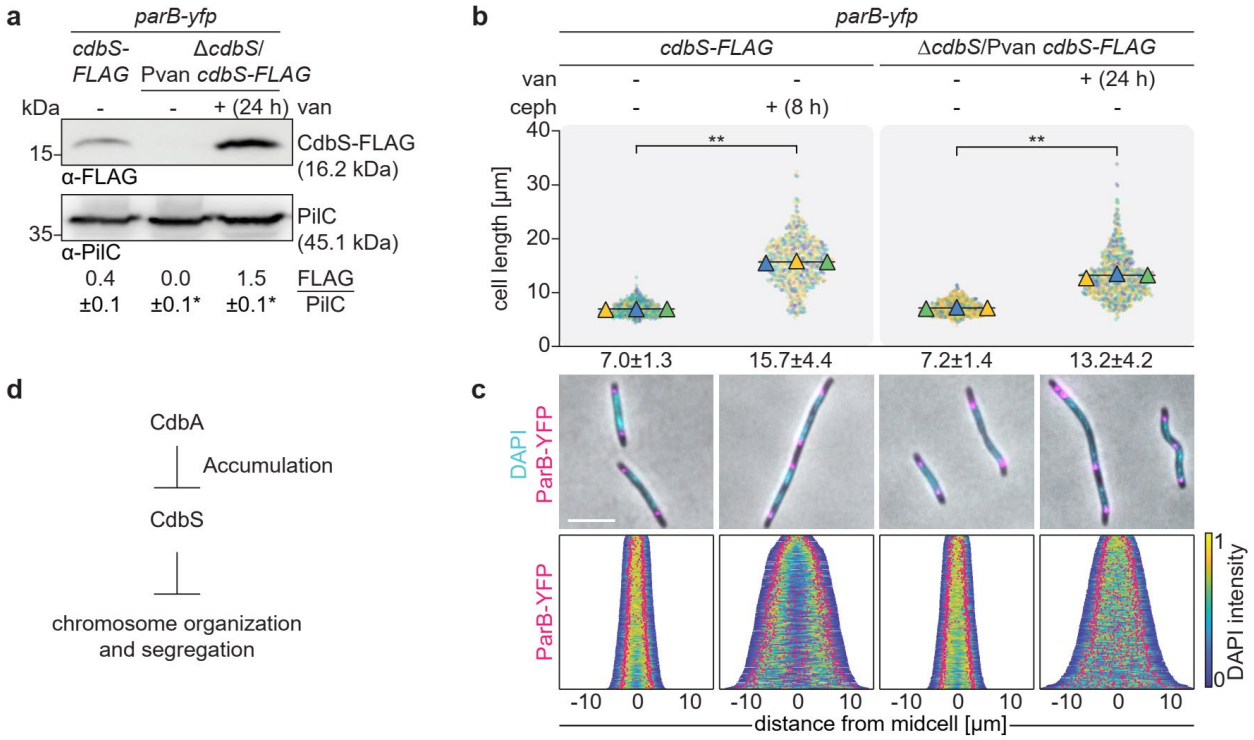

Figure 14: Increased accumulation of CdbS-FLAG phenocopies a strain depleted of CdbA-mCh. (a) Immunoblot analysis of CdbS-FLAG accumulation. Overexpression was induced with 500 µM vanillate for 24 h before sample preparation. The *cdbS-FLAG* strain expresses this allele from the native site. Cell lysate from the same number of cells was loaded per lane. PilC was used as a loading control. Numbers below show the mean level of CdbS-FLAG normalized by the PilC level ± STDEV in the indicated strains calculated from three independent experiments. *, $p < 0.05$ in Student's t test in which samples were compared to WT. (b) Cell length analyses of indicated strains without vanillate or supplemented with 500 µM vanillate for 24 h or with cephalexin (ceph) for 8 h. Measurements of three biological replicates are shown in different coloured dots with the respective means as triangles. Numbers above

indicate mean ± STDEV in µm. ** $p < 0.0001$, ns not significant in 2way ANOVA multiple comparisons test. (c) Fluorescence microscopy of cells stained with DAPI and synthesizing ParB-YFP. In the demographs, cells are sorted by cell length, DAPI signals are shown according to the intensity scale, and ParB-YFP signals in pink. Scale bar, 5 µm. N = 400 cells for all strains. d) Genetic pathway visualizing the working model of CdbA and CdbS. CdbA blocks the increased accumulation of CdbS, while CdbS itself disrupts chromosome organization and segregation.

The conditional *cdbS-FLAG* overexpression strain had an average cell length similar to WT in the absence of vanillate, and the nucleoid as well as ParB-YFP were organized as in cells expressing *cdbS-FLAG* from the native site (Figure 14b,c). Importantly, when supplemented with 500 µM vanillate for 24 h (and, thus, overaccumulating CdbS-FLAG), these cells became filamentous with an average cell length of 13.2 µm. The nucleoid as well as ParB-YFP localization were highly disorganized, essentially phenocopying cells depleted of CdbA-mCh (Figure 14b,c). As a control, we treated WT cells with cephalexin for 8 h to specifically inhibit cell division but not chromosome organization and segregation (Treuner-Lange *et al.*, 2013). These cells elongated to an average cell length of 15.7 µm (Figure 14b). However, these cells had two to four well-separated DAPI signals and an increased number of ParB-YFP foci arranged evenly along the cell length (Figure 14d), as previously described (Skotnicka *et al.*, 2020). These observations suggest that the primary defect in CdbS-FLAG overaccumulating cells is in chromosome organization and segregation, and not in cell division.

We conclude that an elevated CdbS level causes the disruption of chromosome organization as well as segregation, thereby causing *M. xanthus* cells to elongate. Because this phenotype mimics the phenotype caused by CdbA-depletion, these observations suggest a genetic pathway in which CdbA inhibits accumulation of CdbS (Figure 14d). Upon CdbA depletion, this inhibition is relieved and CdbS accumulates at an increased level. This increased level of CdbS, in turn, interferes with chromosome organization and segregation, thereby inhibiting cell division.

2.6 CdbS does not affect the accumulation and localization of CdbA

To investigate whether CdbS affects CdbA, we tested if the CdbA-mCh level or localization is altered in response to different CdbS levels. Therefore, we generated a strain that expresses *cdbA-mCh* from the native site (genotype *cdbA::cdbA-mCh*, from here on *cdbA-mCh*). Next, we introduced the Δ*cdbS* mutation or ectopically overexpressed *cdbS-FLAG* for 24 h from the vanillate promoter in the *cdbA-mCh* strain. By immunoblot analysis, neither lack nor the overexpression of CdbS-FLAG affected the accumulation of CdbA-mCh (Figure 15a). Because CdbA-mCh co-localizes with the nucleoid (Skotnicka *et al.*, 2020), we investigated its localization in response to altered CdbS levels. CdbA-mCh co-localized with the nucleoid, and this localization was not visibly altered in cells lacking or overaccumulating CdbS-FLAG (Figure 15b). Thus, while depletion of CdbA leads to an increased CdbS level, CdbS does not affect the CdbA level and likely also not the localization of CdbA. These observations are in agreement with the genetic pathway (Figure 14d) in which CdbA inhibits accumulation of CdbS; upon CdbA depletion, this inhibition is relieved and CdbS accumulates at an increased level. This increased level of CdbS, in turn, interferes with chromosome organization and segregation, thereby inhibiting cell division.

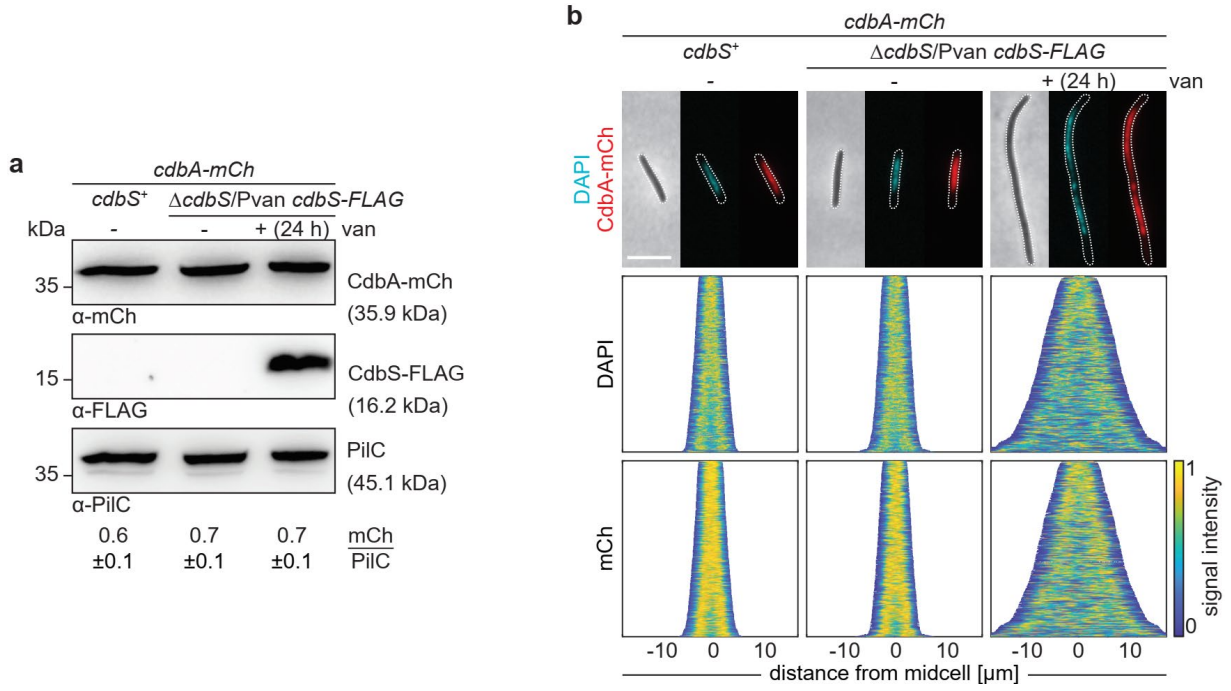

Figure 15: CdbS does not affect CdbA accumulation or localization. (a) Immunoblot analysis of *cdbA-mCh* expressing strains with varying CdbS levels. Overexpression of *cdbS-FLAG* was induced with 500 μM vanillate for 24 h. Cell lysate

from the same number of cells was loaded per lane. PilC was used as a loading control. Numbers below show the mean level of CdbA-mCh normalized by the PilC level ± STDEV in the indicated strains calculated from three independent experiments. No statistical differences in Student's t test were observed in which samples were compared to WT. (b) Fluorescence microscopy of cells stained with DAPI and expressing CdbA-mCh. In the demographs, cells are sorted by cell length, DAPI and mCh signals are shown according to the intensity scale. Scale bar, 5 µm. N = 400 cells for all strains.

2.7 CdbS activity is independent of c-di-GMP binding

As His_6-CdbS binds c-di-GMP with a K_D approximating the estimated c-di-GMP concentration of ~1.4 µM in *M. xanthus* (Skotnicka *et al.*, 2020), this suggests that c-di-GMP binding by CdbS could be important *in vivo*. To investigate the role of c-di-GMP binding by CdbS, we overexpressed the *cdbS*^{R9A}*-FLAG* variant from the vanillate-inducible promoter on a plasmid integrated in a single copy at the Mx8 *attB* site in a Δ*cdbS* strain. When supplemented with 500 µM vanillate for 24 h, CdbS^{R9A}-FLAG, similarly to ectopically synthesized cdbS^{WT}-FLAG, accumulated at a ~4-fold increased level compared to the native CdbS-FLAG level (Figure 16a).

Moreover, cells overaccumulating the CdbS^{R9A}-FLAG variant for 24 h phenocopied cells overexpressing CdbS^{WT}-FLAG, with the formation of elongated cells with irregularly organized nucleoids and ParB-YFP foci (Figure 16b, c). Therefore, we conclude that under these conditions, the effect of CdbS overaccumulation is independent of c-di-GMP binding.

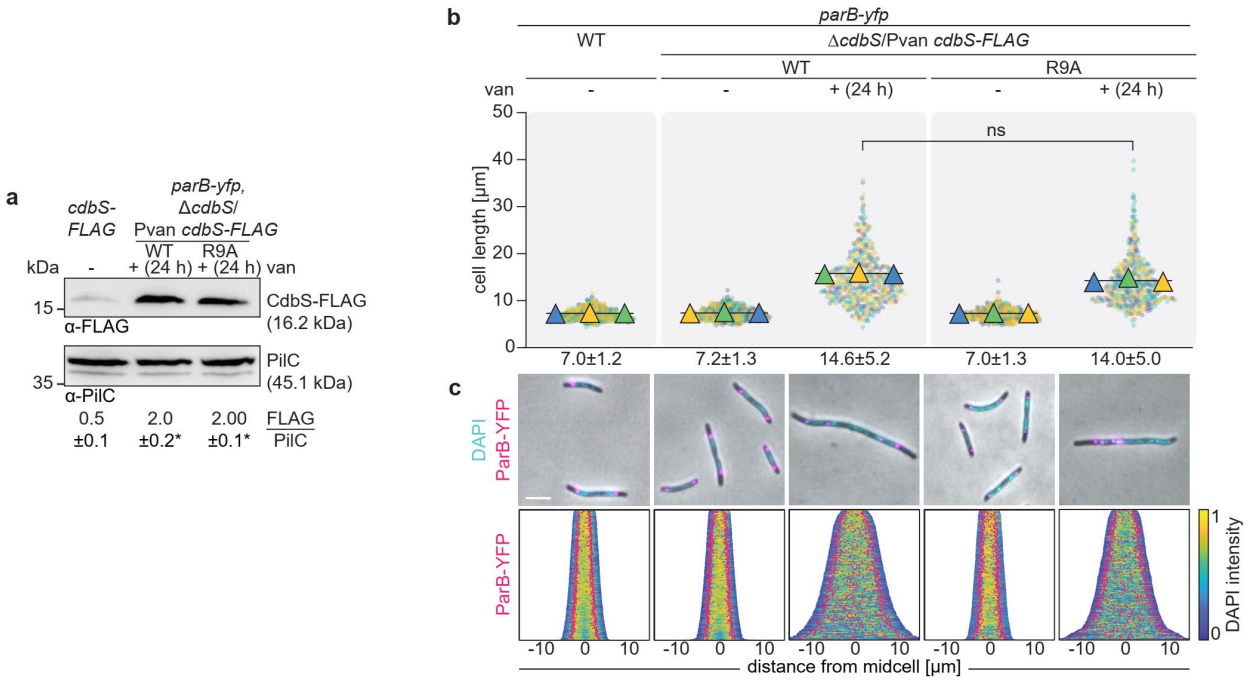

Figure 16: The *cdbS* overexpression phenotype is independent of c-di-GMP binding. (a) Immunoblot analysis of strains with the indicated genotypes. Overexpression was induced with 500 µM vanillate for 24 h before sample preparation. PilC was used as a loading control. Numbers below show the mean level of CdbS-FLAG normalized by the PilC level ± STDEV in the indicated strains calculated from three independent experiments. *, $p < 0.05$ in Student's t test in which samples were compared to WT. (b) Cell length analyses of indicated strains supplemented with 500 µM vanillate for 24 h or without. Measurements of three independent experiments are shown in different coloured dots with the respective means as triangles. Numbers above indicate mean ± STDEV in µm. The two *cdbS-FLAG* overexpression strains were not significantly different in 2way ANOVA multiple comparisons test. (c) Fluorescence microscopy of cells stained with DAPI and synthesizing ParB-YFP. In the demographs, cells are sorted by cell length, DAPI signals are shown according to the intensity scale, and ParB-YFP signals in pink. Scale bar, 5 µm. N = 400 cells for all strains.

2.8 Identification of interaction candidates of CdbS and their bioinformatical analyses

To understand how overaccumulation of CdbS may result in disruption of chromosome organization and segregation, we considered that PilZ domain proteins are typically involved in protein-protein interactions (Galperin and Chou, 2020, Hengge, 2009). To identify CdbS interaction partner candidates, we performed an *in vivo* pull-down followed by liquid chromatography-mass spectrometry (LC-MS) using a strain in which CdbS-FLAG is synthesized

from the native site as a bait. As a negative control, we used a strain synthesizing GFP-FLAG under the regulation of the constitutively active *pilA* promoter integrated at the Mx8 *attB* site. In this experiment, we detected a total of 982 proteins. Using a $\log_2$ fold difference ≥ 3 between the bait sample and the negative control and a *p*-value ≥ 0.005 as thresholds, we identified 12 significantly enriched proteins in the CdbS-FLAG sample (Figure 17, Table 2).

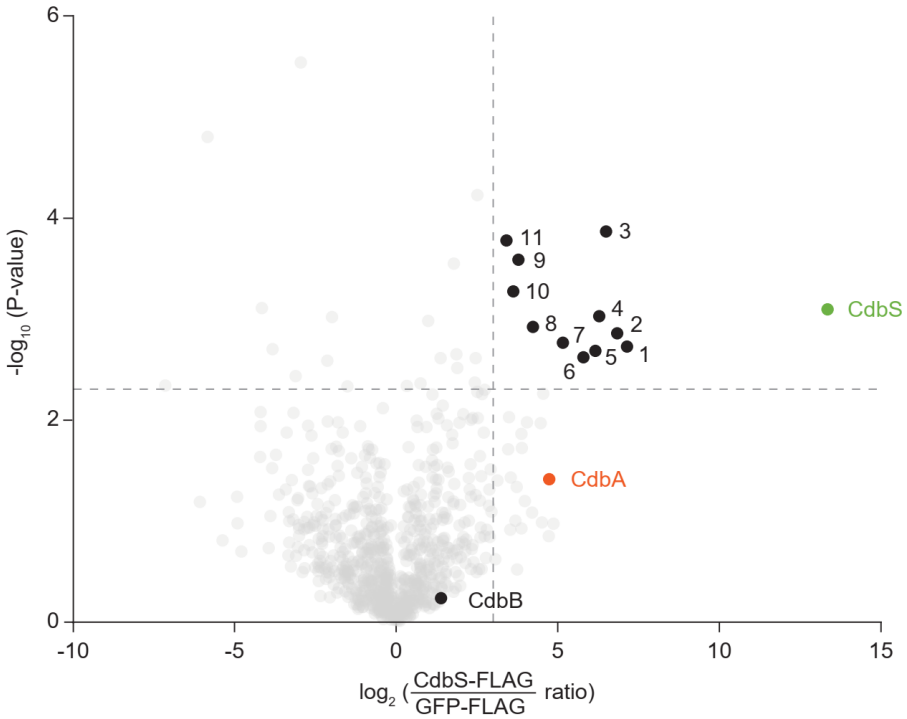

Figure 17: Volcano plot visualizing potential interaction candidates of CdbS. *In vivo* pull-down using CdbS-FLAG as bait compared to GFP-FLAG. Samples from four biological replicates were analyzed by LC-MS. Cut-offs were fold enrichment ≥ 3 fold and *P*-value ≥ 0.005, indicated by dotted lines. Enriched interaction candidates were numbered and explained in more detailed in Table 2.

Table 2: List of identified interaction partners of CdbS in *in vivo* pull-down experiments*

Nr	Gene locus	Protein description	Name
1	*mxan_6605,*	DnaK family	CsdK2
2	*mxan_3802*	hypothetical protein	
3	*mxan_6672*	GrpE family	GrpS (Weimer *et al.*, 1998)
4	*mxan_2152*	dehydrogenase family	
5	*mxan_2277*	putative lipoprotein	
6	*mxan_3057*	haloacid dehalogenase-like family	
7	*mxan_3879*	hybrid histidine kinase	

8	*mxan_5084*	DNA helicase	DnaB (Rosario and Singer, 2007)
9	*mxan_3778;*	DnaK family	CsdK1
10	*mxan_0750*	DnaJ family	DnaJ1
11	*mxan_1092*	Hsp20 family	

* Proteins are numbered as in Figure 17 and listed according to their log2-fold enrichment.

As expected, the most highly enriched protein in the bait sample compared to the negative control was CdbS (Figure 17). Among the 11 enriched proteins, we identified five proteins involved in protein folding and heat shock response. In addition, we detected the DnaB helicase that acts during DNA replication to unwind double stranded DNA (LeBowitz and McMacken, 1986, Rosario and Singer, 2007). The remaining five proteins included two hypothetical proteins, a dehydrogenase, a dehalogenase and a hybrid histidine protein kinase. These five proteins have not been analyzed previously.

Of note, we did not significantly enrich CdbA in the CdbS-FLAG pull-down. Consistently, in a CdbA-FLAG pull-down experiment, we did not enrich CdbS but only CdbB and the lipoprotein Mxan_5771 (Figure 18). This observation is agreement with data from a bacterial two-hybrid experiments demonstrating that that CdbA and CdbB can interact (Skotnicka *et al.*, 2020). Altogether, this supports that the effect of CdbA-depletion on CdbS accumulation does not depend on direct interactions between CdbA and CdbS.

Because our data suggest that the elevated CdbS accumulation in CdbA-depleted cells is based on either increased translation or increased stability, and CdbA-depletion leads to disrupted chromosome biology, we focused on the five proteins associated with protein folding and heat shock response as well as DnaB.

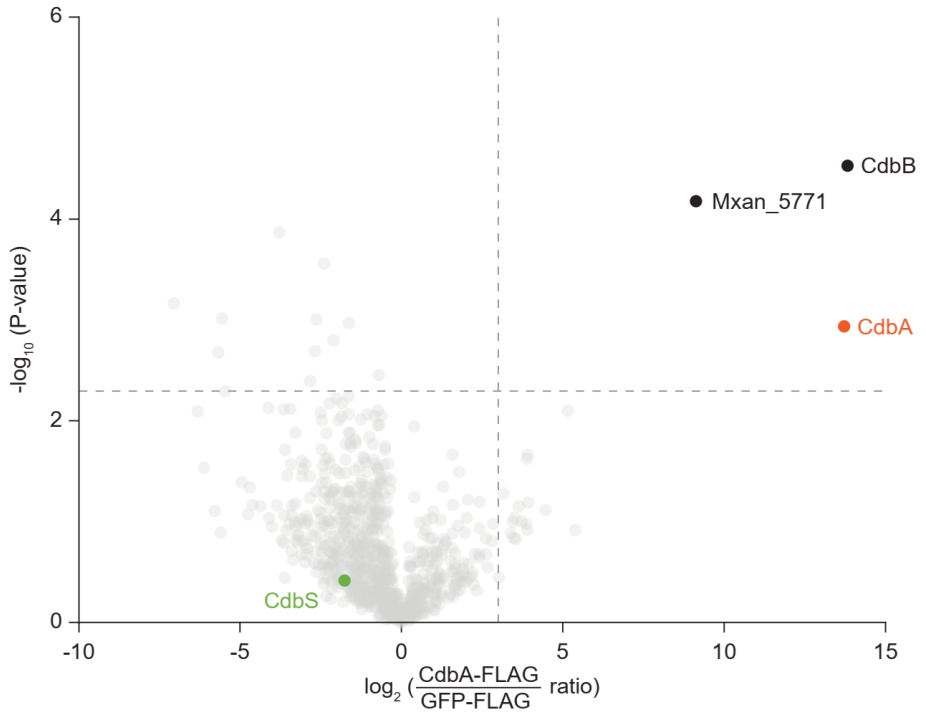

Figure 18: Volcano plot visualizing interaction candidates of CdbA. *In vivo* pull-down using CdbA-FLAG as bait compared to GFP-FLAG. Samples from four biological replicates were analyzed by LC-MS. Cut-offs are fold enrichment ≥ 3 fold and *p*-value ≥ 0.005, indicated by dotted lines.

We identified Mxan_3778 and Mxan_6605, which we renamed to CsdK1 and CsdK2 (CdbS stabilizing DnaK 1 and 2, respectively), both contain a PilZ domain and a DnaK/Hsp70 domain (Figure 19a) and are two of the 15 proteins in *M. xanthus* with a DnaK/Hsp70 domain. CsdK1 contains 772 amino acids and its N-terminal PilZ domain only has the second half of the bipartite c-di-GMP binding motif (Figure 19a, b), suggesting that this protein does not bind c-di-GMP. This domain is followed by the DnaK/Hsp70, which has 36/57% identity/similarity to DnaK from *E. coli*. This domain contains the important residues for chaperone activity as well as for interacting with its partner DnaJ and GrpE co-chaperones (Zuiderweg *et al.*, 2013), suggesting that CsdK1 likely has ATPase activity and might function as a DnaK-like chaperone (Figure 19c).

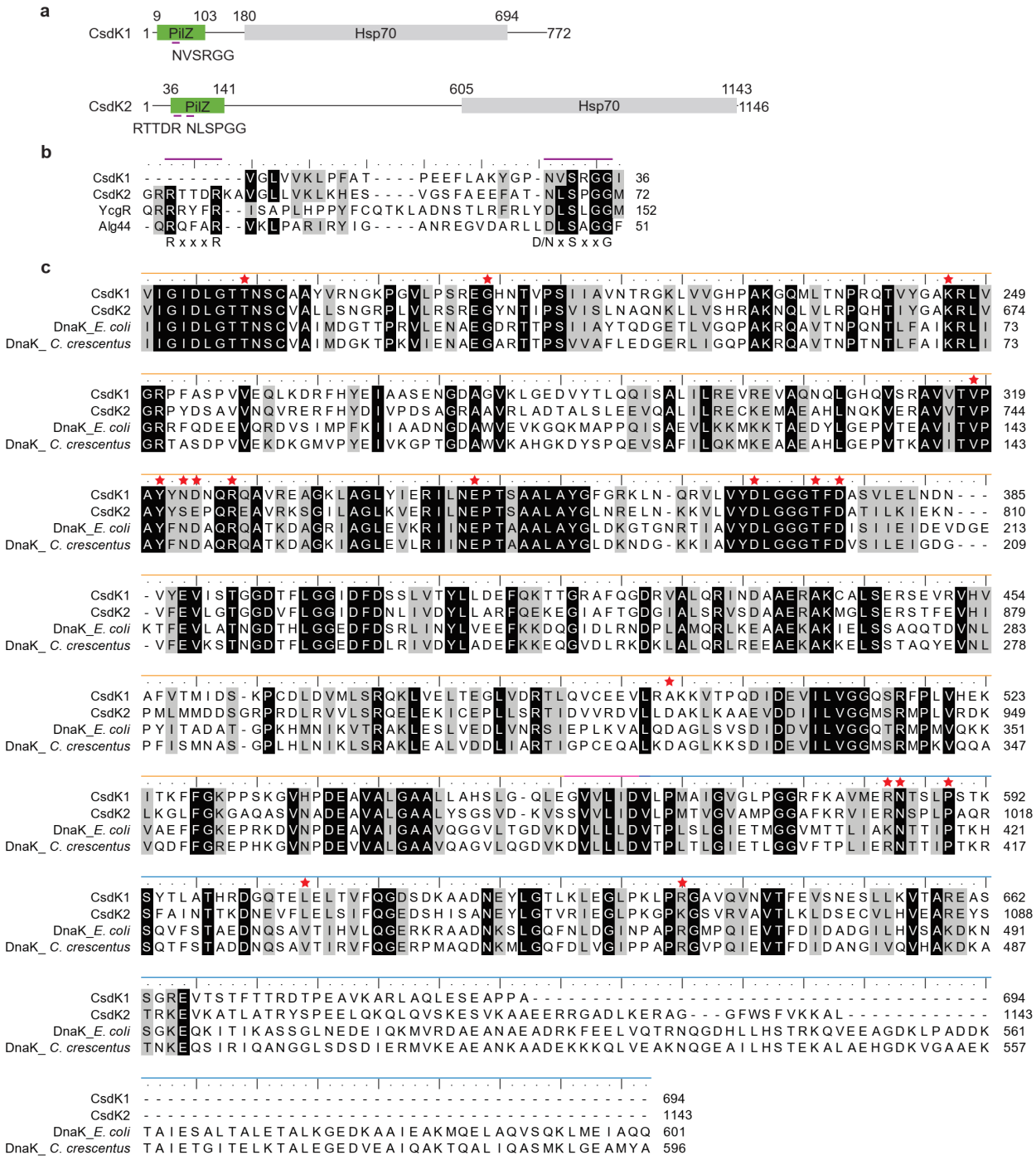

Figure 19: Sequence analysis of CsdK1 and CsdK2. (a) Domain architecture of CsdK1 and CsdK2. The PilZ and DnaK/Hsp70 ATPase domains are shown in green and grey, respectively. c-di-GMP binding motifs are marked in pink with the respective residues below. (b) Alignment of the residues 9-36 of CsdK1 and 36-72 of CsdK2 with the corresponding residues of YcgR from *E. coli* and Alg44 from *P. aeruginosa*. The amino acids of the c-di-GMP binding motif are marked in pink and the consensus sequence is shown below. (c) Alignment of the DnaK/Hsp70 domains with those of DnaK proteins from *E. coli* and *C. crescentus*. The nucleotide-binding subdomain (orange), the linker (pink)

and the substrate-binding domain (blue) are indicated. Residues important for chaperone activity of the Hsp70 domain of DnaK from *E.coli* are marked with a red asterisk (Zuiderweg *et al.*, 2013).

CsdK2 consists of 1146 amino acid and its two domains are separated by a 417 amino acid long unstructured region. Its N-terminal PilZ domain has the fully conserved bipartite c-di-GMP binding motif, indicating that this protein likely binds c-di-GMP (Figure 19a). The DnaK/Hsp70 domain of CsdK2 has 34/55% identity/similarity to *E. coli* DnaK and contains the residues for ATPase activity and the interactions with DnaJ and GrpE homologs (Zuiderweg *et al.*, 2013), suggesting that also CsdK2 likely has ATPase activity and might function as a DnaK-like protein (Figure 19c). While the nucleotide-binding domains in CdK1 and CdK2 show high conservation, the substrate-binding domains are more diverse (Figure 19c). CsdK2 was the most enriched putative interaction partner of CdbS in the pull-down experiment (Figure 17,Table 2).

Mxan_0750 contains the J-domain as well as a glycine-rich J-central domain. This classifies this protein as a class I J-domain protein, similar to the canonical DnaJ of *E. coli* (Figure 20a). Full-length Mxan_0750 shares 50/69% identity/similarity with DnaJ from *E. coli* and contains important residues, such as the HPD motif, that are vital for the interaction with a Hsp70 domain (Figure 20b), suggesting it can act as a DnaJ co-chaperone. *M. xanthus* encodes 16 proteins with a J-domain, from hereon we refer to Mxan_0750 as DnaJ1.

Mxan_6672 was identified in previous work and suggested to be a GrpE homolog, and the protein was named GrpS (Weimer *et al.*, 1998). GrpS is one of two GrpE homologs in *M. xanthus* and contains the GrpE domain (Figure 21a). The domain shares 33%/55% identity/similarity to GrpE from *E. coli* and contains the residues important for the interaction of canonical GrpE proteins with their cognate DnaK, suggesting that GrpS can function as a co-chaperone for DnaK proteins (Gelinas *et al.*, 2003, Gelinas *et al.*, 2004) (Figure 21b).

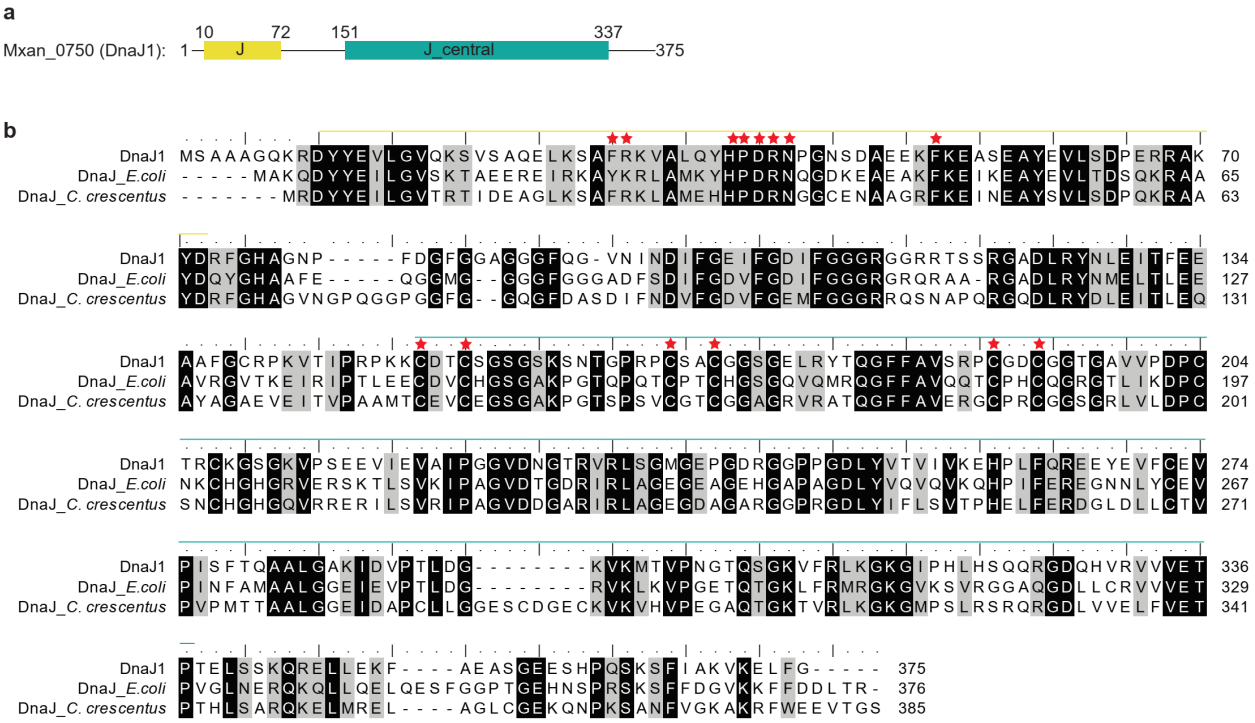

Figure 20: Sequence analysis of DnaJ1. (a) Domain architecture of DnaJ1. The J-domain is marked in yellow, rhe J_central domain in turquoise. (b) Alignment of full-length DnaJ1 with DnaJ from *E. coli* and a homolog in *C. crescentus*. The J domain is marked in yellow and the J_central domain in turquoise. Residues important for the activity of DnaJ from *E. coli* are marked with a red asterisk.

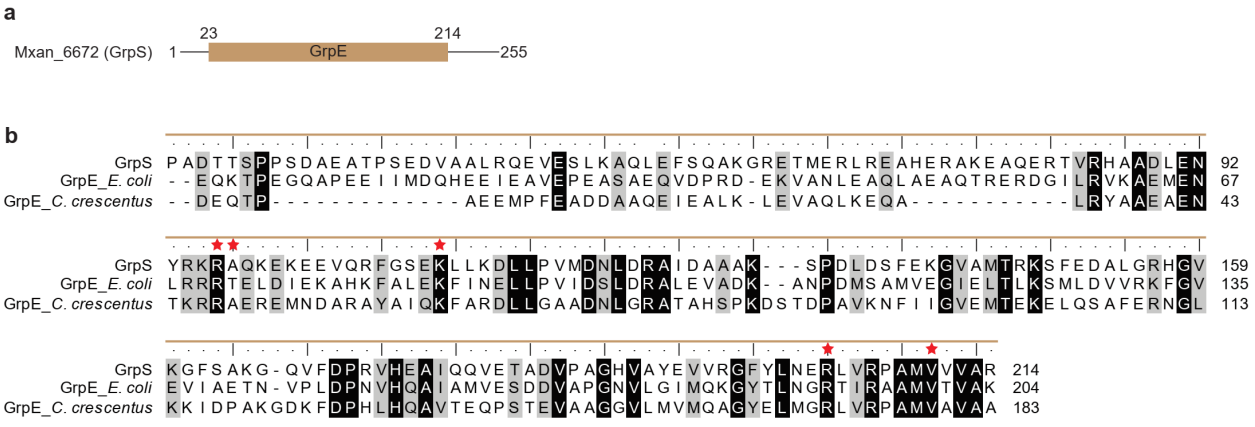

Figure 21: Sequence analysis of GrpS. (a) Domain architecture of GrpS. The GrpE domain is marked in brown. (b) Alignment of the GrpE domain of GrpS with those of GrpE from *E. coli* and the domain of a homolog in *C. crescentus*. The GrpE domain is marked in brown. Characterized residues of the *E. coli* GrpE for dimerization and interaction with a Hsp70 domain are marked with a red star.

Mxan_1092 is one of three Hsp20/α-crystallin domain proteins in *M. xanthus* (Figure 22a). A well-described Hsp20 is IbpA of *E. coli*, which binds to misfolded proteins to generate a pool of misfolded protein clients that then get transferred to a KJE system (Haslbeck *et al.*, 2019). The Hsp20 domain of Mxan_1092 is 20.7/40.5% identical/similar to that of IbpA of E. coli (Figure 22b), suggesting that it has Hsp20 activity.

Figure 22: Sequence analysis of Mxan_1092. (a) Domain architecture of Mxan_1092. The Hsp20 domain is marked in cyan. (b) Alignment of the Hsp20 domains of Mxan_1092 with those of IbpA from *E. coli* and the domain of CC_3592 from *C. crescentus*. The Hsp20 domain is marked in cyan.

Mxan_5084 encodes the DnaB homolog (Rosario and Singer, 2007). Accordingly, it has both the DnaB_N domain, which was demonstrated in the *E. coli* homolog to be involved in oligomerization and the formation of a hexameric ring, and the DnaB_C ATPase domain that hydrolyses ATP to unwind dsDNA (Arai *et al.*, 1981, Chodavarapu and Kaguni, 2016). Full-length DnaB of *M. xanthus* shares 41.5/60.4% identity/similarity with DnaB of *E. coli* (Figure 23).

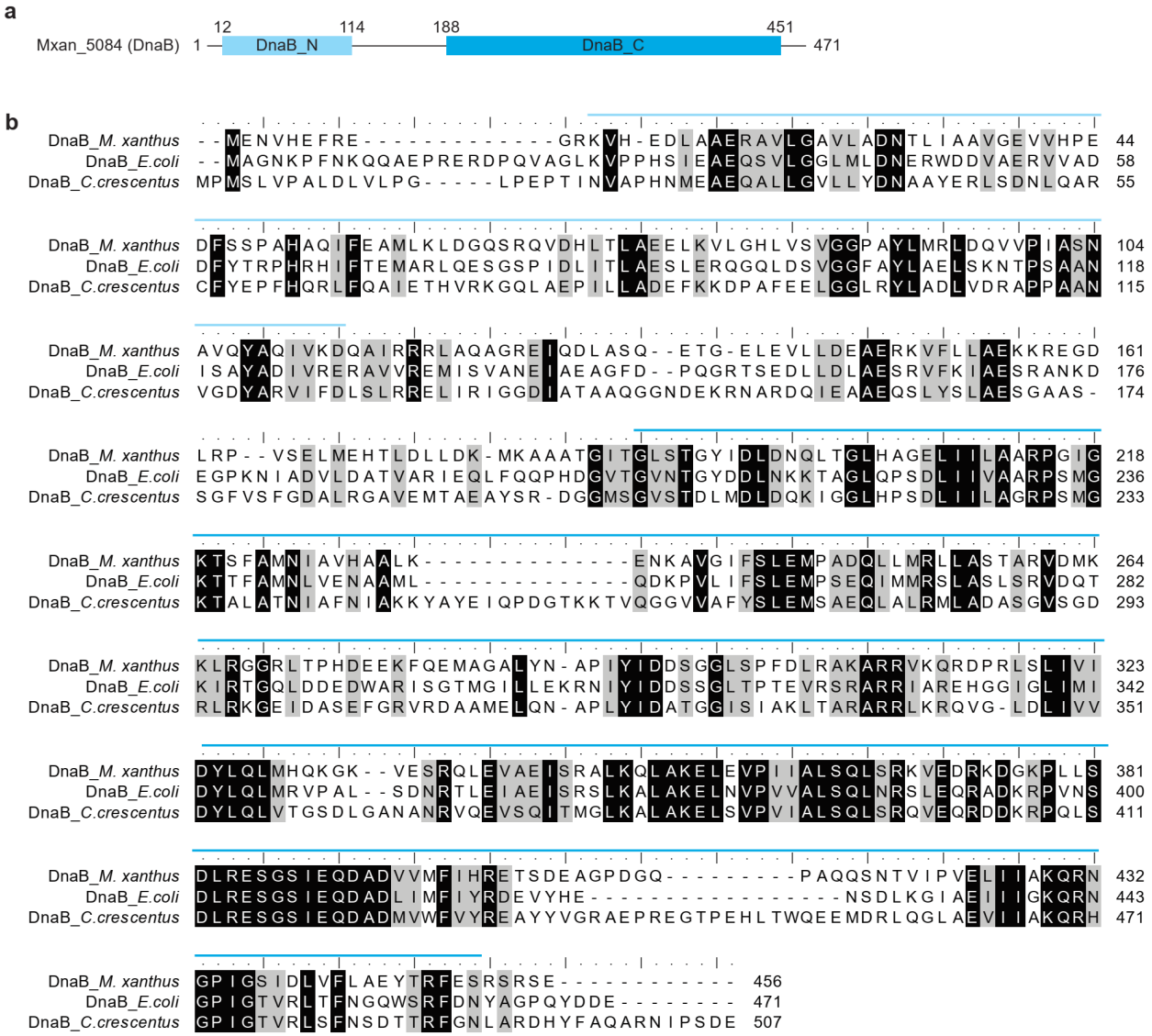

Figure 23: Bioinformatic analysis of DnaB (Mxan_5084). (a) Domain architecture of DnaB. The DnaB_N domain is marked in light blue and the DnaB_C domain in dark blue. (b) Alignment of full-length DnaB with the in *E. coli* and *C. crescentus*. The DnaB_N domain (light blue) and the DnaB_C domain (blue) are indicated with coloured lines.

2.9 Investigation of the putative PilZ-KJE protein folding machinery and its clients

DnaK/Hsp70 proteins are the central chaperones in DnaKJE chaperone/co-chaperone systems and interact directly with the client proteins for protein folding and stability, while J-domain and GrpE proteins function as co-chaperones. J-domain proteins present the client to the partner DnaK/Hsp70 and also stimulates their ATPase activity, while GrpE proteins are NEFs that stimulate ADP for ATP exchange by DnaK/Hsp70. Therefore, it is possible that the proteins that were enriched in the CdbS-FLAG pull-down experiments make up a KJE chaperone system and its clients. To investigate this hypothesis, we focused on understanding the interactions between CsdK1, CsdK2, DnaJ1, GrpS, CdbS and DnaB (Figure 24a,b).

To map interactions between these proteins, the BACTH system was used. To this end, the full-length genes of interest were fused N- and C-terminally to the T18 and T25 fragments of the adenylate cyclase from *Bordetella pertussis* and co-transformed into BTH101 *E. coli* cells. If the proteins of interest interact, the two fragments of the adenylate cyclase come into close contact, which enables the BTH101 cells to produce cAMP. This allows the cells to metabolize 5-brom-4-chlor-3-indoxyl-β-D-galactopyranosid (X-Gal), and the colony appears blue instead of white. As a positive control, the T18-Zip and T25-Zip plasmids were co-transformed.

CdbS only interacted with CsdK2 in this experiment (Figure 24a,b). CsdK2 also interacted with DnaJ1 and DnaB. For CsdK1, we observed an interaction with DnaB (Figure 24a,b). DnaJ1 not only interacted with CsdK2, but also DnaB (Figure 24a,b). Moreover, GrpS and DnaB self-interacted as expected (Arai et al., 1981, Harrison et al., 1997). DnaJ proteins form dimers (Mayer, 2021) but we did not detect self-interaction of DnaJ1 (Figure 24a,b).

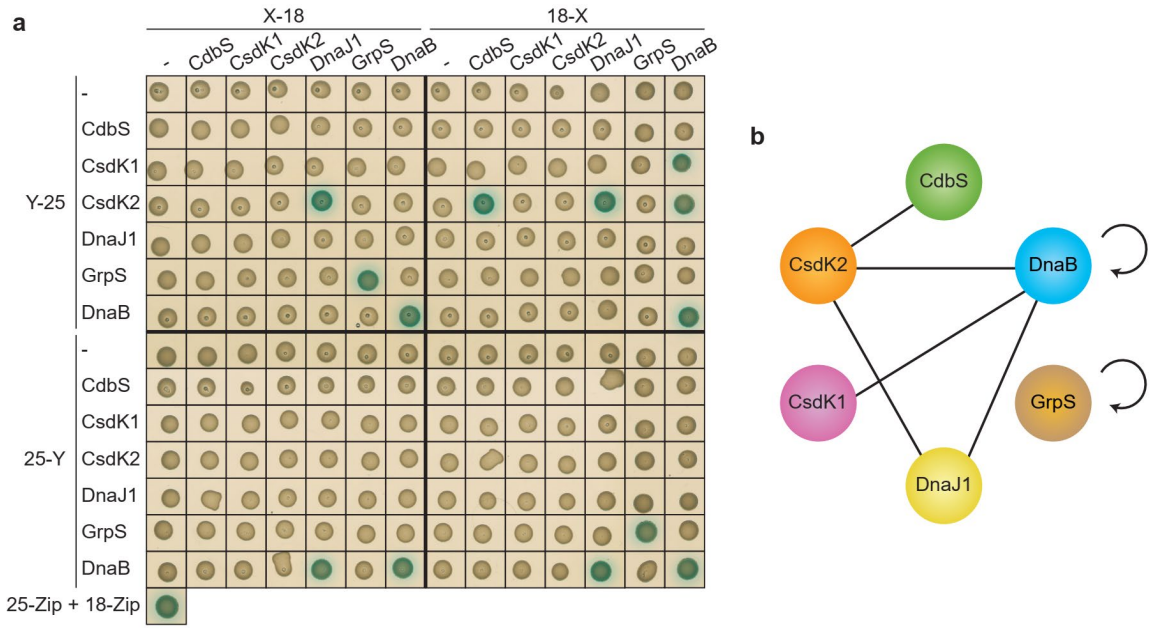

Figure 24: BACTH analysis of CdbS and the interaction candidates identified in the *in vivo* pull-down experiment. (a) The indicated full-length proteins were fused to the N- or the C-terminus of T18 or T25 as indicated. Blue and white colony colours indicate an interaction and no interaction, respectively. – indicates empty plasmids as a negative control. The Zip-constructs serve as positive control in the bottom left. Co-transformed cells were spotted on different plates with all controls and the images were edited together to create the figure. The same results were observed in two biological replicates. (b) Schematic of the observed interactions.

Because CdbS and CsdK2 interact directly, and CdbS binds c-di-GMP while CsdK2 has a PilZ domain that is predicted to bind the second messenger, we performed an additional BACTH assay to investigate this interaction in detail. To this end, we fused the T18 and T25 fragments to the CdbS^{R9A} variant that does not bind c-di-GMP, the CsdK2^{R38A} variant, which contains the Arg38 to Ala substitution in the c-di-GMP binding motif (see also Figure 19a) and is expected not to bind c-di-GMP (Ryjenkov *et al.*, 2006), or variants of CsdK2 containing only the PilZ or the DnaK/Hsp70 domain (Figure 25). We observed that the variants of CdbS and CsdK2 that do not (CdbS) or likely do not (CsdK2) bind c-di-GMP still showed a positive interaction, supporting that c-di-GMP binding by the two proteins is not important for their interaction. Moreover, CdbS interacted with the DnaK/Hsp70 domain of CsdK2 but not with its PilZ domain (Figure 25a,b). Together, these observations support that CdbS is a client of CsdK2 independently of c-di-GMP binding.

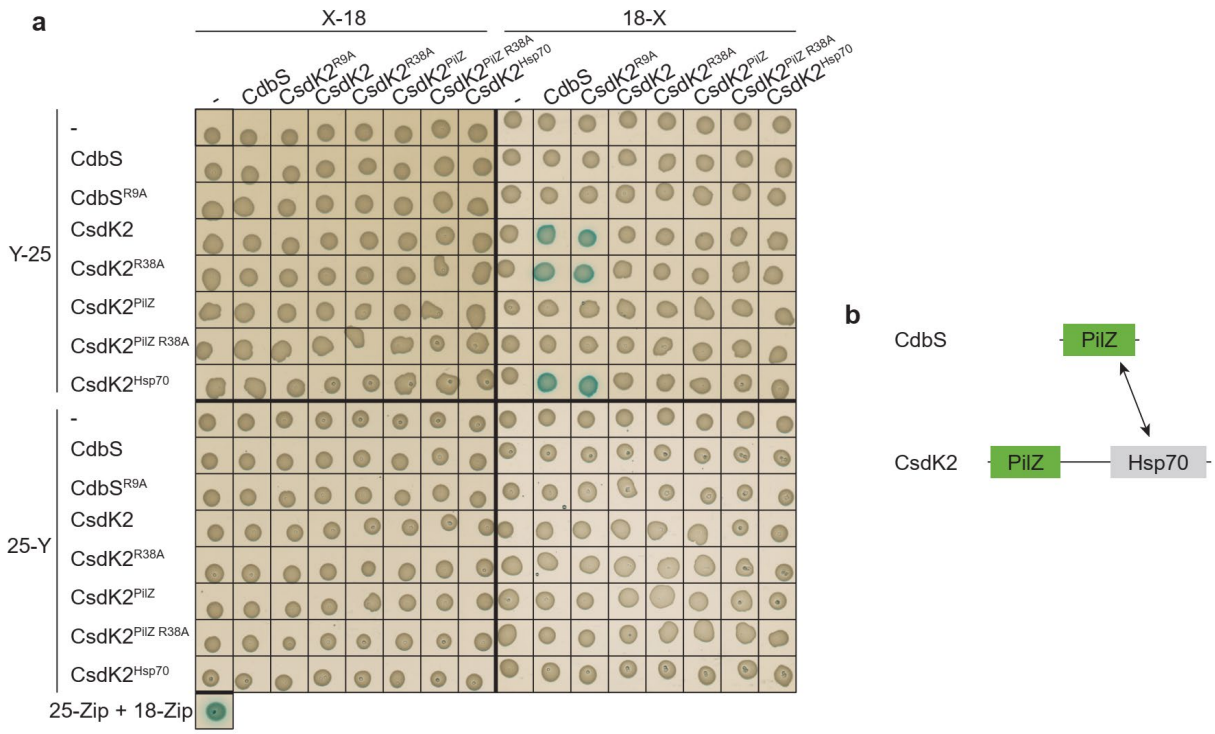

Figure 25: BACTH analysis of CdbS and CsdK2 interactions. (a) The indicated protein variants were fused to the N- or the C-terminus of T18 or T25 as indicated. Blue and white colony colours indicate an interaction and no interaction, respectively. – indicates empty plasmids as a negative control. The Zip-constructs serve as positive control in the bottom left. Co-transformed cells were spotted on different plates with all controls and the images were edited together to create the figure. The same results were observed in two biological replicates. (b) Schematic of the observed interactions.

Based on these results from the pull-down and BACTH analyses, we suggest that CsdK2 and DnaJ1 may constitute a DnaK/DnaJ pair. It is tempting to speculate that GrpS functions together with CsdK2; however, we have not shown a direct CsdK2/GrpS interaction. Moreover, our data strongly support that CdbS is a client of CsdK2 and that CdbS interacts with CsdK2 independently of c-di-GMP binding by the two proteins. Our data also support that DnaB could be a client of CsdK1 and CsdK2. We note that most of the proteins were not detected to bind to CdbS in the BACTH assay. We do not believe that these proteins are false positives from the pull-down experiments because they were highly and significantly enriched; therefore, we speculate that the interaction between CdbS and CsdK1 is too weak to be detected in the BACTH. Moreover, we speculate that DnaJ1 and GrpS were pulled-down because they interact with CsdK1 and CsdK2, and because CsdK1 and CsdK2 interact with DnaB.

2.10 CsdK1 and CsdK2 act during CdbA-depletion

Typically, a KJE chaperone system and Hsp20 proteins are involved in protein folding and stability. Therefore, we hypothesized that the five chaperones and co-chaperones might stabilize CdbS during CdbA-depletion. To test whether these protein act during CdbA-depletion, we generated in-frame deletions of *csdK1*, *csdK2*, *dnaJ1*, *grpS* and *hsp20* in the CdbA-mCh depletion strain that also expressed *parB-YFP* from a plasmid integrated in a single copy at the MxB *attB* site. We then spotted these strains on CTT agar plates containing 0 µM or 500 µM vanillate and tested for viability (Figure 26).

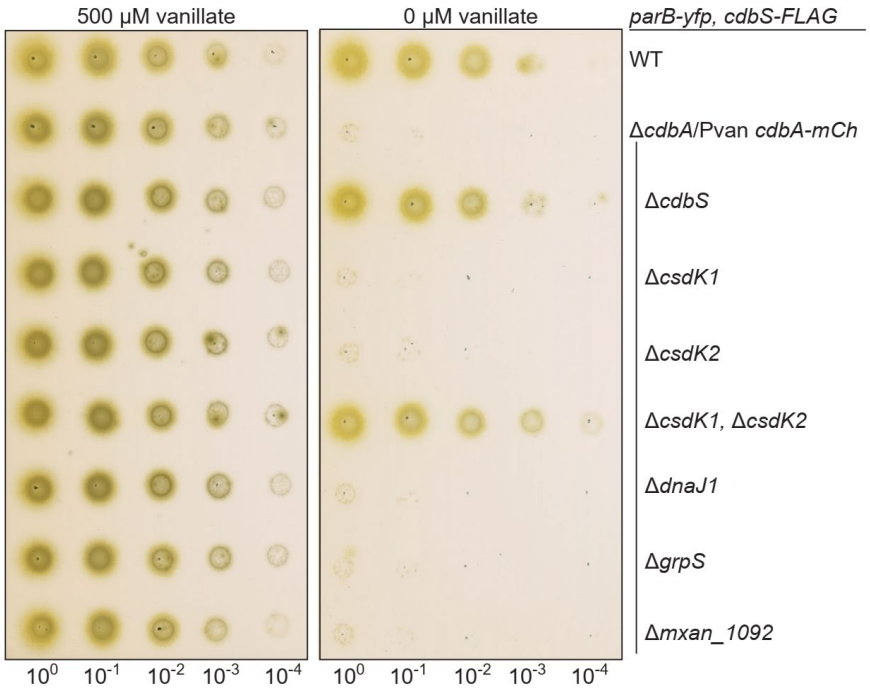

Figure 26: Cells lacking CsdK1, CsdK2 and depleted of CdbA-mCh are viable. Both plates contain CTT agar, the plate shown on the left additionally contains 500 µM vanillate.. After spotting 10 µl of each dilution, the plates were incubated for 96 h. Similar results were observed in three independent experiments.

We again observed that the CdbA-depletion strain is only viable when supplemented with vanillate, while cells depleted of CdbA-mCh and lacking CdbS were viable in the absence of vanillate (as seen in Figure 11a). Cells depleted of CdbA-mCh and lacking either CsdK1, CsdK2, DnaJ1, GrpS or Hsp20 were not viable in the absence of vanillate (Figure 26). Remarkably, the

Δ*csdK1* Δ*csdK2* double mutant in the CdbA-mCh depletion background was viable in the absence of vanillate, i.e. in the absence of CdbA-mCh. These observations support that CsdK1 and CsdK2 have redundant functions and could be involved in enabling the increased CdbS accumulation upon CdbA depletion. The Δ*dnaJ1*, Δ*grpS* and Δ*hsp20* mutations do not have the same effect on viability upon CdbA-mCh depletion, suggesting that other DnaJ protein(s), the second GrpE homolog and other small heat shock proteins can take over their function, or that DnaJ1 and GrpS do not make up a KJE system with CsdK1 and CsdK2. For these reason, we focused on understanding the function of CsdK1 and CsdK2.

2.11 CsdK1 and CsdK2 are important for the increased CdbS accumulation during CdbA-depletion

CsdK1 and CsdK2 were reported to not be involved in motility, EPS accumulation, fruiting body formation, or sporulation (Kuzmich *et al.*, 2021). We observed that cells lacking either or both CsdK1 and CsdK2 in an otherwise WT background had WT-like cell length and chromosome organization and segregation (Figure 27a,b). To test whether CsdK1 and CsdK2 are important for the accumulation of CdbS, we analyzed the CdbS-FLAG level synthesized from the native site in the absence of CsdK1 and CsdK2 in immunoblots. Cells lacking either or both proteins accumulated CdbS-FLAG at the same level as WT (Figure 27c).

Next, we tested whether CsdK1 and CsdK2 are important for the increased accumulation of CdbS during CdbA-depletion. In control experiments, we observed that cells depleted of CdbA-mCh accumulated CdbS-FLAG at a ~4-fold increased level compared to WT. The individual Δ*csdK1* and Δ*csdK2* mutations did not affect this elevated CdbS-FLAG level in this background (Figure 28). By contrast, the Δ*csdK1* Δ*csdK2* double mutant only accumulated CdbS-FLAG at an ~1.6-fold increased level compared to WT (Figure 28) supporting that CsdK1 and CsdK2 act redundantly during CdbA-depletion to enable the increased CdbS-FLAG accumulation.

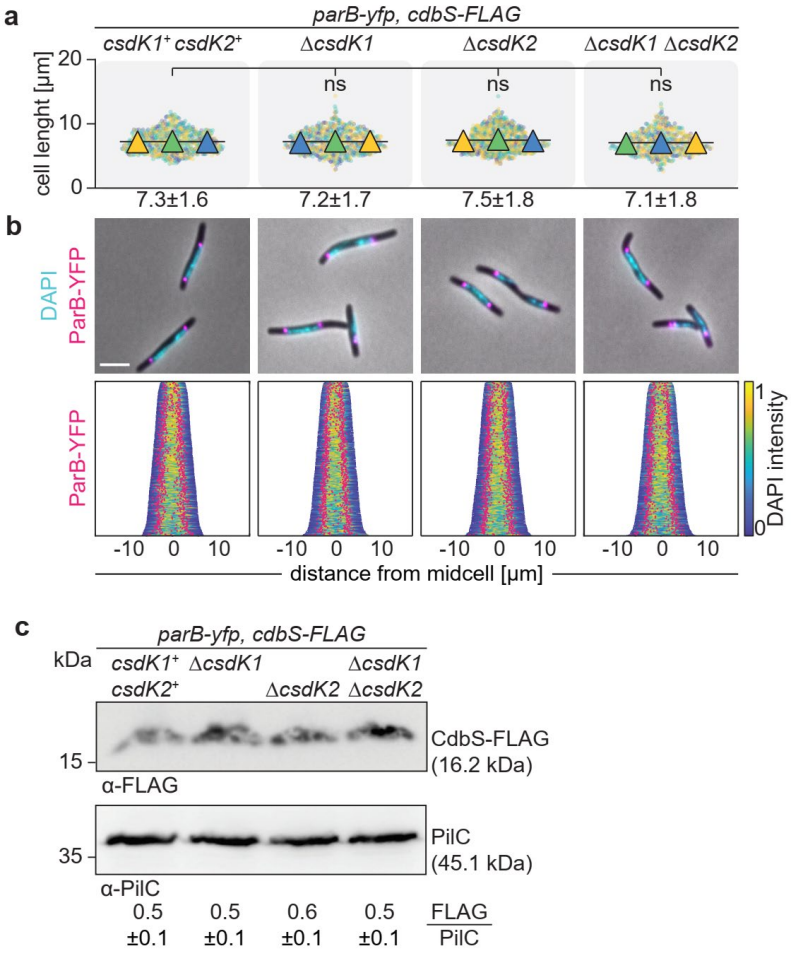

Figure 27: Lack of CsdK1 or CsdK2 does not affect CdbS accumulation, cell length and chromosome organization and segregation. a) Cell length analysis of indicated strains. Measurements of three independent experiments are shown in different coloured dots with the respective means as triangles. No significant differences were observed in 2way ANOVA multiple comparisons test among the strains. b) Fluorescence microscopy of cells stained with DAPI and synthesizing ParB-YFP. In the demographs, cells are sorted by cell length, DAPI signals are shown according to the intensity scale, and ParB-YFP signals in pink. Scale bar, 5 µm. N = 400 cells for all strains. c) Immunoblot analysis of CdbS-FLAG accumulation. Cell lysate from the same number of cells was loaded per lane. PilC was used as a loading control. Numbers below show the mean level of CdbS-FLAG normalized by the PilC level ± STDEV in the indicated strains calculated from three independent experiments. No statistical differences in Student's t test were observed in which samples were compared to WT.

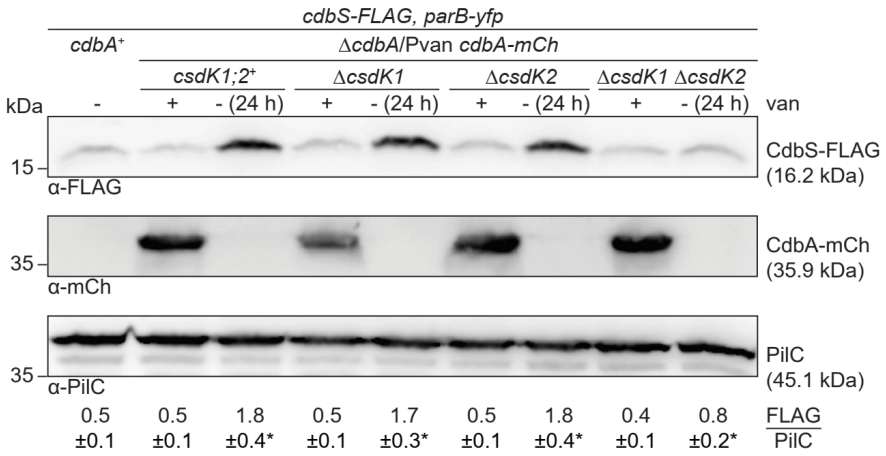

Figure 28: CsdK1 and CsdK2 enable increased CdbS-FLAG accumulation during CdbA-mCh depletion. Cells were grown in the presence or absence of 500 µM vanillate for 24 h before sample preparation. The mCh antibody has a light unspecific band at around 36 kDa. Cell lysate from the same number of cells was loaded per lane. PilC was used as a loading control. Numbers below show the mean level of CdbS-FLAG normalized by the PilC level ± STDEV in the indicated strains calculated from three independent experiments. *, $p < 0.05$ in Student's t test in which samples were compared to WT.

Following these observations, we analyzed the strains for cell length and chromosome organization and segregation. Cells depleted of CdbA-mCh and lacking either CsdK1 or CsdK2 had an average cell length similar to cells only lacking CdbA-mCh (Figure 29a). In addition, these mutant strains also had disrupted chromosome organization and segregation (Figure 29b). In contrast, cells depleted of CdbA-mCh and lacking CsdK1 as well as CsdK2 only had a slight although significant increase in cell length and most cells had WT-like chromosome organization and segregation (Figure 29a,b).

Altogether, these results demonstrate that CsdK1 and CsdK2 act during CdbA-depletion to enable the increased CdbS accumulation. Thus, lack of both CsdK1 and CsdK2 also suppresses the CdbA depletion phenotype and cells are viable in the absence of CdbA-mCh. Because CsdK1 and CsdK2 enable the increased CdbS accumulation in response to CdbA-depletion and this increase is regulated at the post-transcriptional level, we suggest that CsdK1 and CsdK2 function to stabilize CdbS during CdbA depletion. Furthermore, we suggest that the increased CdbS accumulation in response to CdbA-depletion is the result of increased CdbS stability and not a result of increased translation of *cdbS*.

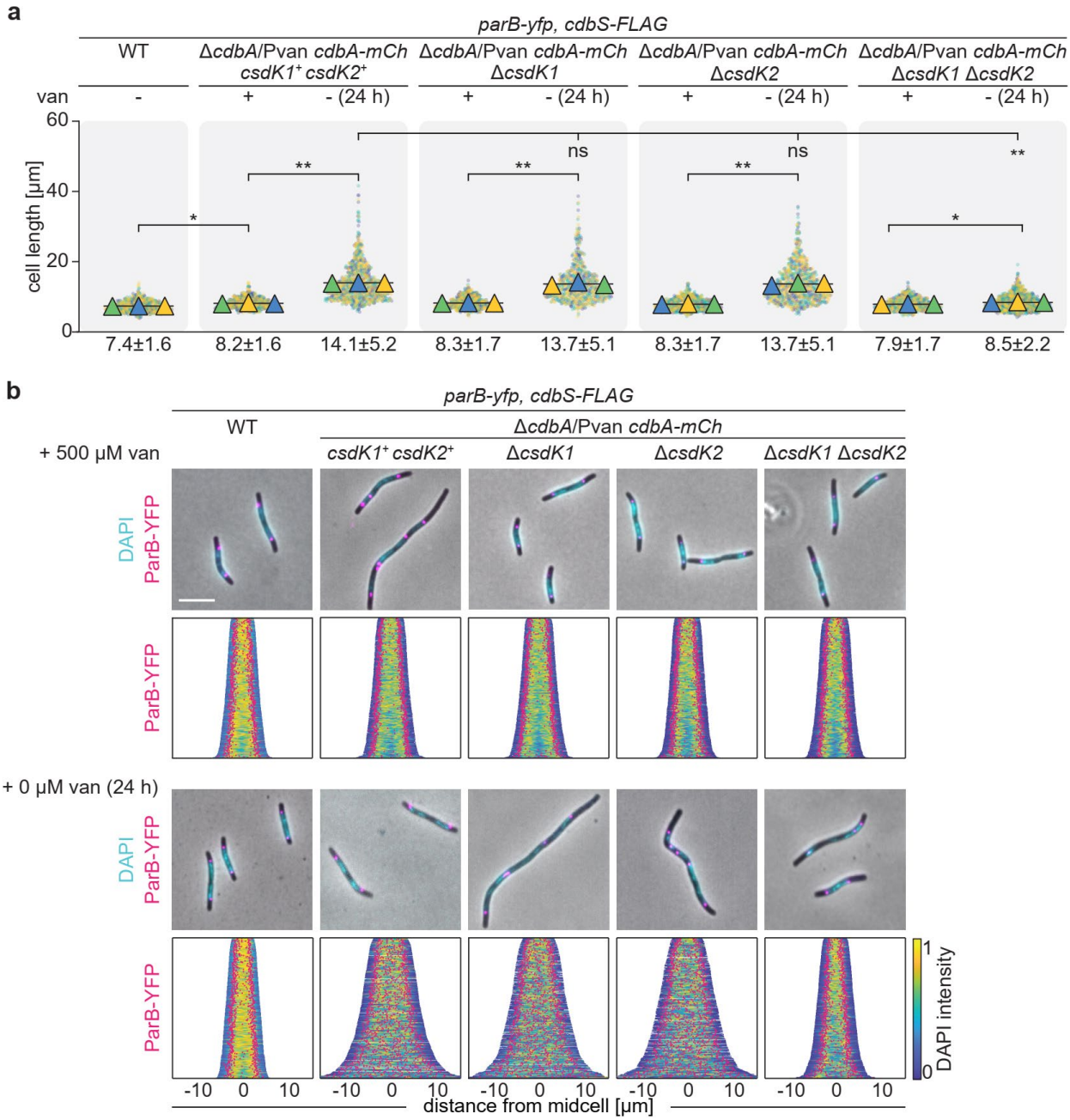

Figure 29: Lack of CsdK1 and CsdK2 partially suppresses the CdbA-depletion phenotype. a) Cell length analyses of indicated strains supplemented with or without 500 µM vanillate for 24 h. Measurements of three independent experiments are shown in different coloured dots with the respective means as triangles. Numbers above indicate mean ± STDEV in µm. * $p < 0.001$, ** $p < 0.0001$, ns, not significant in 2way ANOVA multiple comparisons test. b) Fluorescence microscopy of cells stained with DAPI and synthesizing ParB-YFP. In the demographs, cells are sorted by cell length, DAPI signals are shown according to the intensity scale, and ParB-YFP signals in pink. Scale bar, 5 µm. N = 400 cells for all strains.

2.12 CdbA-depletion induces increased *csdK1* and *csdK2* transcription and accumulation

Next, we sought to understand the connection between CdbA and CsdK1 and CsdK2. Because CdbA is a DNA-binding protein, we asked whether it binds in the gene loci of *csdK1* and *csdK2* using published ChIP-seq data (Skotnicka *et al.*, 2020). CdbA binds in two regions close to the *csdK1* locus, with one peak centered at -1976 bp and a second peak centered at +382 bp relative to the transcriptional start site of *csdK1* at +1 bp (Figure 30a). In the same experiment, CdbA was reported to bind in the intergenic region of *csdK2* with a ChIP-seq peak centered around position -2 bp relative to the transcriptional start site of *csdK2* (Figure 30b).

Based on CdbA binding to the genetic regions of *csdK1* and *csdK2*, we aimed to understand whether CdbA-depletion regulates the expression and accumulation of CsdK1 and CsdK2. To this end, we used strains in which a *csdK1-HA* allele or a *csdK2-mV* allele is expressed from their respective native sites (genotypes are *csdK1::csdK1-HA* or *csdK2::csdK2-mV*, from here on *csdK1-HA* and *csdK2-mV*). Using RT-qPCR, we determined the expression of *csdK1-mV* and *csdK2-HA* in the CdbA-mCh depletion mutant compared to the level in otherwise WT cells. When supplemented with vanillate, i.e. in the presence of CdbA-mCh, *csdK1-HA* was expressed at a similar level to that of otherwise WT cells. Cells depleted of CdbA-mCh for 24 h expressed the gene at a ~1.8-fold elevated level compared to the WT level (Figure 30c). Moreover, cells accumulating CdbA-mCh expressed *csdK2-mV* at a level similar to otherwise WT cells, but when depleted of CdbA-mCh for 24 h, the cells showed significantly increased transcription of *csdK2-HA* at a ~2.4-fold level compared to the WT level (Figure 30c)

Following these observations, we determined the accumulation of CsdK1-mV and CsdK2-HA in the presence and absence of CdbA-mCh. We found that cells synthesizing CdbA-mCh accumulated CsdK1-mV at its WT level, but at ~1.6-fold elevated level when depleted of CdbA-mCh for 24 h (Figure 30d). Similarly, in the presence of CdbA-mCh, the cells accumulated CsdK2-HA at its WT level, but at an ~1.8-fold increased level in the absence of CdbA-mCh (Figure 30e).

These results show that CdbA represses the transcription of *csdK1* and *csdK2*. When CdbA-mCh is depleted, the expression and the accumulation of CsdK1 and CsdK2 are increased, and we suggest that this increased level of the chaperones then stabilizes CdbS.

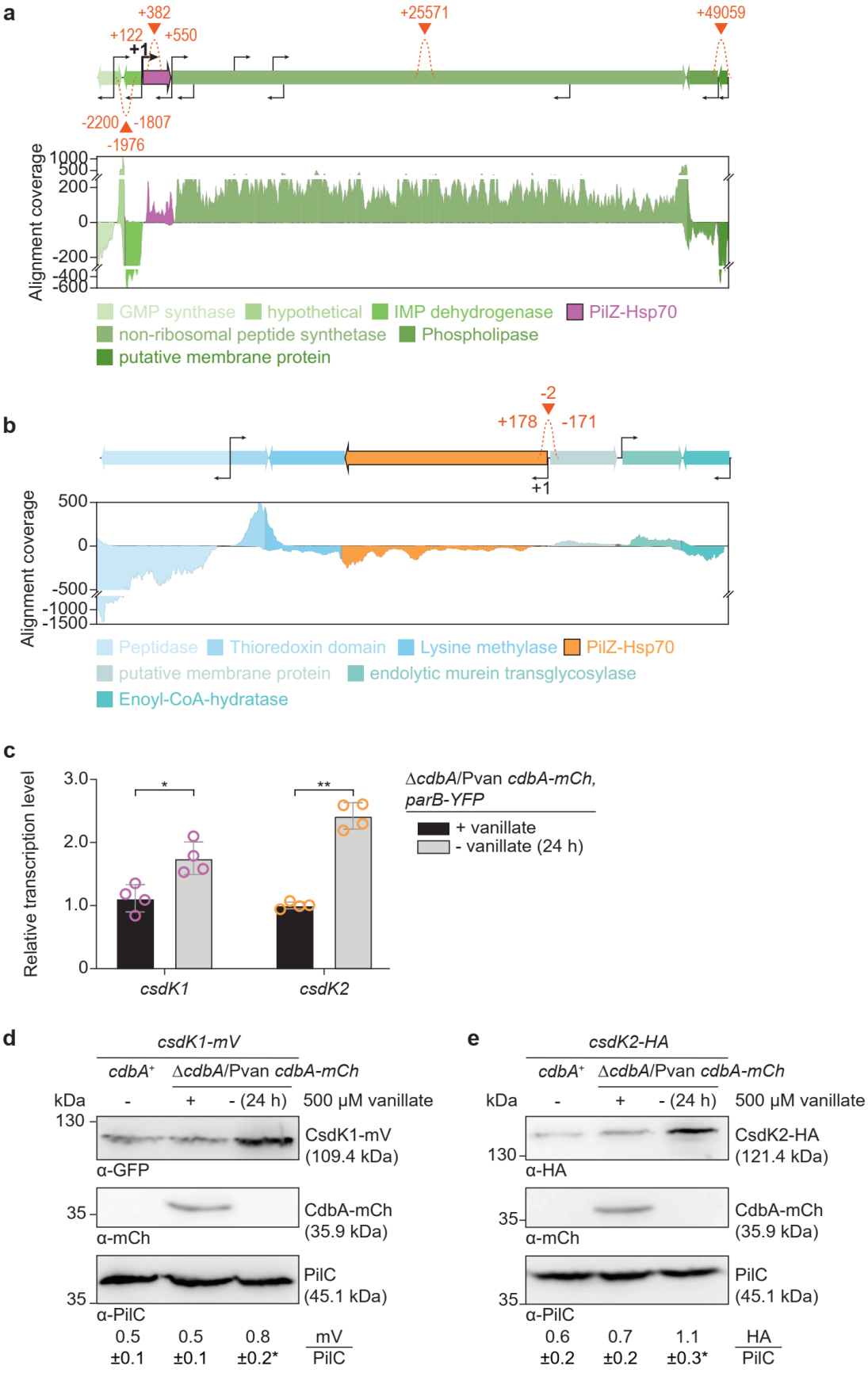
a
+382
+122
+550
+1
+25571
+49059
-2200
-1807
-1976
Alignment coverage
1000
500
200
0
-200
-400
-600
GMP synthase
hypothetical
IMP dehydrogenase
PilZ-Hsp70
non-ribosomal peptide synthetase
Phospholipase
putative membrane protein
b
-2
+178
-171
+1
Alignment coverage
500
0
-500
-1000
-1500
Peptidase
Thioredoxin domain
Lysine methylase
PilZ-Hsp70
putative membrane protein
endolytic murein transglycosylase
Enoyl-CoA-hydratase
c
Relative transcription level
3.0
2.0
1.0
0
*
**
csdK1
csdK2
ΔcdbA/Pvan cdbA-mCh, parB-YFP
+ vanillate
- vanillate (24 h)
d
csdK1-mV
cdbA+
ΔcdbA/Pvan cdbA-mCh
kDa
-
+
- (24 h)
500 µM vanillate
130
CsdK1-mV (109.4 kDa)
α-GFP
35
CdbA-mCh (35.9 kDa)
α-mCh
35
PilC (45.1 kDa)
α-PilC
0.5 ±0.1
0.5 ±0.1
0.8 ±0.2*
mV / PilC
e
csdK2-HA
cdbA+
ΔcdbA/Pvan cdbA-mCh
kDa
-
+
- (24 h)
500 µM vanillate
130
CsdK2-HA (121.4 kDa)
α-HA
35
CdbA-mCh (35.9 kDa)
α-mCh
35
PilC (45.1 kDa)
α-PilC
0.6 ±0.2
0.7 ±0.2
1.1 ±0.3*
HA / PilC

Figure 30: CdbA-depletion leads to increased transcription and accumulation of CsdK1 and CsdK2. a) Visualization of the CdbA binding site as identified by ChIP-seq analysis relative to the transcription start site of *csdK1*. Upper schematic illustrates *csdK1* and its neighbouring genes to scale. Dotted red lines indicate the peaks of CdbA in ChIP-seq anaylsis from Skotnicka *et al.*, 2020, with the peak coordinates in red, and its summit as red triangles. Coordinates indicate bp relative to transcriptional start site, which overlaps with the start codon of *csdK1* at +1 bp. Kinked arrows indicate transcription start sites as detected in Kuzmich *et al.*, 2022. Lower graph shows RNA-seq data from Kuzmich *et al.*, 2022 in the same colours. Dark grey indicates intergenic region. Gene annotations listed below. b) Schematic of the CdbA binding site as identified by ChIP-seq analysis relative to the transcription start site of *csdK2,* which overlaps with the start codon at position +1 bp, as in Figure 30a. c) RT-qPCR analysis of *csdK1* (purple) and *csdK2* (orange) expression in the conditional CdbA-mCh depletion strain supplemented with or without 500 µM vanillate for 24 h normalized to the transcript in WT. Transcript levels are shown as mean ± STDEV from four biological replicates with three technical replicates each. Individual data points are shown as coloured dots. * $p < 0.01$, ** $p < 0.0001$ in a two-sided Student's t-test. d) Immunoblot analysis of CsdK1-mV accumulation in the conditional CdbA-mCh depletion strain compared to otherwise WT. Cells were grown in the presence or absence of 500 µM vanillate for 24 h before sample preparation. Cell lysate from the same number of cells was loaded per lane. PilC was used as a loading control. Numbers below show the mean level of CsdK1-mV normalized by the PilC level ± STDEV in the indicated strains calculated from three independent experiments. *, $p < 0.05$ in Student's t test in which samples were compared to WT. e) Immunoblot analysis of CsdK2-HA accumulation in the conditional CdbA-mCh depletion strain compared to otherwise WT. Cells were grown in the presence or absence of 500 µM vanillate for 24 h before sample preparation. PilC was used as a loading control. Numbers below show the mean level of CsdK2-HA normalized by the PilC level ± STDEV in the indicated strains calculated from three independent experiments. *, $p < 0.05$ in Student's t test in which samples were compared to WT.

2.13 CdbS overaccumulating cells have no defect in DNA replication

In the pull-down experiment, we identified the DNA helicase DnaB as a potential interaction partner of CdbS, suggesting that CdbS might affect DNA replication via an interaction with DnaB. If CdbS at high levels blocks or interferes with the function of DnaB, the phenotype caused by high levels of CdbS is expected to mimic the phenotype of cells accumulating a non-functional DnaB variant. To test this hypothesis, we analyzed the temperature-sensitive $DnaB^{A116V}$ mutant. This mutant grows like WT at 32°C, but when grown at 37°C, the mutant cells complete one round of DNA replication and then arrest replication (Rosario and Singer, 2007).

When grown at 32°C, both WT and the *dnaB*^{A116V} mutant had similar cell lengths, and both strains elongated when grown at 37°C for 12 h (Figure 31a). The two strains had similar chromosome organization and segregation patterns at 32°C. After 12 h at 37°C, WT cells still had well-organized chromosomes; by contrast, the DnaB^{A116V} mutant had highly condensed chromosomes centered around midcell (Figure 31b). This phenotype differs from the phenotype caused by elevated CdbS levels suggesting that the defect in CdbS overaccumulating cells is not solely caused by CdbS inhibiting DnaB.

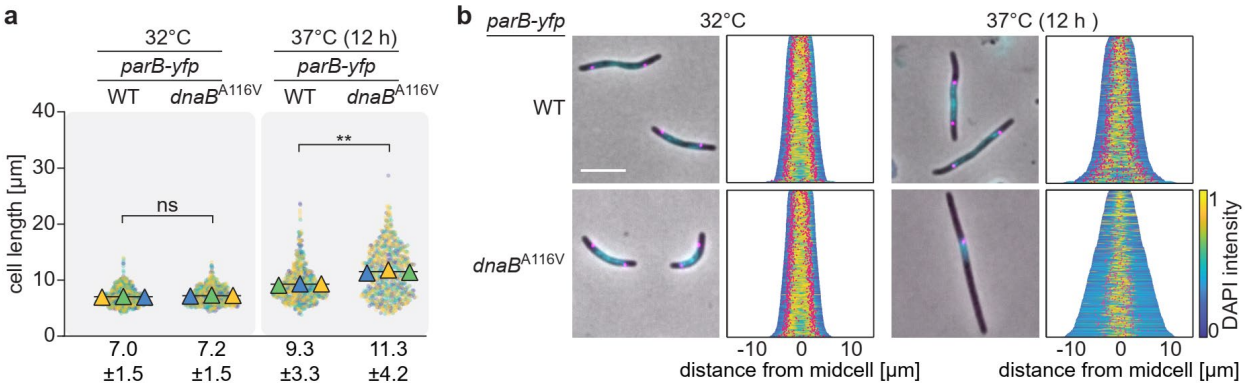

Figure 31: The temperature-sensitive *dnaB*^{A116V} mutant elongates and has a condensed chromosome centered around midcell at the non-permissive temperature. a) Cell length analysis of indicated strains. Cultures were incubated at 37°C for 12 h before the analysis. Measurements of three independent experiments are shown in different coloured dots with the respective means as triangles. ** $p < 0.0001$, ns, not significant in 2way ANOVA multiple comparisons test. b) Fluorescence microscopy of cells stained with DAPI and synthesizing ParB-YFP. In the demographs, cells are sorted by cell length, DAPI signals are shown according to the intensity scale, and ParB-YFP signals in pink. Scale bar, 5 µm. N = 400 cells for all strains.

As an additional test whether increased levels of CdbS interfere with DNA replication, we analyzed the *ori*/ter ratio of cells overexpressing *cdbS-FLAG* from the vanillate promoter. To quantify the *ori* region by qPCR, we targeted *dnaA* (*mxan_0001*) as well as *mxan_7483*, and to quantify the *ter* region, we targeted *csdK1* as well as *mxan_4058* (Figure 32). To calculate the individual *ori*/*ter* ratios, the $2^{-\Delta CT}$ method was used as described (Fernández-Coll *et al.*, 2020). As a negative control for elongated cells, we used WT cells treated with cephalexin for 8 h, which inhibits cell division but not DNA replication.

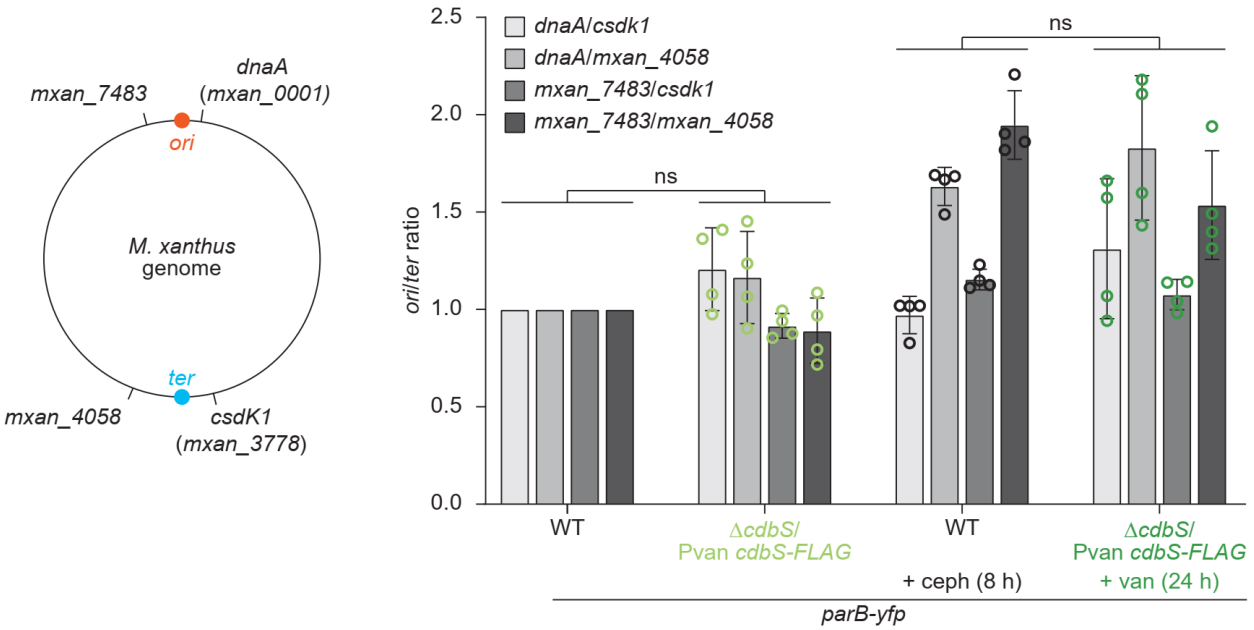

Figure 32: High CdbS levels do not affect DNA replication. Schematic on the left visualizes the quantified genetic regions close to *ori* and *ter*. Graph on the right shows qPCR analysis of *ori*/*ter* ratios in indicated strains, normalized to WT levels. WT was treated with cephalexin for 8 h, *cdbS-FLAG* overexpression was induced with 500 µM vanillate for 24 h before sample preparation. Ratios are shown as mean ± STDEV from four biological replicates with three technical replicates each. Individual data points are shown as coloured circles. No significant difference was observed in 2way ANOVA multiple comparisons test.

We found that WT cells and the uninduced *cdbS-FLAG* overexpression strain had no significant differences in their *ori*/*ter* ratios (Figure 32). Similarly, cells overexpressing *cdbS-FLAG* had *ori*/*ter* ratios similar to WT cells treated with cephalexin for 8 h (Figure 32). These observations support the notion an increased CdbS level does not interfere with DNA replication and that the primary defect upon CdbS overaccumulation is in chromosome organization and segregation.

2.14 The CdbS level increases during heat stress

Under the conditions tested so far, cells lacking CdbA as well as CdbS are viable and have no phenotypes with respect to cell length and chromosome organization and segregation. Therefore, the question arises what the function of this intricate system could be. To address this question, we asked which environmental perturbations might activate this system. In this system,

an increased CdbS level is required and sufficient to disrupt chromosome organization and segregation; therefore, we used the CdbS accumulation as a readout for activation of the system. CdbS levels were followed using a strain synthesizing CdbS-FLAG from the native site.

A significantly increased c-di-GMP level is necessary for *M. xanthus* to complete the starvation-induced developmental program, which results in the formation of fruiting bodies containing diploid myxospores (Skotnicka *et al.*, 2016b, Tzeng and Singer, 2005). As CdbA, CdbS and potentially also CsdK2 and CsdK2 are all associated with c-di-GMP, we determined CdbS accumulation during development. We found that CdbS-FLAG accumulation was decreased at two hours of starvation, and at four hours and later it was not detected.

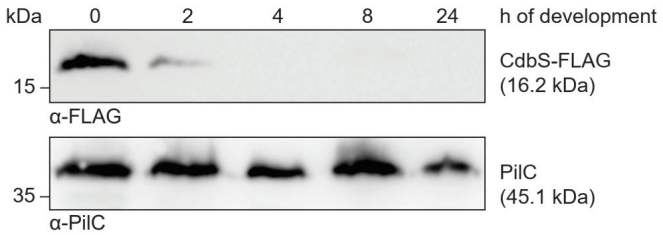

Figure 33: CdbS accumulation decreases during development. Cells were developed under submerged conditions in MC7 buffer. Cells were harvested at the indicated timepoints. Cell lysate from the same number of cells was loaded per lane. PilC was used as a loading control. Similar results were obtained in two independent experiments.

Next, we exposed cells to different stresses and tested for the accumulation of CdbS-FLAG. Therefore, we grew the cells at different growth temperatures, or in minimal medium. Furthermore, we exposed the cells to mitomycin C, nalidixic acid and UV light to induce DNA damage. In addition, we grew the cells in presence of 300 mM NaCl to induce osmotic stress or exposed them to 1.5 mM H_2O_2 to induce oxidative stress as described (Pan *et al.*, 2021). Interestingly, we found that CdbS overaccumulated when the cells were grown at 37°C, while it accumulated at a reduced level in response to all other tested stresses (Figure 34).

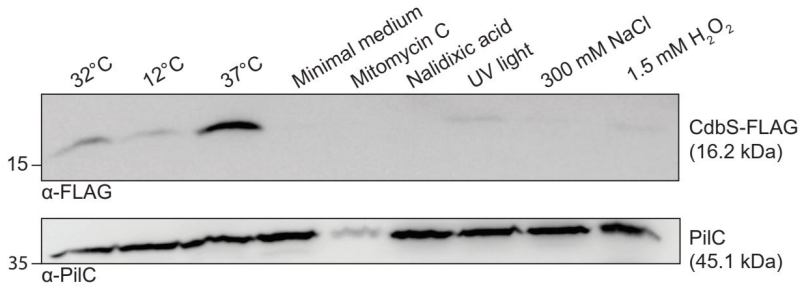

Figure 34: CdbS-FLAG overaccumulates at 37°C. Immunoblot analysis of CdbS-FLAG accumulation under indicated stress conditions. Cells were stressed for 18 h, or for 30 min with H_2O_2. Cell lysate from the same number of cells was loaded per lane. PilC was used as a loading control. Similar results were obtained in two biological replicates.

To further investigate the response to the elevated growth temperature, we analyzed the accumulation of CdbS-FLAG, CdbA-mCh, CsdK1-mV, and CsdK2-HA at 37°C over time in immunoblot analyses (Figure 35). We observed that the CdbS-FLAG level increased steadily over time and peaked at a ~4-fold increased level compared to 32°C at 12-18 h, and then decreased slightly. By contrast, the CdbA-mCh level in the same strain did not significantly change (Figure 35a). Furthermore, the CsdK1-mV level increased moderately over time and with a ~1.9-fold increase at 8-18 h (Figure 35b). Similarly, the CsdK2-HA level rose over time, with a ~2-fold increase at 12 h to 18 h (Figure 35c). At 24 h, the level of both chaperones had slightly decreased (Figure 35b,c). In line with the here presented data, we observed that the drastically increased accumulation of CdbS-FLAG at 37°C was dependent on CsdK1 and CsdK2, as cells lacking both proteins accumulated CdbS-FLAG at a constant level at 37°C with only a slight but significantly ~1.6-fold elevated level at 18 h at 37°C (Figure 35d).

Based on the increased levels of CdbS-FLAG, CsdK1-mV and CsdK2-HA at 37°C, we had expected a decrease in the CdbA-mCh level at 37°C but did not detect any noticeable change in its level. Hence, we investigated the localization of CdbA-mCh via fluorescence microscopy. At 32°C as well as at 37°C, CdbA-mCh co-localized with the nucleoid (Figure 36).

In summary, we observed that the CdbS level increases specifically in response to elevated temperatures, while it decreases during low temperatures, DNA damage, nutrient limitation, osmotic and oxidative stress. While CsdK1 and CsdK2 also accumulate at an elevated level at higher temperatures, and the increased accumulation of CdbS at 37°C is dependent on both CsdK1 and CsdK2, the CdbA level and localization is unaffected by the shift in temperature.

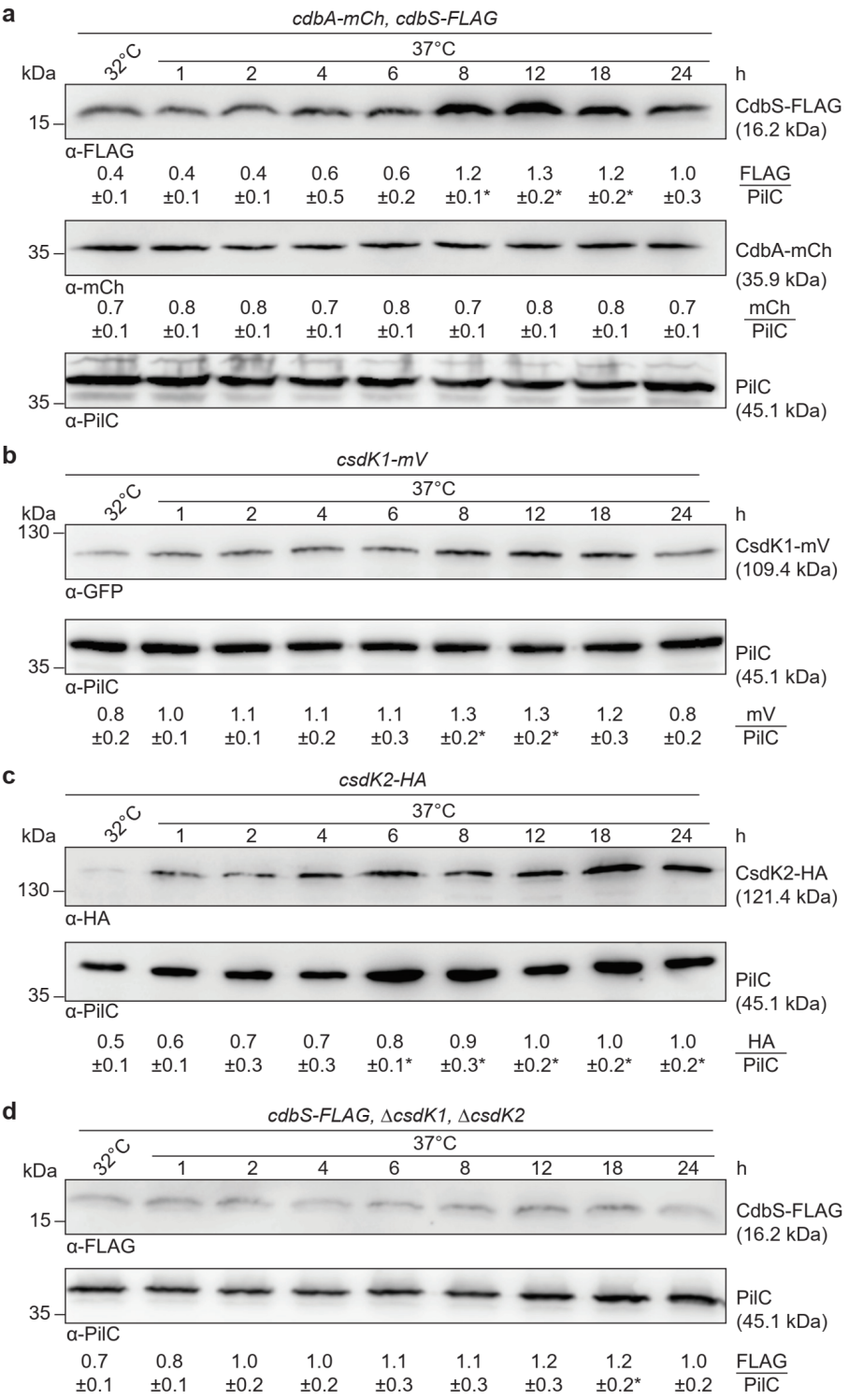

Figure 35: High temperature leads to an increased level of CdbS, CsdK1 and CsdK2, while the CdbA level is unaffected. Cells accumulating CdbS-FLAG and CdbA-mCh (a), CsdK1-mV (b), CsdK2-HA (c), or CdbS-FLAG in the absence of CsdK1 and CsdK2 (d) were grown at 37°C. At the indicated time points, samples were prepared for immunoblot analysis. Cell lysate from the same number of cells was loaded per lane. PilC was used as a loading control for all

experiments. Numbers below show the level of the respective protein normalized by the PilC level in the indicated strains calculated from three independent experiments. *, $p < 0.05$ in Student's t test in which samples were compared to the respective protein level at 32°C.

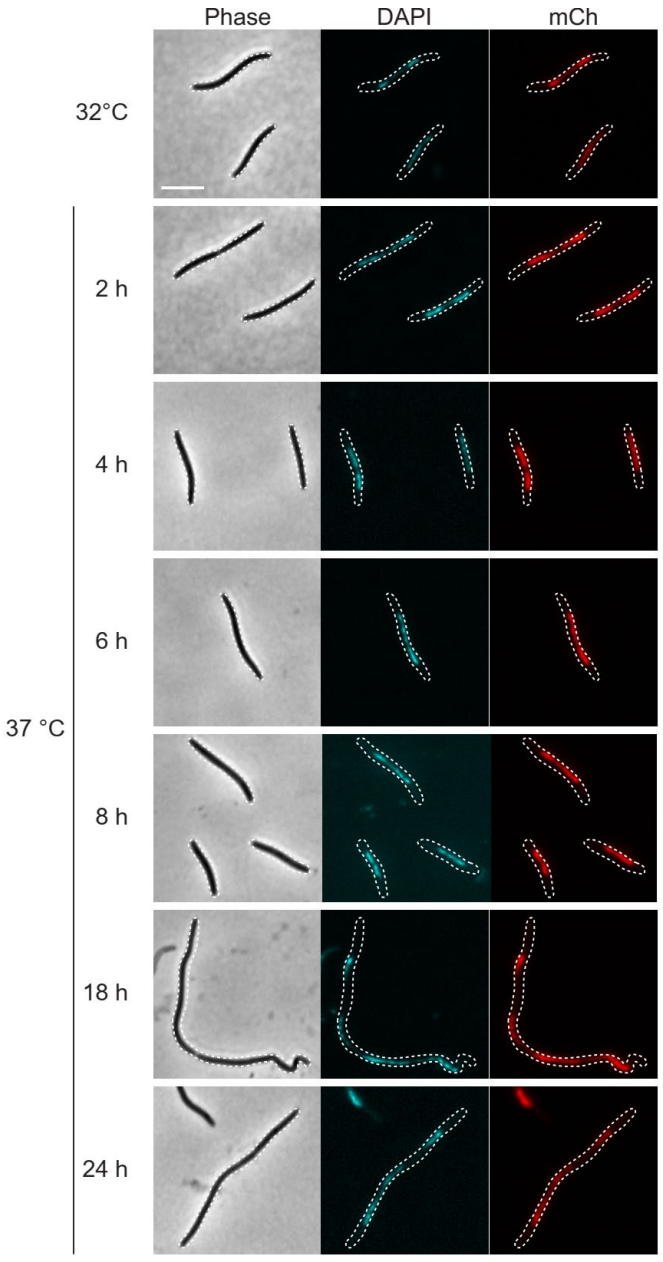

Figure 36: The localization of CdbA-mCh over the nucleoid is not affected at 37°C. Fluorescence microscopy of CdbA-mCh synthesizing cells stained with DAPI, incubated at the indicated temperature for the indicated time. Scale bar, 5 µm.

2.15 CdbS accelerates cell death during heat stress

M. xanthus cells have been described to elongate when grown at 37°C (Janssen *et al.*, 1977, Kimura *et al.*, 2005, Tzeng and Singer, 2005). To determine whether this cell elongation is connected to CdbS and the CsdK proteins, we investigated the cell length of WT, the Δ*cdbS* and the Δ*csdK1* Δ*csdK2* mutants at 37°C. Cells of all three strains elongated over time at 37°C with a significant difference compared to their cell length at 32°C (Figure 37a). However, when compared to each other at 18 h and later, the Δ*cdbS* and the Δ*csdK1* Δ*csdK2* cells had not elongated as drastically as WT (Figure 37a).

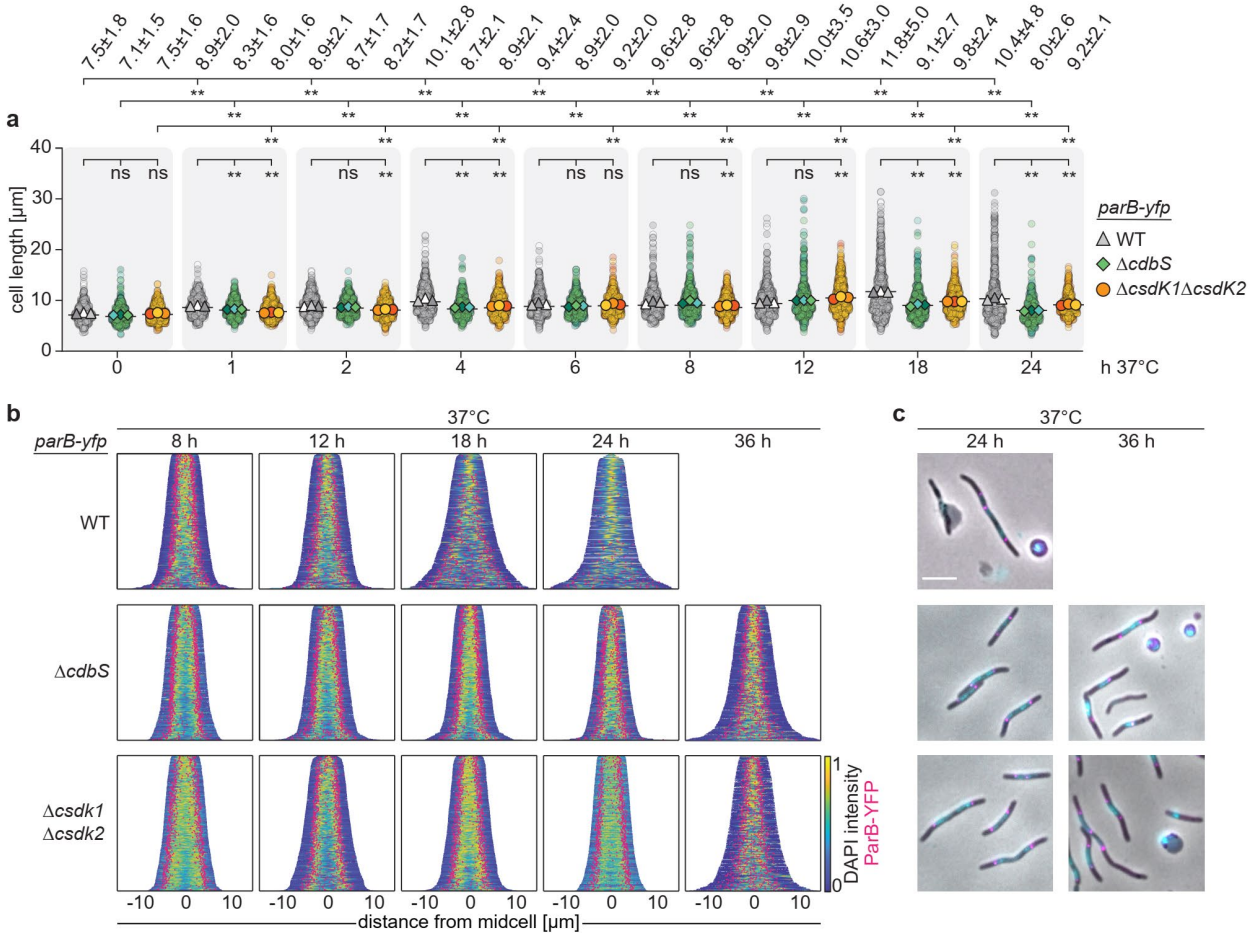

Figure 37: CdbS accelerates the disruption of chromosome organization and segregation at 37°C. a) Cell length analysis of indicated strains. Measurements of three independent experiments are shown in different coloured dots with the respective means as triangles (WT, grey), rhombus (Δ*cdbS*, green) or circles (Δ*csdK1* Δ*csdK2*, orange). Numbers above indicate mean ± STDEV in µm. ** $p < 0.0001$, ns, not significant in 2way ANOVA multiple comparisons to WT. All strains at 37°C are significantly elongated in 2way ANOVA multiple comparisons to their respective cell length at 32°C. b) Demographs depicting DAPI signals according to the intensity scale, and ParB-YFP signals in pink,

from cells sorted by cell length at the indicated time points at 37°C. N = 400 cells for all strains. c) Fluorescence microscopy of cells stained with DAPI and synthesizing ParB-YFP. Scale bar, 5 µm.

Importantly, at 18 h and later at 37°C, WT cells displayed disrupted chromosome organization and segregation (Figure 37b). Also, at 18h, WT cells started to lyse and at 24 h, most WT cells had lysed (Figure 37bc). In addition, we noticed an increasing amount of cells without the ParB-YFP signal (Figure 37bc). By contrast, most cells of the Δ*cdbS* and the Δ*csdK1* Δ*csdK2* strains were not affected in chromosome segregation and organization at 24 h at 37°C and had not lysed at this time point (Figure 37bc). Nevertheless, the Δ*cdbS* and the Δ*csdK1* Δ*csdK2* strains showed disrupted chromosome organization and segregation and started to lyse at 36 h of growth at 37°C (Figure 37b).

These observations suggest that growth at 37°C is lethal for WT, while the Δ*cdbS* and Δ*csdK1* Δ*csdK2* mutants are less affected. We, therefore, investigated the growth of these strains in suspension and in a plate-based assay. In suspension culture, WT had a strong growth defect at 37°C compared to 32°C, and at 24 h OD values decreased indicating that cells were lysing. The Δ*cdbS* and Δ*csdK1* Δ*csdK2* mutants also had slower growth at 37°C compared to 32°C but less so than WT; at 36 h OD values decreased indicating that cells were lysing (Figure 38a). Accordingly, in the plate-based assay, all strains were viable at 32°C, but not at 37°C (Figure 38b). Based on these observations, we conclude that 37°C is a lethal temperature for *M. xanthus*. Moreover, CdbS, CsdK1 and CsdK2 overaccumulate at 37°C and accelerate this viability defect.

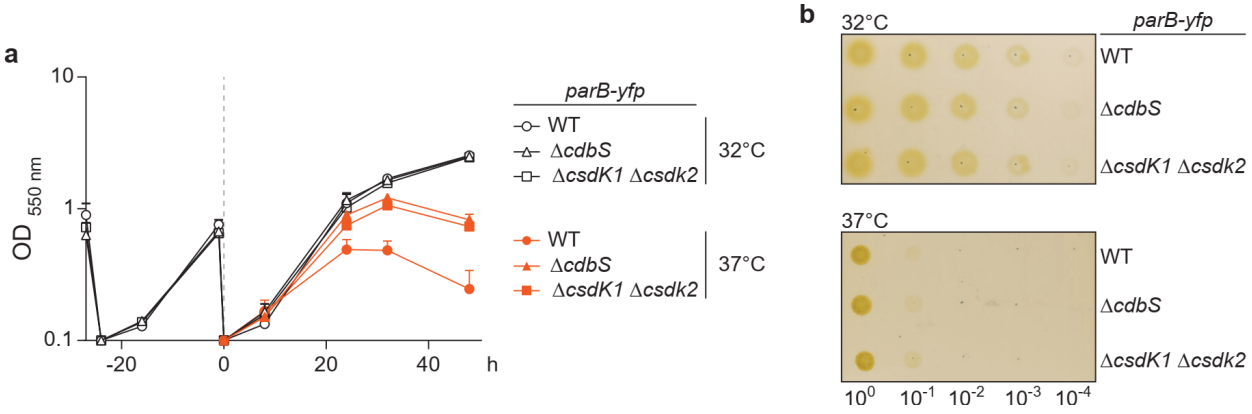

Figure 38: *M. xanthus* cells are not viable at 37°C and CdbS accelerates cell death. (a) Cells were grown in liquid CTT medium. After growth at 32°C (timepoint 0), each culture was split and either grown at 32°C or 37°. Similar results were obtained in three biological replicates. (b) Cells were grown on CTT agar for 96 h. Similar results were obtained in three biological replicates.

3 Discussion

3.1 Model of the CdbA/CdbS system

In a previous study, CdbA was identified as a c-di-GMP binding protein and characterized as an essential NAP whose DNA binding activity is ligand-binding regulated (Skotnicka *et al.*, 2020). Depletion of CdbA caused disrupted chromosome organization and segregation (Skotnicka *et al.*, 2020). As most NAPs typically are not essential, we aimed to understand how CdbA is essential in *M. xanthus*.

Using a suppressor screen with CdbA-depleted cells, we identified loss-of-function mutations in the gene for the PilZ-domain protein CdbS as suppressors of the lethal CdbA-depletion phenotype. We further showed that cells lacking CdbA as well as CdbS, or cells only lacking CdbS, are fully viable and show chromosome organization and segregation like WT under the tested conditions. This demonstrates that the essentiality of CdbA depends on the presence of CdbS, and that CdbS is a crucial player in the cell death caused by CdbA-depletion. Lack of CdbA leads to increased transcription and accumulation of CsdK1 and CsdK2, two proteins with a PilZ domain and a Hsp70 domain. The two CsdK proteins function redundantly during CdbA-depletion, resulting in ~4-fold increased CdbS accumulation. Importantly, cells overaccumuating CdbS phenocopied cells depleted of CdbA. Altogether, these observations demonstrate that while CdbA is a proposed NAP, lack of CdbA only causes major architectural and topological chromosome defects in *cdbS*$^{+}$ cells. This suggests that lack of CdbA *per se* only causes minor architectural and topological chromosome defects, and the increased CdbS level causes the major defect in chromosome organization and segregation.

Moreover, we showed that CdbS, CsdK1 and CsdK2 accumulate at an increased level at 37°C, however the level and localization of CdbA was not affected by this elevated temperature. The increased CdbS accumulation at 37°C depends on CsdK1 and CsdK2 and accelerated the disruption of chromosome organization and segregation as well as cell death at this temperature. Following these observations, we suggest two possible working models for the CdbA/CdbS system.

In model 1 (Figure 39, top), we suggest that CdbA acts as a NAP and globally binds the *M. xanthus* chromosome, thereby contributing to the correct architecture and topology of the chromosome. Upon depletion of CdbA, the chromosome undergoes minor architectural and topological changes that are sufficient to result in elevated transcription of *csdK1* and *csdK2*, and, therefore, increased accumulation of CsdK1 and CsdK2. These two proteins then facilitate the increased accumulation of CdbS, likely by stabilizing it. The elevated CdbS level then causes major defects in chromosome organization and segregation via an unknown mechanism that will be discussed in chapter 3.2.

In model 2 (Figure 39, bottom), CsdK1 and CsdK2 accumulate at an increased level during growth at 37°C, leading to an elevated CdbS level. CdbS, in turn, enhances cell death at 37°C via a mechanism involving perturbed chromosome organization and segregation, while cells lacking CdbS show delayed cell death. As we observed no noticeable change in the accumulation and localization of CdbA at 37°C, this may indicate that this pathway is independent of CdbA. Alternatively, DNA-binding of CdbA is slightly altered at the elevated temperature, possibly by a local pool of c-di-GMP, thereby causing the increased *csdK1* and *csdK2* transcription and CsdK1 and CsdK2 accumulation. This scenario will be discussed in chapter 3.5.

With the presented data and the suggested models, several questions remain open for future research. First, cells of the conditional CdbA-depletion mutant expressing *cdbA-mCh* were reported to be slightly elongated compared to WT cells but do not show a defect in chromosome organization and segregation (Skotnicka *et al.*, 2020). We observed the same phenotype, also when these mutant cells additionally lack CsdK1 or CsdK2, or both. In contrast, cells expressing *cdbA-mCh* from the vanillate promoter and lacking CdbS show WT cell length. This suggests that CdbS might affect cell length independently of chromosome organization and segregation. Following these observations, we would expect that the *cdbA-mCh* expressing CdbA-depletion mutant cells would accumulate CdbS at an elevated level compared to WT cells. However, we detected that these cells accumulate CdbS at the WT level, suggesting that another unknown factor affects cell length in these strains.

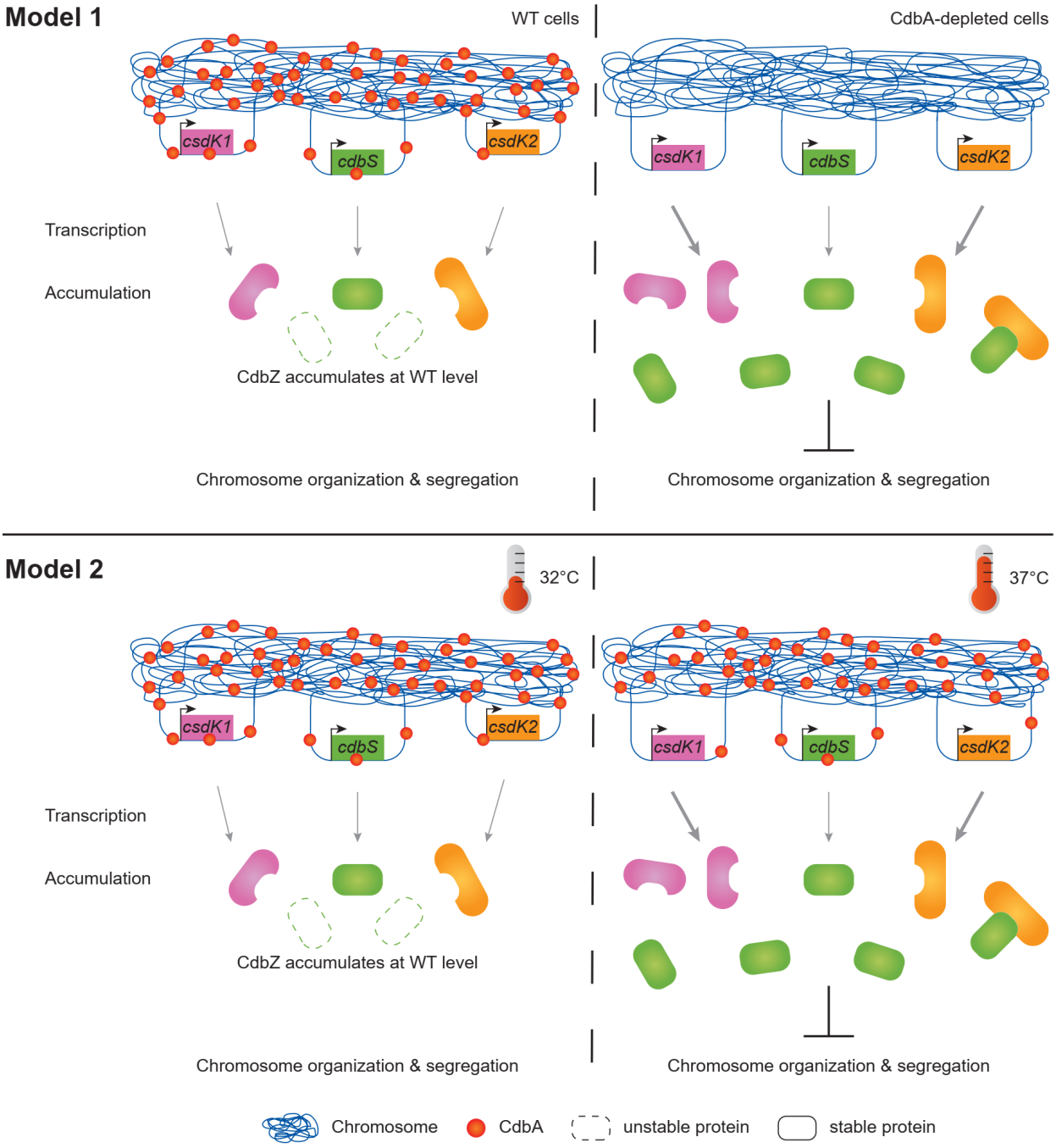

Figure 39: Two suggested working model for the CdbA/ScbS system. See text for details.

Additionally, we observed that the ~4-fold increased accumulation of CdbS during CdbA-depletion is not the result of increased transcription but occurs at the post-transcriptional or post-translational level. We demonstrated that both CsdK1 and CsdK2 are important during CdbA-depletion so that CdbS can accumulate at the elevated level. Additionally, we demonstrated that CsdK2 and CdbS interact directly. As Hsp70 chaperones can either positively promote the accumulation of their clients or negatively by targeting them for degradation, it is speculative how these PilZ-DnaK chaperones modulate the CdbS level. Under non-stress conditions, DnaK in *E. coli* facilitates the degradation of sigma factor σ^{32}. Upon heat shock, DnaK is titrated away from σ^{32} by misfolded proteins, which leads to an elevated σ^{32} level that induces the expression of heat shock genes (Gamer *et al.*, 1996, Tomoyasu *et al.*, 1998).

Hence, the CsdK proteins could either directly stabilize CdbS during CdbA-depletion or facilitate the degradation of CdbS in WT cells. In the latter instance, CdbS would be stabilized upon sequestration by other clients during CdbA-depletion. Because WT cells lacking both CsdK proteins accumulate CdbS at the WT level, we suggest that the CsdK proteins are not involved in the degradation of CdbS in WT cells. Therefore, it is more likely that the chaperones positively affect CdbS stabilization during CdbA-depletion. As our data show that the elevated CdbS accumulation is regulated on the post-transcriptional level, we hypothesize that CdbS is synthesized in a misfolded state in WT cells and is, therefore, degraded in a CsdK1/CsdK2-independent manner. When CdbA is depleted, CsdK1 and CsdK2 accumulate at an elevated level and these additional chaperones assist in refolding of CdbS, leading to its increased accumulation.

Intriguingly, a strain depleted of CdbA and both CsdK proteins still accumulated CdbS at a ~1.6-fold increased level compared to the WT, indicating that additional unknown mechanisms are involved in CdbS stabilization. As Hsp70 proteins bind misfolded clients promiscuously, we hypothesize that also other chaperones could stabilize CdbS in the absence of CdbA but to a lower extent than CsdK1 and CsdK2. This suggests CdbS is a specific client of CsdK1 and CsdK2.

3.2 The role of CdbS in chromosome biology

Cells overexpressing *cdbS* have disrupted chromosome organization and segregation, elongate and eventually undergo cell death. This combined phenotype is intriguing, as depletion of the essential chromosome-partitioning protein ParB only results in defects in chromosome segregation but not in filamentous *M. xanthus* cells (Harms *et al.*, 2013). Cells blocked in cell division form filaments but do not show defects in chromosome segregation, as also observed in this study (Harms *et al.*, 2013, Treuner-Lange *et al.*, 2013). Somewhat elongated cells with disrupted chromosome biology have been observed for strains lacking *smc* and *scpAB* (Anand *et al.*, 2020). *smc* and *scpAB* mutants were reported to have enlarged subpolar regions free of the nucleoid (Anand *et al.*, 2020), which differs from *cdbS* overexpressing cells in which the nucleoids appear to be anchored correctly. As CdbS accelerates the disruption of chromosome organization and segregation during heat stress, and Δ*cdbS* cells eventually display defective chromosome organization and segregation, we speculate that CdbS acts as an adaptor for another protein, which causes this phenotype.

In our search to identify interaction partners of CdbS, we performed in vivo pull-down experiments in cells containing CdbA, i.e. these cells have a WT level of CdbS. Under this condition, we significantly enriched DnaB as an interaction candidate. However, we found that the chromosome of *cdbS* overexpressing cells is fully replicated, indicating that the defect must be in chromosome segregation and organization. While we focused our work on investigating DnaB and proteins related to protein folding, the remaining five interaction partner candidates of CdbS are interesting targets for future research. Similarly, in future experiments it would be important to identify CdbS-interacting proteins under conditions where CdbS is over-accumulating, causing a defect in chromosome organization and segregation.

To further understand the cellular function of CdbS, it would be interesting to analyze its localization *in vivo*. So far, all localization studies of fluorescently labeled CdbS were unsuccessful as the constructs were cleaved and free fluorescent protein accumulated at a higher level than the full-length fusion proteins (data not shown).

3.3 CdbA is a NAP that also influences gene expression

CdbA was characterized as a NAP as it binds the *M. xanthus* chromosome globally with no or only minor affects on transcription, typically having a slight positive effect on gene expression (Skotnicka *et al.*, 2020). Although CdbA binds in the promoter region of *cdbS* (Skotnicka *et al.*, 2020), we demonstrated in the here presented study that CdbA does not affect its expression. In contrast, CdbA represses the transcription of *csdK1* and *csdK2* slightly but significantly, and binds in the coding region of *csdK1* and in the promoter region of *csdK2* (Skotnicka et al., 2020). Does that mean CdbA is a transcriptional regulator?

Generally, NAPs are characterized as small proteins that bind DNA with low sequence-specificity, primarily affecting the overall DNA architecture and topology by bending, bridging, or wrapping the DNA (Badrinarayanan *et al.*, 2015, Dillon and Dorman, 2010). The moderate changes in gene expression caused by NAPs were typically attributed to changes in the topology of the chromosome (Dillon and Dorman, 2010). This was proposed to separate NAPs from canonical transcription factors that usually bind to specific targets and dramatically alter gene expression.

Nevertheless, over time it has become clear that some DNA-binding proteins share traits with NAPs and transcriptional regulators. One example is FIS (Factor for Inversion Stimulation), which is typically defined as a NAP but was demonstrated to interact with RNA polymerase to activate transcription of its target promoters like canonical transcriptional regulators (Bokal *et al.*, 1997). The mIHF protein of *Mycobacterium tuberculosis* binds the chromosome non-specifically and was characterized as an essential NAP, as mIHF-depleted cells elongated and showed a defect in DNA segregation. A lack of mIHF represses the expression of many housekeeping genes involved in tRNA and DNA synthesis (Odermatt *et al.*, 2018). On the other hand, the well-studied CRP was described to be a transcription factor as it binds to promoters in a sequence-specific manner and regulates the expression of target genes. Still, it was later shown to bind the *E. coli* chromosome globally and to affect its structure (Grainger *et al.*, 2005). Today, NAPs are recognized to influence gene expression by altering the architecture and topology of the chromosome upon changes in the environment. Therefore, it becomes increasingly harder to

clearly define what a transcription factor is and what a NAP is (Dorman *et al.*, 2020, Hołówka and Zakrzewska-Czerwińska, 2020).

For CdbA, in ChIP-seq analysis, it was shown that it binds with a peak at 1972 bp upstream and 382 bp downstream of the first nucleotide of the start codon and the overlapping transcription start site and of *csdK1*, and with a peak 2 bp upstream of the first nucleotide of the start codon and the overlapping transcription start site *csdK2* (Skotnicka *et al.*, 2020). Therefore, we suggest that lack of CdbA triggers structural changes in these regions, resulting in increased the transcription of both genes.

Both CdbA and CdbS, as well as CsdK1 and CsdK2, are conserved only in some members of Myxococcales (Kuzmich *et al.*, 2021, Skotnicka *et al.*, 2020), but another essential NAP has been reported in *C. crescentus*. GapR was first characterized as an essential NAP that, when depleted or overexpressed, causes defects in cell shape and cell division without major effects on transcription (Ricci *et al.*, 2016). A following study demonstrated that GapR is vital to stimulate topoisomerase IV and gyrase activity to allow DNA replication to occur efficiently (Guo *et al.*, 2018). This shows that some NAPs have diverse functions and affect different cellular processes in addition to their conventional role in maintaining the architecture of the nucleoid. This highlights NAPs as fascinating targets for research in the future.

3.4 CdbA and CdbS share characteristics of toxin-antitoxin systems

WT cells express and accumulate CdbS, but the chromosome disruption phenotype only becomes apparent when CdbS accumulates at an elevated level in the cell. While CdbA is highly abundant, with ~7000 monomers per cell (Skotnicka *et al.*, 2020), the CdbS level is relatively low and increases significantly in the absence of CdbA. Conceptually, this is reminiscent of a toxin-antitoxin system, where an antitoxin directly blocks a toxin or protects the toxin targets from toxin activity (Unterholzner *et al.*, 2013). The toxins can affect a broad spectrum of cellular processes such as DNA replication, translation, cell shape, and cytoskeleton (Jurėnas *et al.*, 2022). One of the best-understood toxin-antitoxin systems is the CcdAB system, where the CcdB toxin blocks DNA gyrase and ultimately leads to cell death (Bernard and Couturier, 1992).

Eight different types of toxin-antitoxin systems have been described, but only five types consist solely of proteinaceous toxins and antitoxins. In a type II system, the antitoxin directly binds to the toxin to inactivate it. In a type IV system, the antitoxin counteracts the activity of the toxin. A type V antitoxin is annotated as an RNAse and degrades the transcript of the toxin, preventing its accumulation. Type VI antitoxins target their cognate toxin for degradation. In a type VII system, the antitoxin post-translationally modifies its toxin to inactivate it (Jurėnas *et al.*, 2022).

The mode of action of CdbA and CdbS does not match any currently known toxin-antitoxin systems, as no direct interaction between CdbA and CdbS was detected, and CdbA is not predicted to have RNAse activity or other enzymatic activity similar to known antitoxins (Skotnicka *et al.*, 2020). Furthermore, toxin-antitoxin systems are typically encoded in an operon or are part of a genetic island (Jurėnas *et al.*, 2022, Singh *et al.*, 2021b). *cdbA* (*mxan_4361*) and *cdbS* (*mxan_4328*) do not form an operon but are encoded 33 genes apart on the *M. xanthus* genome. In closely related species, *cdbA* and *cdbS* orthologs are also encoded in close proximity. As demonstrated, CsdK1 and CsdK2 act downstream of CdbA to facilitate an increased CdbS level. Intriguingly, tripartite toxin–antitoxin–chaperone modules have been identified, where SecB homologs act as chaperons to stabilize the antitoxin (Bordes *et al.*, 2011, Bordes *et al.*, 2016).

While CdbA is conserved in all fully sequenced Myxococcales, we identified CdbS homologs only in *Cystobacterineae* and *Nanocystineae*, indicating that the function of this system is conserved in several species. This raises the question why these soil bacteria encode a self-killing system that can be induced in the response to heat stress. Similarly, the role of chromosomal encoded toxin-antitoxin systems have been controversially discussed (Jurėnas *et al.*, 2022). However, it became clear that some chromosomal toxin-antitoxin systems act in response to environmental stresses and can increase the fitness of a population, such as the MazEF system in *E. coli*, which is upregulated during heat, oxidative and other stresses (Engelberg-Kulka *et al.*, 2006). This type II system consists of the antitoxin MazE and the toxin MazF, which is an endoribonuclease that blocks protein synthesis (Zhang *et al.*, 2005). Intriguingly, *E. coli* cells lacking MazEF are more resistant to heat stress, but are eventually not viable (Hazan *et al.*, 2004), just like *M. xanthus* cells lacking CdbS. Nevertheless, the physiological role of CdbA/CsdK1/CsdK2/CdbS remains elusive. Our data demonstrates that WT cells need to limit the accumulation of CsdK1, CsdK2 and CdbS under a certain threshold to

survive. Therefore, it is interesting to think of this system as a well-balanced unit that, when disrupted such as during heat stress or lack of CdbA, has a detrimental effect on cell viability.

3.5 The putative role of c-di-GMP in heat shock response

In this study, we identified the PilZ domain protein CdbS and showed that it binds c-di-GMP *in vitro*. However, its effect on chromosome organization and segregation appears to be c-di-GMP independent manner. Similarly, the PilZ domain protein PixA in *M. xanthus* was shown to bind c-di-GMP *in vitro*, but its role in modulating cellular reversals was independent of c-di-GMP binding under the tested conditions (Kuzmich *et al.*, 2021). Furthermore, the PilZ domain protein PlpA contains the fully conserved c-di-GMP binding motif, but was reported to not bind c-di-GMP *in vitro* (Pogue *et al.*, 2018). This suggests that the interplay between PilZ domain proteins and c-di-GMP might be more complex and not fully understood.

CdbS is a suppressor of the lethal CdbA-depletion phenotype, and CdbA was already shown to bind c-di-GMP (Skotnicka *et al.*, 2020). Without CdbA, CdbS accumulates at a higher level due to the PilZ-Hsp70 proteins CsdK1 and CsdK2, both of which have yet to be tested for c-di-GMP binding. Based on bioinformatics analyses, only CsdK2 is expected to bind c-di-GMP, and CsdK2 was also identified as a c-di-GMP receptor in the c-di-GMP capture compound pull-down that identified CdbA (Skotnicka, personal communication). In a BACTH assay, variants of CdbS and CsdK2 that are suggested not to bind c-di-GMP still interacted, indicating that this interplay may not rely on c-di-GMP. Taken together, we have identified three c-di-GMP-associated proteins that work together to disrupt chromosome biology eventually, but seemingly in a c-di-GMP binding independent manner. This raises the question of the role of the second messenger in this system.

During growth, *M. xanthus* accumulates c-di-GMP at a constant level during the exponential and stationary phase, but the level increases significantly during starvation-induced development (Skotnicka *et al.*, 2016a, Skotnicka *et al.*, 2016b). Therefore, it was interesting to test whether CdbS acts during development. However, we observed that the CdbS level decreases upon starvation. Instead, we detected an increased accumulation of CdbS when cells were incubated at 37°C, eventually leading to cell death. In addition, CsdK1 and CsdK2

accumulate at an elevated level at 37°C. However, the CdbA level and localization were unaffected. Hence, it is intriguing to speculate whether c-di-GMP serves as a signaling molecule during heat shock.

The first indication of a link between c-di-GMP and temperature was reported in *V. cholerae*, which shows biofilm formation due to increased c-di-GMP synthesis at low temperatures (Townsley and Yildiz, 2015). In the same study, it was observed that also *P. aeruginosa* accumulates c-di-GMP at an elevated level at low temperatures, but *Listeria monocytogenes* does not (Townsley and Yildiz, 2015). In another study, the protein Bp1026b_II2523 was proposed as a putative thermoregulated DGC that promotes biofilm formation at 30°C but limits it at 37°C; however, the molecular mechanism was unknown (Plumley *et al.*, 2017). More evidence followed with the identification of TdcA, a protein with the GGEEF motif and a PAS domain, as a thermosensory DGC in *P. aeruginosa*, as it was reported to have an up to 100-fold increased catalytic rate in synthesizing c-di-GMP over a 10°C change (Almblad *et al.*, 2021). Fusing PAS_{TdcA} with other enzymatically active proteins rendered those protein chimeras temperature-sensitive, indicating that PAS_{TdcA} is the part of the protein that transduces a signal in response to temperature changes (Almblad *et al.*, 2021).

The closest homolog of TdcA in *M. xanthus* is Mxan_5791, which is annotated as a DGC with a receiver domain and was previously shown to be dispensable for motility, EPS accumulation, and development (Skotnicka *et al.*, 2016a, Skotnicka *et al.*, 2016b). Of note, two of the 18 DGCs in *M. xanthus* are predicted to have the PAS domain: TmoK and Mxan_4257, both of which lack critical residues for catalytic activity with c-di-GMP synthesis (Skotnicka *et al.*, 2016a). It remains interesting to test whether Mxan_5791 acts as a thermoregulated DGC.

So far, only metabolically active DGCs have been proposed as temperature regulated. All proteins investigated in the present study are receptors, so how could c-di-GMP fit into this system? For CdbA, it was reported that it binds DNA and c-di-GMP in a mutually exclusive manner and that c-di-GMP might fine-tune DNA-binding *in vivo* (Skotnicka *et al.*, 2020). We demonstrated that CdbS, CsdK1 and CsdK2 all accumulate at an increased level when *M. xanthus* is grown at 37°C, but also when cells lack CdbA. However, CdbA accumulation was seemingly unaffected at 37°C. Following these observations, we propose two different hypotheses for this system during heat stress: Either, the increased accumulation of CsdK1 and CsdK2 at 37°C is independent of

CdbA, and the synthesis of the chaperones is regulated by an unknown mechanism. Alternatively, we speculate that elevated temperatures trigger an increased c-di-GMP level in *M. xanthus*, which has already been observed in other bacteria such as *P. aeruginosa* (Almblad *et al.*, 2021). This altered c-di-GMP then might cause reduced DNA-binding by CdbA. Of note, a strain with a ~7-fold increased c-di-GMP level due to overexpression of a heterologous DGC was reported to not show defects in cell length and chromosome organization (Skotnicka *et al.*, 2016a). Hence, we hypothesize that the binding of CdbA to DNA might be controlled via a local c-di-GMP pool, which could be created in response to heat shock. Alternatively, a simple increase in the cellular level of c-di-GMP is not sufficient to cause induction of *csdK1* and *csdK2* transcription. Nevertheless, we speculate that at elevated temperatures, a local c-di-GMP pool is generated at specific locations of the chromosome that titrate specific clusters of CdbA away from the chromosome. This modulates the expression of *csdK1* and *csdK2*, and the respective proteins accumulate at an increased level. Both chaperones then allow CdbS to accumulate at an increased level, which accelerates the disruption of chromosome organization and segregation via an unknown mechanism.

4 Material & Methods

4.1 Reagents, kits and equipment

Table 3: Reagents, enzymes and antibodies used in this study

Reagents	Supplier
Chemicals	Roth (Karlsruhe), Merck (Darmstadt), Sigma-Aldrich (Taufkirchen)
Media components, agar	Roth (Karlsruhe), Merck (Darmstadt), Difco (Heidelberg), Invitrogen (Darmstadt)
ROTILAB®GelRed	Roth (Karlsruhe)
1 kB Plus DNA Ladder	New England Biolabs (Frankfurt a. M.)
6x gel loading dye	New England Biolabs (Frankfurt a. M)
PageRuler™ Plus Prestained Protein Ladder	Thermo Scientific (Dreieich)
Oligonucleotides	Eurofins MWG Operon (Ebersberg)
Antarctic Phosphatase	New England Biolabs (Frankfurt a. M)
Phusion High-Fidelity DNA Polymerase	Thermo Scientific (Dreieich)
RedTaq DNA Polymerase Master Mix	VWR International (Darmstadt)
Restriction Enzymes	New England Biolabs (Frankfurt a. M)
T4 DNA Ligase	New England Biolabs (Frankfurt a. M)
Carbenicillin disodium salt, chloramphenicol, gentamycin sulfate, kanamycin sulfate, oxytetracycline dehydrate, streptomycin sulfate, tetracycline hydrochloride	Roth (Karlsruhe)
SeaKem LE agarose	Lonza (Basel, Switzerland)
InstantBlue® Coomassie Protein Stain	Abcam (Camebridge, UK)
Amersham™ Protran™ Nitrocellulose 0.2 µm membrane	Cytiva (Marlborough, USA)
Luminata Western HRP Substrate	Merck Millipore (Darmstadt)
cOmplete protease inhibitor EDTA-free	Roche Diagnostics GmbH (Mannheim)
anti-FLAG® M2 magnetic beads	Merck Millipore (Darmstadt)
2'-Biotin-16-c-diGMP	BioLog (Bremen)

Table 4: Kits used in this study

Kits	Supplier
Bacterial Adenylate Cyclase Two-Hybrid System Kit	Euromedex (Souffelweyersheim, France)
MasterPure™ DNA Purification Kit	Epicentre Biotechnologies (Wisconsin, USA)

NucleoSpin® Gel and PCR Clean-up Kit	Macherey-Nagel (Düren)
NucleoSpin® Plasmid Kit	Macherey-Nagel (Düren)
LunaScript® RT SuperMix Kit	New England Biolabs (Frankfurt a. M)
Luna® Universal qPCR Master Mix	New England Biolabs (Frankfurt a. M)

Table 5: Equipment used in this study

Device	Manufacturer	Application
Amicon® Ultra-4 3K centrifugal unit	Merck	Concentration of protein sample
Äkta pure with Fraction Collector F9-C - 5 ml HiTrap Chelating HP - 5 ml HiTrap SP HP	GE Healthcare Europe GmbH (Freiburg)	Affinity purification of recombinant and anion-exchange chromatography
BLItz™ system - Streptavidin SA biosensor	forteBio (Fremont, USA)	Biolayer interferometry
Avanti J-26 XP, Centrifuge 5424 R Multifuge 1 S-R	Beckman Coulter (Krefeld), Eppendorf (Hamburg), Heraeus/Thermo Scientific (Dreieich)	Centrifugation
UP200St sonifier	Hielscher Ultrasonics GmbH (Teltow)	Cell disruption
Fuji Photo Film FPM 100A Luminescent image analyser LAS-4000	Fujifilm (Düsseldorf)	Chemiluminescence detection
E-BOX VX2 imaging system	PeqLab (Erlangen)	DNA illumination
MicroPulser Electroporator	Bio-Rad (Munich)	Electroporation
Q Exactive Plus Hybrid Quadrupole-Orbitrap Mass Spectrometer	Thermo Scientific (Dreieich)	Mass spectrometry
DM IRE2 Inverted microscope	Leica Microsystems (Wetzlar)	Microscopy
Hamamatsu ORCA-flash V2 Digital CMOS camera	Hamamatsu Photonics (Hersching)	Microscope camera
DS-11 spectrophotometer	DeNovix (Wilmington, USA)	Nucleic acid quantification
Ultrospec 2100 pro Spectrophotometer	Amersham Biosciences (Munich)	Determination of optical densities
Mastercycler® nexus X2	Eppendorf (Hamburg)	Polymerase chain reaction
7500 Real-Time PCR system	Applied Biosystems (Darmstadt)	qRT-PCR
Mini-PROTEAN® electrophoresis chambers	Bio-Rad (Munich)	Protein gel electrophoresis
ThermoMixer® C	Eppendorf (Hamburg)	Heating block

TransBlot® Turbo™Transfer System	Bio-Rad (Munich)	Western Blotting

Table 6: Software used for data acquisition and analysis

Software	Supplier	Application
Alphafold PyMOL	(Jumper *et al.*, 2021) Schrödinger LLC (New York, USA)	Protein structure prediction and visualization
Metamorph® v 7.5	Molecular Devices (Union City, USA)	Microscopy image processing
LAS X	Leica Microsystems (Wetzlar)	Microscopy image acquisition
MATLAB R2020a	MathWorks (Natick, USA)	Fluorescence microscopy image data analysis
MEGA-X	(Kumar *et al.*, 2018)	Generation of alignments and phylogenies
Oufti	(Paintdakhi *et al.*, 2016)	Fluorescence microscopy image analysis
Perseus	(Tyanova *et al.*, 2016)	Proteomic data analysis
Snapgene®	GSL Biotech LLC (San Diego, USA)	*In silico* cloning of plasmids

4.2 Media

Table 7: Media

Medium	Composition
CTT	1% (w/v) Bacto casitone 10 mM Tris-HCl pH 8.0 1 mM potassium phosphate buffer pH 7.6 8 mM $MgSO_4$
LB	1% (w/v) tryptone 0.5% (w/v) yeast extract 1% (w/v) NaCl
TPM	10 mM Tris-HCl pH 7.6 1 mM KH_2PO_4 pH 7.6 8 mM $MgSO_4$
2xYT	1.6% (w/v) tryptone 1% (w/v) yeast extract 0.5% (w/v) NaCl

For TPM agarose slides, 1% (w/v) SeaKem LE agarose (Lonza) was added to TPM. To prepare agar plates using the media listed in Table 7, 1.5% (w/v) agar was added to the respective medium. If required, the respective antibiotic or additive was added.

Table 8: Additives for growth media

Additive	Solvent	Final concentration
Carbenicillin	H_2O	100 µg/ml
Cephalexin	H_2O	35 µg/ml
Galactose	H_2O	2.5% (v/v)
Gentamycin	H_2O	10 µg/ml
Kanamycin sulfate	H_2O	50 µg/ml
Oxytetraclycine	0.1M HCl	10 µg/ml
Streptomycin	H_2O	20 mg/ml
Tetracycline	99.99% EtOH	15 µg/ml
Vanillate (pH 7.6, KOH)	H_2O	500 µM
IPTG	H_2O	0.5 mM
X-Gal	DMF	40 µg/ml

4.3 Microbiological methods

4.3.1 *E. coli* strains

Table 9: *E. coli* strains used in this study

Strain	Genotype	Reference
ArcticExpress(DE3) RP	*E. coli B F⁻ ompT hsdS(r_B- m_B-) dcm+ (TetR) gal endA Hte* [*cpn10 cpn60 (Gent^R)*] [*argU proL (StrR)*]	Agilent Technologies (Waldborn)
NEB Turbo	*F⁻ proA⁺B⁺ lacI^q ΔlacZM15 / fhuA2 Δ(lac-proAB) glnV galK16 galE15 R(zgb- 210::Tn10)Tet^S endA1 thi-1 Δ(hsdS-mcrB)5*	New England Biolabs (Frankfurt a. M.)
BTH101	F⁻ *cya-99 araD139 galE15 galK16 rpsL1 (Str^R) hsdR2 mcrA1 mcrB1*	Euromedex (Souffelweyersheim, France)

4.3.2 M. xanthus strains

Table 10: *M. xanthus* strains used in this study

Strain	Genotype	Reference
DK1622	WT	(Kaiser *et al.*, 1979)
SA5690	Δ*cdbA*; *mxan18-19*::P_{van} *cdbA-mCh*	(Skotnicka *et al.*, 2020)
SA5691	Δ*cdbA*; *mxan18-19*::P_{van} *cdbA-mCh*; *parB⁺/attB::P_{nat} parB-YFP*	(Skotnicka *et al.*, 2020)
SA5693	*parB⁺/attB::P_{nat} parB-YFP*	(Skotnicka *et al.*, 2020)
SA8813	*cdbA::cdbA-FLAG*	(Skotnicka *et al.*, 2020)

SA10209	Δ*cdbA*; *mxan18-19*::P_{van} *cdbA-mCh*; *cdbS::cdbS-FLAG; parB*$^{+}$/*attB::*P_{nat} *parB-YFP*	This study
SA10217	*cdbS::cdbS-FLAG; parB*$^{+}$/*attB::*P_{nat} *parB-YFP*	This study
SA10220	Δ*cdbS; parB*$^{+}$/*attB::*P_{nat} *parB-YFP*	This study
SA10225	∆*cdbS*; *mxan18-19*::P_{van} *cdbS-FLAG*; *parB*$^{+}$/*attB::*P_{nat} *parB-YFP*	This study
SA10226	∆*cdbS*; *mxan18-19*::P_{van} *cdbS*^{R9A}*-FLAG*; *parB*$^{+}$/*attB::*P_{nat} *parB-YFP*	This study
SA10249	*cdbS::cdbS-FLAG*; Δ*csdK1; parB*$^{+}$/*attB::*P_{nat} *parB-YFP*	This study
SA10251	*cdbS::cdbS-FLAG*; Δ*csdK2; parB*$^{+}$/*attB::*P_{nat} *parB-YFP*	This study
SA10260	*cdbA::cdbA-mCh; parB*$^{+}$/*attB::*P_{nat} *parB-YFP*	This study
SA10262	Δ*cdbA*; *mxan18-19*::P_{van} *cdbA-mCh*; *cdbS::cdbS-FLAG;* Δ*csdK1; parB*$^{+}$/*attB::*P_{nat} *parB-YFP*	This study
SA10264	Δ*cdbA*; *mxan18-19*::P_{van} *cdbA-mCh*; *cdbS::cdbS-FLAG;* Δ*csdK2; parB*$^{+}$/*attB::*P_{nat} *parB-YFP*	This study
SA10267	*cdbS::cdbS-FLAG*; Δ*csdK1*; Δ*csdK2; parB*$^{+}$/*attB::*P_{nat} *parB-YFP*	This study
SA10270	Δ*cdbA*; *mxan18-19*::P_{van} *cdbA-mCh*; *cdbS::cdbS-FLAG;* Δ*grpS; parB+/attB::*P_{nat} *parB-YFP*	This study
SA10273	Δ*cdbA*; *mxan18-19*::P_{van} *cdbA-mCh*; *cdbS::cdbS-FLAG;* Δ*mxan_1092; parB+/attB::*P_{nat} *parB-YFP*	This study
SA10274	*cdbA::cdbA-mCh; cdbS::cdbS-FLAG; parB+/attB::*P_{nat} *parB-YFP*	This study
SA10275	*cdbA::cdbA-mCh;* ∆*cdbS*; *mxan18-19*::P_{van} *cdbS-FLAG*; *parB+/attB::*P_{nat} *parB-YFP*	This study
SA10277	Δ*cdbA*; *mxan18-19*::P_{van} *cdbA-mCh*; *cdbS::cdbS-FLAG;* Δ*csdK1;* Δ*csdK2; parB+/attB::*P_{nat} *parB-YFP*	This study
SA10288	*csdK1::csdK1-mV*	This study
SA10289	*csdK2::csdK2-HA*	This study
SA11494	*attB::*P_{pilA} *gfp-FLAG*	Dr. Anke Treuner-Lange
SA12204	Δ*cdbA*; *mxan18-19*::P_{van} *cdbA-mCh*; *csdK1::csdK1-mV*	This study
SA12205	Δ*cdbA*; *mxan18-19*::P_{van} *cdbA-mCh*; *csdK2::csdK2-HA*	This study
SA12206	Δ*cdbA*; mxan18-19::P_{van} *cdbA-mCh*; Δ*cdbS; parB+/attB::*P_{nat} *parB-YFP*	This study
SA12209	Δ*cdbA*; *mxan18-19*::P_{van} *cdbA-mCh*; *cdbS::cdbS-FLAG;* Δ*mxan_0750; parB+/attB::*P_{nat} *parB-YFP*	This study
SA12222	Δ*cdbA*; mxan18-19::P_{van} *cdbA-mCh*; Δ*cdbS; attB::*P_{nat} *cdbS-FLAG::*P_{nat} *parB-yfp*	This study
SA12238	*dnaB::dnaB*^{A116V}; *parB+/attB::*P_{nat} *parB-YFP*	This study

4.3.3 Bacterial cultivation methods

E. coli cells were grown in liquid LB medium with 220 rpm horizontal shaking or on LB agar plates at 37°C. The optical densities of the cultures were determined photometrically at 600 nm. For long-term storage, 1 ml of an overnight culture was harvested, resuspended in 900 µl fresh LB, and supplemented with 100 µl 75% (w/v) glycerol. After shock-freezing in liquid nitrogen, the cells were stored at -80°C.

M. xanthus cells were grown in liquid CTT media in the dark with 220 rpm horizontal shaking or on CTT agar plates at 32°C. In general, gentamycin was added in all CTT media. The optical densities of the cultures were determined photometrically at 550 nm. For long-term storage, 10 ml of an overnight culture were harvested, resuspended in 900 µl fresh CTT, and supplemented with 100 µl 75% (w/v) glycerol. After shock-freezing in liquid nitrogen, the cells were stored at -80°C.

4.3.4 Development assay under submerged conditions to test CdbS-FLAG accumulation

Exponentially growing cells were harvested to an $OD_{550\ nm}$ of 0.875 via centrifugation at 11000 rpm for 1 min and resuspended in MC7 buffer (10 mM MOPS pH 7.0, 1 mM $CaCl_2$). From this mix, 400 µl were placed in a well of a 15 mm microtitre dish and incubated at 32°C. After the indicated time points, the cells were harvested in a total volume of 1 ml MC7. Cells were then centrifuged and resuspended in SDS loading buffer to an $OD_{500\ nm}$ of 14.

4.3.5 Stress conditions to test CdbS-FLAG accumulation

To test for protein accumulation during different stress conditions, 5 ml CTT per condition of interest were inoculated with exponentially growing cells to an $OD_{500\ nm}$ of 0.1. To check accumulation at different temperatures, the culture was then incubated at either 15°C, 32°C or 37°C for 18 h. To check for the accumulation with limited nutrients, the culture was grown in EZ minimal medium (Teknova, Hollister, USA). To induce DNA damage, 20 µg/ml mitomycin c or 20 µg/ml nalidixic acid were added to the culture for 18 h, or 1 ml of concentrated cells was treated with 500 J UV light for 10 s before inoculation. To induce osmotic stress, 300 mM NaCl was added to the culture for 18 h. To induce oxidative stress, the cells were treated with 1.5 mM H_2O_2 for 30

min before washing twice in CTT with a following recovery time of 18 h, similar but slightly modified to Pan *et. al*, 2020.

4.3.6 BACTH assay

The respective full-length genes of interest were cloned into the appropriate vectors to construct N- and C-terminal fusions with the T18 and T25 fragments of the adenylate cyclase from *Bordetella pertussis*. 20 ng of a plasmid containing a gene of interest fused to the T18 fragment and 20 ng of a plasmid containing a second gene of interest fused to the T25 fragment were co-transformed respectively into *E. coli* BTH101 cells. The cells were plated on LB agar plates containing Streptomycin, Kanamycin, Carbenicillin, X-Gal and 0.5 mM IPTG. The plate was incubated over night at 32°C. As a positive control, the pUT18C-zip and pKNT25-zip plasmids (Euromedex) were co-transformed. To study and compare protein interactions, two to three colonies of each combination were inoculated into 200 µl LB containing Streptomycin, Kanamycin and Carbenicillin and incubated for 4-6 h at 32°C while shaking. Of each culture, 2 µl were spotted onto LB agar plates containing Streptomycin, Kanamycin, Carbenicillin, X-Gal and 0.5 mM IPTG. After incubation at 32°C for 24 h, the plates were further incubated at 4°C for 48 h to intensify colouration of the colonies before a picture of the plate was taken. The experiment was performed in two biological replicates with two technical parallels.

4.3.7 Fluorescence microscopy and image analysis

For live-cell imaging, a *M. xanthus* overnight culture was diluted to an OD_{550} of 0.1 and grown for 24h until they reached an OD_{550} of 0.5 - 0.7. If required, 395 µl of cell culture were stained with 5 µl 80 µg/ml DAPI and incubated for 10 min at 32°C with shaking in the dark. 5 µl of culture were mounted onto a 1.5% TPM agarose patch. The cell spot was covered with a 0.17 mm coverslip, and cells were allowed to attach. A Leica DMi8 inverted microscope was used for imaging. Phase contrast and fluorescence snapshots were taken using a Hamamatsu ORCA-flash V2 Digital CMOS camera. For image processing, Metamorph_ v 7.5 (Molecular Devices) was used. Using a custom-made Matlab R2020a (MathWorks) script, cells and fluorescent signals were detected automatically using Oufti48.

4.4 Molecular methods

4.4.1 Plasmids and oligonucleotides

Table 11: Primers used for cloning

Primer	Sequence	Purpose
CdbS_E	GAGGCGCTCCAGTACATCGC	EF/GH primers for *cdbS*
CdbS_F	CCGCCAACATCCTGTCGCAG	
CdbS_G	ACCTCCGTTTCGACAAGGTC	
CdbS_H	GTCGTCCTGCGTCTCATAGG	
CdbA_E	GAAGCCGGAGTCGCTC	EF/GH primers for *cdbA*
CdbA_F	GCCAGCCGAAAGGCTC	
CdbA_G	CAGTCGCTGTACTTCCCC	
CdbA_H	CTCGTCGCCAGTCACA	
CsdK1_E	CACCTTCACCGCGTCCACGC	EF/GH primers for *csdK1*
CsdK1_F	GGGCTCCGCGCCGCAGAA	
CsdK1_G	TTCCCCCGGTTCCTCCCAAT	
CsdK1_H	ATGGAGGGCACCGTGTTGTG	
CsdK2_E	TGTGAACCACGCCAGGCTGCC	EF/GH primers for *csdK2*
CsdK2_F	GCAGTGCCCGTCCTCGCGCTT	
CsdK2_G	AAGGGCTTCCCCAAGTGCGCC	
CsdK2_H	TTGAGCTCGCGGTTGAGACCG	
4328 fw_NdeI	ATGCATATGATGTTTGAGCGTCCTCACGA	Overexpression of His-CdbS or His-CdbS^{R9A}
oMS002	ATGTCTAGAATGTTTGAGCGTCCTCACGAGCGCGCGTCCCACCTC	
oMS004	GTTAAGCTTTCAGTGCATCACCCGCTCGCGGTCG	
oMS041	GAGGAATTCTCACTTGTCGTCGTCGTCCTTG	Amplification of FLAG fragments
oMS024	GATAAGCTTGGTTCAGCCCGGAATCGTGCC	In-frame insertion of *cdbS-FLAG*
oMS013	CTGCCCGCCGCGCTGCCCGCGCTGCCGTGCATCACCCGCTCGCGGTC	
oMS025	GCGGGCAGCGCGGCGGGCAGCGGCGAGTTCGACTACAAGGACGACGACGACAAGTGACGTCCGCCCGGGGCCCGTGAGG	
oMS026	CAGTGAATTCGAGCTCATCCCGGACATC	
oMS068	CCTTCTAGAGAGGCGTGTCATCGTCACCCG	Generation of pMS047
oMS069	GCCTGCATGCTCACTTGTACAGCTCGTCCA	
oMS070	TACGAATTCGAGCTCGGTACCGGGGATCCTCTAGAGTCGACCTGCAGGCATGCAAGCTTGGCAC	Generation of pMS048
oMS071	GTGCCAAGCTTGCATGCCTGCAGGTCGACTCTAGAGGATCCCCGGTACCGAGCTCGAATTCGTA	
oMS082	GCCAAGCTTCGGACCGCGGTGGAATGGAG	In-frame insertion of *cdbA-mCh*
oMS083	TCTTCTAGAGGATCCCTCCTCCCGAGGGTCCTGGC	
oMS084	GAGGGATCCTCTAGAAGATCTGCTAGCGGCAGCGCGGCGGGCAGCGGCATGGTGAGCAAGGGCGAGGAG	
oMS085	GTCCGTCGTAGCCATCCGTCGTTACTTGTACAGCTCGTCCATG	

oMS086	CATGGACGAGCTGTACAAGTAACGACGGATGGCTACG ACGGAC	
oMS087	AGTGAATTCGAGACGGCTATGGCACGGCGC	
oMS092	GCCAAGCTTATCGGTTATACGGACATCAAG	In-frame deletion of *mxan_0750*
oMS093	CTTCACCTTGGCGATGTCGCGTTTCTGACCCGCCGC	
oMS094	ATCGCCAAGGTGAAGGAGCTG	
oMS095	AGTGAATTCGAAGAAGAGGACGCCGGCCTG	
oMS096	CAACCCTGCGGACAGGTTCAG	EF/GH primers for *mxan_0750*
oMS097	GGCGTCATCCGCCCGCGAATG	
oMS098	GAAATCTGTCTCCGCGCAGGA	
oMS099	CTCCGCGAACTTCTCCAGCAG	
oMS100	GCCAAGCTTGAGCGCCTCCTCAAGGAAGTG	In-frame deletion of *grpS*
oMS101	GGAAGAGTTCTCGGACTTGTCGTTCGAGCCGGCCAC	
oMS102	GTCCGAGAACTCTTCCGGGGGGAGTCAG	
oMS103	CAGTGAATTCGCAGGACACTGAGCCCGGCGA	
oMS104	GATGACTGCCCCATGGAGGAG	EF/GH primers for *grpS*
oMS105	AGCTCCAGGATGGAGATATCG	
oMS106	CATTGACGCGGCGGTTCGCAG	
oMS107	CTCGGTGTCGGTCGTGGCGGTG	
oMS116	GCCAAGCTTATGATGCGCGACAGACGTCCG	In-frame deletion of *mxan_1092*
oMS117	GACTTCGATGACGCGGGCGGAGTTGAACGGATTGCGA GTCTGCAT	
oMS118	CGCGTCATCGAAGTCAAGGTC	
oMS119	AGTGAATTCCCTGCGCACGTTCCTCATCAC	
oMS120	GCACCAGCGTCTTGCCGTTGTC	EF/GH primers for *mxan_1092*
oMS121	CAGCGGAATCATGCAGCAAGAG	
oMS122	CGAGCTGACGCAGCCCATGTG	
oMS123	GTCAGCGTCAGCACACCCTGC	
oMS177	GCCAAGCTTGACGAAGAGCTACACCCTG	In-frame insertion of *csdK1-mV*
oMS231	CCGCGCTGCCCGCGCTGCCGGCTCTTCCGAACAACCC	
oMS194	CGGGCAGCGCGGCGGGCAGCGGCGAGTTCATGGTGA GCAAGGGCGAG	
oMS232	CGCAGTGCGCGTTTTCACTTGTACAGCTCGTCCATG	
oMS228	GAAAACGCGCACTGCGTG	
oMS180	CAGTGAATTCCGCGAGTGAGAGGATGC	
oMS182	GCCAAGCTTGTCAACGCGGACGAAGCC	In-frame insertion of *csdK2-HA*
oMS183	TGGGACGTCGTATGGGTACTTCCTGCCCAGCGCCT	
oMS184	TACCCATACGACGTCCCAGACTACGCTTGATGGTCACA TCCTCAATTCGAAAAG	
oMS185	CAGTGAATTCCGCTGGAGCACCGACAAC	
oMS187	GATAAGCTTGTGGTGCCCATCGCGTC	In-frame insertion of *dnaB-sGFP*
oMS188	CCGCGCTGCCCGCGCTGCCCTCGCTCCGCGACCGGC TC	
oMS029	GCGGGCAGCGCGGCGGGCAGCGGCGAGTTCATGAGC AAAGGAGAAGAACTT	
oMS193	GAACACGGAGGGCTGTTATTTGTAGAGCTCATC	
oMS189	CAGCCCTCCGTGTTCGCG	
oMS190	GTAGAATTCCCACCACCAGTCGGTGC	
oMS191	GCATCGGCAAGACGTCC	

oMS192	CGGTGAAGTGCGGCATG	EF primers for *dnaB*
oMS068	CCTTCTAGAGAGGCGTGTCATCGTCACCCG	Amplification for the insert of pMS102
oMS211	CTGTTCGCATATGTCACTTGTACAGCTCGTCCA	
oMS212	AAGTGACATATGCGAACAGAAAGTAATCGTATGCTCTG CGGGGTGAAGAC	
oMS131	GACTCTAGAGATGTTTGAGCGTCCTCACGAG	BACTH CdbS
oMS132	GCTCGGTACCTTGTGCATCACCCGCTCGCGGTC	
oMS133	GACTCTAGAATTGACGGAATCGAATCAGGCG	BACTH CsdK1
oMS134	CTCGGTACCTTGGCTCTTCCGAACAACCCCTTG	
oMS135	GACTCTAGAAGTGGTCTGCCCACCTGTCGAC	BACTH CsdK2
oMS136	ATTGAATTCTTCTTCCTGCCCAGCGCCTTCTT	
oMS141	ATTGAATTCTTAGTTCTTCCTGCCCAGCGCCTTCTT	
oMS137	GACTCTAGAAATGTCAGCGGCGGCGGGTCAG	BACTH Mxan_0750
oMS138	CTCGGTACCTTGCCGAACAGCTCCTTCACCTT	
oMS139	GACTCTAGAAGTGCGCGCCGTGGCCGGCTCG	BACTH GrpS
oMS140	CTCGGTACCTTCTGACTCCCCCCGGAAGAGTT	
oMS154	GACTCTAGAGATGGAGAACGTCCACGAG	BACTH DnaB
oMS155	CTCGGTACCAGCTCGCTCCGCGACCGGCTC	
oMS204	GATCAAGGCAGGGCCACCACGGACAGG	Amplification of csdK2^{R38A}
oMS205	CCTGTCCGTGGTGGCCCTGCCTTGATC	
oMS206	GTAGAATTCGGGCTCACGTCCTCGGCCA	Amplification of certain CsdK2 domains
oMS207	GTATCTAGAAGACTACAAGGACGACGACGACAAGCTG GACATCGATGAGCC	
oMS208	GTAGAATTCCTATGGGCTCACGTCCTCGGCCAG	

Table 12: Primers used for colony PCRs and sequencing

Test-Primer	**Sequence**
mxan18-19 C fwd	CCCACGGAGAGCTGCGTGAC
mxan18-19 C rev	GAGAAGGGTGCCGTCACGTC
mxan18-19 P rev	CCCTGGCCGCCATTCGTAAC
mxan18-19 P pDS75 rev	GTCTGACGCTCAGTGGAAC
attB left	CGGCACACTGAGGCCACATA
attB right	GGAATGATCGGACCAGCTGAA
attP left	GGGAAGCTCTGGGTACGAA
KA231	GGATGTGCTGCAAGGCGATTAAGTTGG
KA232	GCTTTACACTTTATGCTTCCGGCTCG
KA254	GTGCGCACCTGGGTTGGCATGCG
pKNT25 fwd	TCCGGCTCGTATGTTGTGTG
pKNT25 rev	CGCCACGGCCTTGATGCCAT
pKT25 fwd	GGCGATTCGGTGACCGATTA
pKT25 rev	GGGTTTTCCCAGTCACGACG
pMR369X fwd	CTCCCTCGACTCGTCCCCATG
pMR369X rev	GAACTAGTGGATCCCCCGGGCTGC
pUT18 fwd	TCCGGCTCGTATGTTGTGTG
pUT18 rev	ATTCATGTCGCCGTCGTAGC
pUT18C fwd	CTGGAAACGGTGCCGGCGTC

pUT18C rev	AGCAGACAAGCCCGTCAG
T7	TAATACGACTCACTATAGGG
T7 term	CTAGTTATTGCTCAGCGGT

Table 13: RT-qPCR Primers

Test-Primer	Sequence
cdbS qPCR fwd	CCGTTTCGACAAGGTCTTCA
cdbS qPCR rev	GGACCTCCACGAACATGC
3778_ter 1 qPCR fwd	TTCCACTATGAGATCGCGGC
3778_ter 1 qPCR rev	CTGATGGCCCAACTGGTTCT
6605 qPCR fwd	GGGGATCGAGGGGTCAAAAC
6605 qPCR rev	GCTTCAGCTTCA
rpsS qPCR fwd	GTTCGATCAAGAAGGGTCCGT
rpsS qPCR rev	GACGAACACCGGGATGAACT
ori 1/dnaA fwd	AACCTCATCTGGGAGCGAGA
ori 1/dnaA rev	TTGCCGAGGAACTGGATGTC
ori 2/7483 fwd	TGCCCACCATCAATCCATCC
ori 2/7483 rev	TGAGTTCCTGACGCTTGGTG
ter 2/4058 fwd	GACGCCCTCAAGGACCTG
ter 2/4058 rev	TTCGTACTTCGCGAGCAGAT

Table 14: Plasmids used in this study

Plasmid	Description	Reference
pBJ114	*galK*, Kan^R	(Julien *et al.*, 2000)
pET28a(+)	expression vector, Kan^R	Novagen® Merck (Darmstadt)
pMR3691	*mxan18-19* site integration, *vanR*-P_{van}, Tet^R	(Iniesta *et al.*, 2012)
pSW105	Mx8 *attB* site integration, P_{pilA}, Kan^R	(Jakovljevic *et al.*, 2008)
pSWU19	Mx8 *attB* site integration, Kan^R	(Wu and Kaiser, 1995)
pSWU30	Mx8 *attB* site integration, Tet^R	(Wu and Kaiser, 1997)
pUT18	BACTH plasmid, *cyaAT18* N-terminal fusion, Amp^R	Euromedex (Souffelweyersheim, France)
pUT18C	BACTH plasmid, *cyaAT18* C-terminal fusion, Amp^R	
pKNT25	BACTH plasmid, *cyaAT25* N-terminal fusion, Kan^R	
pKT25	BACTH plasmid, *cyaAT25* N-terminal fusion, Kan^R	
pDJS94	pBJ114; Δ*csdK2*, Kan^R	(Kuzmich *et al.*, 2021)
pDJS151	pSWU19; P_{nat} *parB-eYFP*, Kan^R	(Skotnicka *et al.*, 2020)
pDS80	pDS75; P_{nat} *pomZ*^{D90A}, Tet^R	(Schumacher *et al.*, 2017)
pSK42	pBJ114; Δ*csdK1*, Kan^R	(Kuzmich *et al.*, 2021)
pMS007	pET28a(+); His_6-*cdbS*, Kan^R	This study
pMS008	pET28a(+); His_6-*cdbS* R9A, Kan^R	This study
pMS018	pBJ114; *cdbS-FLAG*, Kan^R	This study
pMS024	pMR3691; Pvan *cdbS-FLAG*, Tet^R	This study

pMS026	pMR3691; Pvan *cdbS*^{R9A}*-FLAG*, Tet^{R}	This study
pMS047	pMS048; P_{nat} *parB-eYFP*, Tet^{R}	This study
pMS048	pDS80; MCS of pSWU30, Tet^{R}	This study
pMS054	pBJ114; *cdbA-mCh*, Kan^{R}	This study
pMS055	pBJ114; Δ*mxan_0750*, Kan^{R}	This study
pMS056	pBJ114; Δ*grpS*, Kan^{R}	This study
pMS057	pBJ114; Δ*mxan_1092*, Kan^{R}	This study
pMS088	pBJ114; *csdK1-mV*, Kan^{R}	This study
pMS089	pBJ114; *csdK2-HA*, Kan^{R}	This study
pMS091	pBJ114; *dnaB-sGFP*, Kan^{R}	This study
pMS102	pSWU19; P_{nat} *parB-YFP*; P_{nat} *cdbS-FLAG*; Kan^{R}	This study
pKNT25-CdbS	pKNT25; *cdbS*, Kan^{R}	This study
pKT25-CdbS	pKT25; *cdbS*, Kan^{R}	This study
pUT18-CdbS	pUT18; *cdbS*, Amp^{R}	This study
pUT18C-CdbS	pUT18C; *cdbS*, Amp^{R}	This study
pKNT25-3778	pKNT25; *csdK1*, Kan^{R}	This study
pKNT25-CsdK1	pKT25; *csdK1*, Kan^{R}	This study
pKT25-CsdK1	pKT25; *csdK1*, Kan^{R}	This study
pUT18-CsdK1	pUT18; *csdK1*, Amp^{R}	This study
pUT18C-CsdK1	pUT18C; *csdK1*, Amp^{R}	This study
pKNT25-CsdK2	pKNT25; *csdK2*, Kan^{R}	This study
pKT25-CsdK2	pKT25; *csdK2*, Kan^{R}	This study
pUT18-CsdK2	pUT18; *csdK2*, Amp^{R}	This study
pUT18C-CsdK2	pUT18C; *csdK2*, Amp^{R}	This study
pKNT25-Mxan_0750	pKNT25; *mxan_0750*, Kan^{R}	This study
pKT25-Mxan_0750	pKT25; *mxan_0750*, Kan^{R}	This study
pUT18-Mxan_0750	pUT18; *mxan_0750*, Amp^{R}	This study
pUT18C-Mxan_0750	pUT18C; *mxan_0750*, Amp^{R}	This study
pKNT25-GrpS	pKNT25; *grpS*, Kan^{R}	This study
pKT25-GrpS	pKT25; *grpS*, Kan^{R}	This study

pUT18-GrpS	pUT18; *grpS*, Amp^R	This study
pUT18C-GrpS	pUT18C; *grpS*, Amp^R	This study
pKNT25-DnaB	pKNT25; *dnaB*, Kan^R	This study
pKT25-DnaB	pKT25; *dnaB*, Kan^R	This study
pUT18-DnaB	pUT18; *dnaB*, Amp^R	This study
pUT18C-DnaB	pUT18C; *dnaB*, Amp^R	This study
pKNT25-$CdbS^{R9A}$	pKNT25; *cdbS*^{R9A}, Kan^R	This study
pKT25-$CdbS^{R9A}$	pKT25; *cdbS*^{R9A}, Kan^R	This study
pUT18-$CdbS^{R9A}$	pUT18; *cdbS*^{R9A}, Amp^R	This study
pUT18C-$CdbS^{R9A}$	pUT18C; *cdbS*^{R9A}, Amp^R	This study
pKNT25-$CsdK2^{R38A}$	pKNT25; *csdK2* ^{R38A}, Kan^R	This study
pKT25-$CsdK2^{R38A}$	pKT25; *csdK2* ^{R38A}, Kan^R	This study
pUT18-$CsdK2^{R38A}$	pUT18; *csdK2* ^{R38A}, Amp^R	This study
pUT18C-$CsdK2^{R38A}$	pUT18C; *csdK2* ^{R38A}, Amp^R	This study
pKNT25-$CsdK2^{PilZ}$	pKNT25; *csdK2* ^{PilZ}, Kan^R	This study
pKT25-$CsdK2^{PilZ}$	pKT25; *csdK2* ^{PilZ}, Kan^R	This study
pUT18-$CsdK2^{PilZ}$	pUT18; *csdK2*^{PilZ}, Amp^R	This study
pUT18C-$CsdK2^{PilZ}$	pUT18C; *csdK2* ^{PilZ}, Amp^R	This study
pKNT25-$CsdK2^{PilZ\ R38A}$	pKNT25; *csdK2* $^{PilZ\ R38A}$, Kan^R	This study
pKT25-$CsdK2^{PilZ}$	pKT25; *csdK2* $^{PilZ\ R38A}$, Kan^R	This study
pUT18-$CsdK2^{PilZ\ R38A}$	pUT18; *csdK2*$^{PilZ\ R38A}$, Amp^R	This study
pUT18C-$CsdK2^{PilZ\ R38A}$	pUT18C; *csdK2* $^{PilZ\ R38A}$, Amp^R	This study
pKNT25-$CsdK2^{Hsp70}$	pKNT25; *csdK2* ^{Hsp70}, Kan^R	This study

pKT25-CsdK2^{Hsp70}	pKT25; *csdK2*^{Hsp70}, Kan^{R}	This study
pUT18-CsdK2^{Hsp70}	pUT18; *csdK2*^{Hsp70}, Amp^{R}	This study
pUT18C-CsdK2^{Hsp70}	pUT18C; *csdK2*^{Hsp70}, Amp^{R}	This study

4.4.2 Plasmid construction

Genomic DNA of *M. xanthus* or plasmids were used as templates to amplify genes and genomic regions of interest as described in 4.4.5. The restriction enzyme digest and ligation of the respective DNA fragments was performed as described in 4.4.7. Chemically competent NEB Turbo cells were transformed with the ligated construct as described in 4.4.8. After the colony PCR, a plasmid with an insert of interest was extracted as in 4.4.4 and sent for sequencing to Microsynth Seqlab GmbH (Göttingen). The obtained sequences were then analyzed using Snapgene® (GSL Biotech LLC).

The plasmids **pMS007 and pMS008** are the derivatives of pET28a(+) and were used for the recombinant overproduction of His_6-CdbS and His_6-CdbS R9A respectively. *cdbS* was amplified from genomic DNA using the primers 4328 fw_NdeI and oMS004. To generate the *cdbS* R9A variant, *cdbS* was amplified from genomic DNA using the primers oMS002 and oMS004. The resulting fragment was then used as a template for another PCR and amplified using the primers 4328 fw_NdeI and oMS004. Both inserts were respectively inserted into the pET28a(+) vector via the NdeI/HindII sites.

The plasmid **pMS018** is a derivative of pBJ114 and was used for the native insertion of *cdbS-FLAG*. To amplify the upstream fragment, the primers oMS024 and oMS013 were used using gDNA as a template. To generate the downstream fragment, the primer pairs oMS025 and oMS087 using gDNA as a template. The final fragment was obtained via overlap PCR and was inserted into pBJ114 via the HindIII/EcoRI sites.

The plasmids **pMS024** and **pMS026** are derivatives of pMR3691 and were used for the overexpression of *cdbS-FLAG* and *cdbS*^{R9A}*-FLAG*, respectively, under the vanillate promoter from the *mxan_18-19* site. To amplify FLAG-tagged *cdbS*, the gene was amplified using the primers 4328 fw_NdeI and oMS041 from SA8821. The fragment was then inserted into the pMR3691 vector via the NdeI/EcoRI sites. To amplify the amino substituted variant, the primer pairs oMS002

and oMS041 were used with pMS024 as a template. The resulting fragment was then used for another PCR using 4328 fw_NdeI and oMS041 as primers. This final fragment was inserted into pMR3691 via the NdeI/EcoRI sites.

The plasmid **pMS047** is a derivative of pMS047 and was used to express parB-eYFP under the native promoter from the the *mxan_18-19* site. To amplify the insert, the primer pair oMS068 and oMS069 were used using pDJS151 as a template. The fragment was then inserted into pMS048 via the XbaI/SphI sites.

The plasmid **pMS048** is a derivative of pDS80 and was used to create a host plasmid with the multiple cloning site of pSWU30 for the integration at the *mxan18-19* site with a tetracycline resistance. To create the multiple cloning site, the complementary primers oMS070 and oMS071 were aligned. This fragment was inserted into pDS80 via the HindIII/EcoRI sites. To test for correct integration in *M. xanthus*, the test primer mxan18-19 P pDS75 rev was used.

The plasmid **pMS054** is a derivative of pBJ114 and was used for the native insertion of *cdbA-mCh*. To amplify the upstream fragment, the primers oMS082 and oMS083 were used using gDNA as a template. To amplify the mCherry fragment, the primer pairs oMS084 and oMS085 were used using SA5691 as a template. These two fragments were ligated via the BamHI site. To generate the downstream fragment, the primer pairs oMS086 and oMS087 using gDNA as a template. The final fragment was obtained via overlap PCR and was inserted into pBJ114 via the HindIII/EcoRI sites.

The plasmid **pMS055** is a derivative of pBJ114 and was used for the native deletion of *mxan_0750*. To amplify the upstream fragment, the primers oMS092 and oMS093 were used using gDNA as a template. To generate the downstream fragment, the primer pairs oMS094 and oMS095 using gDNA as a template. The final fragment was obtained via overlap PCR and was inserted into pBJ114 via the HindIII/EcoRI sites.

The plasmid **pMS056** is a derivative of pBJ114 and was used for the native deletion of *grpS*. To amplify the upstream fragment, the primers oMS100 and oMS101 were used using gDNA as a template. To generate the downstream fragment, the primer pairs oMS102 and oMS103 using gDNA as a template. The final fragment was obtained via overlap PCR and was inserted into pBJ114 via the HindIII/EcoRI sites.

The plasmid **pMS057** is a derivative of pBJ114 and was used for the native deletion of *mxan_1092*. To amplify the upstream fragment, the primers oMS116 and oMS117 were used using gDNA as a template. To generate the downstream fragment, the primer pairs oMS118 and oMS119 using gDNA as a template. The final fragment was obtained via overlap PCR and was inserted into pBJ114 via the HindIII/EcoRI sites.

The plasmid **pMS088** is a derivative of pBJ114 and was used for the native insertion of *csdK1-mV*. To amplify the upstream fragment, the primers oMS177 and oMS231 were used using gDNA as a template. To amplify the mVenus fragment, the primers oMS194 and oMS232 were used using pFM60 (Franziska Müller) as a template. To generate the downstream fragment, the primer pairs oMS228 and oMS180 using gDNA as a template. The upstream fragment and the mVenus fragment were then fused via overlap PCR, before the resulting fragment was used to the downstream fragment via a second overlap PCR. This final fragment was then inserted into pBJ114 via the HindIII/EcoRI sites.

The plasmid **pMS089** is a derivative of pBJ114 and was used for the native insertion of *csdK2-HA*. To amplify the upstream fragment, the primers oMS182 and oMS183 were used using gDNA as a template. To generate the downstream fragment, the primer pairs oMS184 and oMS185 using gDNA as a template. The final fragment was obtained via overlap PCR and was inserted into pBJ114 via the HindIII/EcoRI sites.

The plasmid **pMS091** is a derivative of pBJ114 and was used for the native insertion of *dnaB-sGFP*. To amplify the upstream fragment, the primers oMS187 and oMS188 were used using gDNA as a template. To amplify the sGFP fragment, the primers oMS029 and oMS193 were used using SA11494 as a template. To generate the downstream fragment, the primer pairs oMS189 and oMS190 using gDNA as a template. The upstream fragment and the sGFP fragment were then fused via overlap PCR, before the resulting fragment was used to the downstream fragment via a second overlap PCR. This final fragment was then inserted into pBJ114 via the HindIII/EcoRI sites.

The plasmid **pMS102** is a derivative of pSWU19 and was used to express both *parB-YFP* and *cdbS-FLAG* under their respective native promoters from the attachment site. The P_{nat} *parB-YFP* fragment was amplified from pDJS151 using the primers oMS068 and oMS211. The P_{nat} *cdbS-FLAG* fragment was amplified from gDNA using the primer pairs oMS212 and oMS004. The

two fragments were ligated via the NdeI site, and the resulting fragment was inserted into pBJ114 via the XbaI/EcoRI sites.

The **BACTH plasmids** were all constructed in a similar way. For all constructs except CsdK2, the same fragment of each gene was amplified from gDNA and inserted into the respective plasmids via the XbaI/KpnI. For CdbS constructs, the primers oMS131 and oMS132 were used, while for the $CdbS^{R9A}$ variant, the template was pMS026. For CsdK1 constructs, the primers oMS133 and oMS134 were used. For Mxan_0750 constructs, the primers oMS137 and oMS138 were used. For GrpS constructs, the primers oMS139 and oMS140 were used. For DnaB constructs, the primers oMS154 and oMS155 were used. To generate the constructs of CsdK2 for pKNT25, pUT18 and pUT18C, the primers oMS135 and oMS136 were used. For the pKT25-CsdK2 construct, the primer pair oMS135 and oMS141 was used. All CsdK2 fragments were inserted into the respective vector via the XbaI/EcoRI sites.

For the $CsdK2^{R38A}$ variants, the primer pairs oMS135 and oMS204 and additionally oMS205 and oMS206 were used to amplify two fragments that were then fused using overlap PCR. The resulting fragment was then cloned into the BACTH plasmids containing CsdK2 using the XbaI/XmaI sites.

For the $CsdK2^{PilZ}$ variant, the primer oMS135 was used together with oMS208 for the pKT25 construct or oMS206 for pUT18/pUT18C/pKNT25 constructs. Similarly, the same primer pairs were used for the $CsdK2^{PilZ\ R38A}$ variants using pUT18C-$CsdK2^{R38A}$ as a template. For the $CsdK2^{Hsp70}$ variant, the primer oMS207 was used together with oMS141 for the pKT25 construct or oMS136 for pUT18/pUT18C/pKNT25 constructs.

4.4.3 Construction of in-frame deletion and insertion strains

In-frame deletion and insertion *M. xanthus* mutants were constructed by two-step homologous recombination as described previously with small modifications (Shi *et al.*, 2008). In brief, the about 500 bp long upstream (AB fragment) and downstream (CD fragment) flanking regions of the locus of interest were amplified. Both fragments were designed to contain overlapping ends and were used as template to amplify the in-frame deletion or insertion AD fragment. The resulting fragment was then cloned into the pBJ114 vector using the appropriate restriction enzyme sites. Plasmids with the correct sequence were used for transformation of the

respective *M. xanthus* strain via electroporation. If the plasmid integrates into the genome via homologous recombination, the mutant clones become resistant to kanamycin. Growing clones may be checked for upstream or downstream integration using the appropriate E/F primer pair as well as the corresponding combination with KA231 or KA232. Correct integration clones were inoculated into CTT medium containing no kanamycin but 0.5% galactose and grown overnight for a second homologous recombination. The cells were then plated in a serial dilution on CTT plates containing 2.5% galactose for counter selection, as pBJ114 contains *galk* as a second selection marker. GalK converts galactose to galactose-1-phosphate, which *M. xanthus* cannot metabolize and therefore accumulates to toxic levels. For this reason, only cultures that loop out the plasmid can grow on plates containing galactose. Growing colonies were restreaked on CTT plates containing galactose as well as CTT plates containing kanamycin. Clones that only grew in the presence of galactose but not kanamycin were used in a test PCR using the respective E/F and G/H primer pair to test for correct deletion or insertion.

4.4.4 DNA isolation

For isolating genomic DNA of *M. xanthus* DK1622, the MasterPure™ DNA Purification Kit (Epicentre Biotechnologies) was used following the provided protocol. To extract plasmids from *E.coli* NEB Turbo cells, the NucleoSpin® Plasmid kit (Macherey-Nagel) was used following the manufacturer's instructions. The quantity and the quality of extracted DNA was determined using a spectrophotometer (DeNovix).

Crude genomic DNA extracts of *M. xanthus* for colony PCRs was obtained by boiling cells in 20 µl ddH_2O for 5 min at 95°C. After a quick spin down to remove cell debris, 1.5 µl of the supernatant was used in a PCR reaction.

4.4.5 Polymerase chain reaction (PCR)

To amplify specific DNA fragments, the Phusion High-Fidelity DNA Polymerase (Thermo Scientific) was used. For checking the presence of inserts in plasmids in *E. coli* or the genomic integration of plasmids in *M. xanthus*, colony PCR using the RedTaq DNA Polymerase Master Mix (VWR) was performed. The composition and running programs of the PCRS are listed in Table 15 and Table 16.

Table 15: Composition of PCR reactions

Component	Volume
PCR reaction mix using Phusion Polymerase	
5x Phusion GC buffer	10 µl
5x Enhancer	10 µl
10 mM dNTPs	1 µl
10 µM forward primer	1 µl
10 µM reverse primer	1µl
DNA template	50 ng
Phusion DNA polymerase	0.5 µl
ddH_2O	ad 50 µl
Colony PCR	
Red Taq DNA polymerase Master Mix	10 µl
DNA template	1 *E. coli* colony or 1.5 µl *M. xanthus* crude DNA extract
DMSO	2 µl
ddH_2O	ad 20 µl

Table 16: Running programs of PCRs

Step	Temperature	Time	
Touchdown PCR using Phusion Polymerase			
Initial denaturation	95°C	2 min	
Denaturation	95°C	30 sec	10x
Primer annealing	65°C	30 sec	
Elongation	72°C	30 sec/1 kb	
Denaturation	95°C	30 sec	10x
Primer annealing	60°C	30 sec	
Elongation	72°C	30 sec/1 kb	
Denaturation	95°C	30 sec	13x
Primer annealing	55°C	30 sec	
Elongation	72°C	30 sec/1 kb	
Final elongation	72°C	2 min	
Hold	4°C	∞	
Colony PCR			
Initial denaturation	95°C	2 min	
Denaturation	95°C	30 sec	25x
Primer annealing	according to melting temperature	30 sec	
Elongation	72°C	1 min/1 kb	
Final elongation	72°C	2 min	
Hold	4°C	∞	

4.4.6 Agarose gel electrophoresis

Nucleic acid fragments were separated in a 1% agarose gel with 0.1% ROTILAB® GelRed (Roth) in 1x ROTIPHORESE® TBE buffer (Roth) at 120 V. Samples may be mixed with 6x gel

loading dye (New England Biolabs). As a reference, the 1 kb Plus DNA Ladder (New England Biolabs) was used. The agarose gels were imaged using the E-BOX VX2 imaging system (PeqLab).

4.4.7 Restriction enzyme digest of DNA and ligation

Restriction of plasmids and DNA fragments was performed using restriction endonucleases (New England Biolabs) according to the manufacturer's protocol. In addition, digested plasmid DNA was dephosphorylated using Antarctic Phosphatase (New England Biolabs) according to the protocol of the manufacturer. The digested samples were purified using the NucleoSpin® Gel & PCR Clean-up kit (Macherey-Nagel) according to the instructions of the manufacturer.

Digested DNA fragments and plasmids were ligated using T4 DNA ligase (New England Biolabs) according the manufacturer's protocol with a 3-fold molar excess of insert DNA.

4.4.8 Preparation and transformation of chemically competent *E. coli*

For the preparation of chemically competent *E. coli* cells, an overnight culture was used to inoculate 200 ml of LB to an OD_{600} of 0.1 and was grown at 37°C until it reached an OD_{600} of 0.5. After harvesting the cells by centrifugation at 3500 rpm for 10 min at 4°C, the cells were resuspended in a total volume of 50 ml sterile TFB1 buffer (30 mM potassium acetate, 10 mM $CaCl_2$, 50 mM $MnCl_2$, 100 mM RbCl, 15 % glycerol (v/v), pH 5.8 adjusted with acetic acid). Following incubation for 10 min on ice, the cells were centrifuged using the same conditions. After resuspending the cells in a total volume of 4 ml TFB2 buffer (10 mM MOPS pH 6.5 adjusted with KOH, 75 mM $CaCl_2$, 10 mM RbCl, 15 % glycerol (v/v)), the cells were incubated on ice for one hour. 50 µl aliquots were then shock frozen in liquid nitrogen and stored at -80°C.

For transformation, one aliquot was thawed on ice. 100 ng plasmid or 10 µl of ligation mix was added to the cells and incubated for 30 min on ice. The cells were heat shocked at 42°C for 90 sec and then recovered on ice for 2 min before 1 ml LB was added, and the cells were incubated for 45 min at 37°C with shaking. The cells were harvested and plated onto LB agar plates containing the respective antibiotic. After incubation overnight at 37°Cm, grown colonies

were streaked onto a fresh agar plate and checked via colony PCR using backbone-specific primers.

4.4.9 Electroporation of *M. xanthus*

5 ml of overnight culture were harvested by centrifugation at 11,000 rpm for 1 min. After washing the cells in 2 ml ddH_2O, they were harvested again and resuspended in 50 µl ddH_2O. 1 ng of plasmid was added. The solution was then transferred to an electroporation cuvette (Bio-Rad, Munich) and pulsed with 0.65 kV. The cells were resuspended in 2 ml CTT and incubated for at least 6 h at 32°C in the dark with 230 rpm shaking before plating on CTT agar plates containing the respective antibiotic or additive. The plates were incubated at 32°C in the dark. Grown colonies were streaked onto a fresh agar plate, and plasmid integration was verified by colony PCR.

4.4.10 RNA isolation and cDNA synthesis

A 30 ml culture was grown to OD_{550} of 0.7 and harvested by centrifugation at 4,700 rpm for 10 min. The pellet was then resuspended in 1 ml of TRIzol® reagent (Ambion) and incubated for 5 min on ice. After transferring 1 ml of the lysate to a new tube, 200 µl of chloroform was added and the solution was vortexed thoroughly. The solution was kept on ice for 15 min, before it was centrifuged at max speed for 15 min at 4°C. 600 µl of the aqueous phase was transferred to a new tube and mixed with 600 µl of isopropanol followed by 60 min incubation at -20°C. The mix was centrifuged at max speed for 10 min at 4°C, the supernatant discarded and the pellet washed with 200 µl of cold 75% ethanol. After centrifugation at max speed for 10 min at 4°C, the supernatant was removed and the pellet air-dried for 5 min. The pellet was resuspended in 60 µl of RNase-free ddH_2O and stored at -80°C.

To remove any DNA residue, the TURBO™ DNase kit (Ambion) was used following the protocol of the manufacturer. For clean-up, the NucleoSpin® RNA Plus kit (Macherey-Nagel) was used as instructed. The quality of RNA was checked via an agarose gel, before storing the sample at -80°C. The respective cDNA was synthesized according to the LunaScript RT SuperMix Kit (New England Biolabs).

4.4.11 RT-qPCR and *ori*/*ter* measurements

RT-qPCR was performed using cDNA and the Luna Universal qPCR Master Mix (New England Biolabs) and measured on an 7500 Real Time PCR system (Applied Biosystems). The relative gene expression levels were calculated using the comparative C_T method (Schmittgen and Livak, 2008). The experiments were performed with four biological replicates each with three technical replicates.

Do determine the *ori*/*ter* ratio, chromosomal DNA of the strains were isolated as described. The *ori* region was amplified using the primer pairs ori 1/dnaA fwd & ori 1/dnaA rev and ori 2/7483 fwd & ori 2/7483 rev, while the ter region was amplified using the primer pairs 3778_ter 1 qPCR fwd & 3778_ter 1 qPCR rev and ter 2/4058 fwd & ter 2/4058 rev using the Luna Universal qPCR Master Mix (New England Biolabs). Quantification of the *ori*/*ter* ratio was performed using the the $2^{-\Delta CT}$ method as described (Fernández-Coll *et al.*, 2020). The experiments were performed with four biological replicates each with three technical replicates.

4.5 Biochemical methods

4.5.1 SDS polyacrylamide gel electrophoresis (SDS-PAGE)

For separation of proteins using SDS polyacrylamide gel electrophoresis (Laemmli, 1970), SDS gels with acrylamide concentrations of 8 – 15% were used depending on the molecular weight of the proteins of interest (

Table 18).

To denature proteins, the samples were mixed with SDS loading buffer (60 mM Tris-HCl pH 6.8, 10% (v/v) glycerol, 2% (w/v) SDS, 5 mM EDTA, 100 mM DTT, 0.005% (w/v) bromophenol blue) and heated for 10 min at 95°C. To analyze protein accumulation of growing cells, cells of the respective cultures were harvested to an $OD_{500\ nm}$ of 14 in SDS loading buffer.

Gel electrophoresis was performed in 1x ROTIPHORESE® SDS-PAGE buffer (Roth) at 120 V. As a standard, the PageRuler™ Plus Prestained Protein Ladder (Thermo Scientific) was used as comparison to determine protein sizes. If required, the gel was stained with FastGene® Q-Stain (Nippon Genetics) to visualize the separated proteins.

Table 17: Compositions of buffers used for SDS-PAGE

Buffer	Composition
Stacking buffer	1.5 M Tris-HCl pH 8.8, 0.4% (w/v) SDS
Resolving buffer	0.5 M Tris-HCl pH 6.8, 0.4% (w/v) SDS

Table 18: Composition of SDS gels

Component	8%	12%	15%	Stacking gel
ddH_2O	2.3 ml	1.6 ml	1.1 ml	1.25 ml
Resolving buffer	1.3 ml	1.3 ml	1.3 ml	-
Stacking buffer	-	-	-	0.5 ml
30% acrylamide/bisacrylamide	1.3 ml	2.0 ml	2.5 ml	0.25 ml
TEMED	2.5 µl	2.5 µl	2.5 µl	6 µl
10% APS	50 µl	50 µl	50 µl	12 µl

4.5.2 Immunoblot analysis

Following SDS-PAGE, the proteins were transferred onto a 0.2 µm nitrocellulose membrane using the TransBlot® Turbo™ Transfer System (Bio-Rad) at 1.3 A, 25 V for 7 min with transfer buffer (300 mM Tris, 300 mM Glycin, 0.05% (w/v) SDS, pH 9.0). Then, the membrane was blocked in 5% non-fat milk powder (w/v) in TBST (50 mM Tris-HCl ph 7.5, 150 mM NaCl, 0.05% (v/v) Tween-20) for at least 1 h at 4°C. Next, the membrane was incubated in primary antibody solution overnight at 4°C. All antibodies were diluted in 2% non-fat milk powder TBST according to Table 19. After washing the membrane three times with TBST for 5 min, it was incubated in secondary antibody solution for 1 h at 4°C. Following three washings with TBST, the membrane was developed with Luminata Forte chemiluminescence reagent (Merck) on a LAS-4000 imager (Fujifilm).

Table 19 antibodies used for immunoblot analyses

Antibody	Manufacturer	Dilution
α-Cya18	Santa Cruz Biotechnology (Heidelberg)	1:2000
α-FLAG	Rockland Immunochemicals (Limerick, USA)	1:2000
α-GFP	Sigma-Aldrich (Taufkirchen)	1:2000
α-HA	Sigma-Aldrich (Taufkirchen)	1:1000
α-His	Sigma-Aldrich (Taufkirchen)	1:2000
α-mCherry	BioVision (Waltham, USA)	1:2500

α-PilC	(Bulyha *et al.*, 2009)	1:2000
Goat α-rabbit IgG	Sigma-Aldrich (Taufkirchen)	1:10,000
Sheep α-mouse IgG	GE Healthcare Europe GmbH (Freiburg)	1:5000

4.5.3 Protein purification

For protein overproduction, the appropriate plasmid was transformed into *E.coli* ArcticExpress. 2 L of 2xYT was inoculated with an overnight culture to an OD_{600} = 0.1 and grown to an OD_{600} = 0.5 at 30°C. After adding a final concentration of 0.5 mM IPTG, the culture was grown at 11°C for 24 hours.

The cells were harvested by centrifugation at 6,000 rpm for 30 min at 4°C. The pellet was resuspended in 25 ml Lysis Buffer (50 mM Tris-HCl pH 7, 150 mM NaCl, 10% (v/v) glycerol, 1 mM DTT, 10 mM Imidazole, cOmplete protease inhibitor EDTA-free (Roche Diagnostics GmbH)) and sonicated for 30 min with a UP200St sonifier (60% pulse, 50% amplitude, 30 sec on/off time; Hielscher) on ice. To separate the soluble from the insoluble fraction, the solution was centrifuged at 20,000 rpm for 45 min at 4°C. The soluble fraction was then loaded onto a 5 ml HiTrap Chelating HP column that has been loaded with $NiSO_4$ according to the manufacturer. The bound protein was eluted with elution buffer (50 mM Tris-HCl pH 7, 150 mM NaCl, 10% (v/v) glycerol, 1 mM ß-mercaptoethanol) with a linear imidazole gradient from 50 to 500 mM. Fractions containing His_6-CdbS were combined and mixed with anion exchange buffer A (50 mM Tris-HCl pH 7, 10% (v/v) glycerol, 1 mM ß-mercaptoethanol) in a 1:3 ratio and then loaded onto a 5 ml HiTrap SP HP (GE Heathcare) column. Bound protein was eluted along a 5 column volume gradient of anion exchange buffer B (50 mM Tris-HCl pH 7, 10% (v/v) glycerol, 1 mM ß-mercaptoethanol, 2 M NaCl). Using an Amicon® Ultra-4 3K centrifugal filter unit (Merck) according to the manufacturer's protocol, the purest His_6-CdbS samples were pooled and concentrated. Aliquots of 100 µl were shock-frozen in liquid nitrogen and stored at -80°C.

4.5.4 Bio-layer interferometry

Bio-layer interferometry was performed using the BLItz system (forteBio). Tween-20 was added to used assay buffer to a final concentration of 0.02% (w/v) during the experiment. 500 nM biotinylated c-di-GMP (Biolog) was loaded onto a Streptavidin SA biosensor (forteBio) for 120 s

followed by 30 s of washing. To calculate interaction kinetics, varying concentration of the protein of interest were applied to the biosensor for 120 s followed by 120 s of dissociation.

4.5.5 Co-Immunoprecipitation and label-free mass spectrometry-based quantitative proteomics

For each sample, 100 ml CTT were inoculated with an overnight culture to an OD_{550} of 0.1 and grown overnight until it reached an OD_{550} of 0.7 at 32°C. From each culture, an OD_{550} of 20 was harvested by centrifugation of 4,700 rpm at 20°C for 10 min. Each pellet was then resuspended in 10 ml HNN buffer (50 mM HEPES pH 7.2, 150 mM NaCl, 5 mM EDTA, cOmplete protease inhibitor (Roche Diagnostics GmbH), 0.5% (v/v) NP40) and sonicated for 1 min with a UP200St sonifier (60% pulse, 50% amplitude; Hielscher) on ice. To each sample, 10 µl anti-FLAG® M2 magnetic beads (Merck) were added. Next, the samples were placed in an overhead rotor for 90 min at 4°C. The supernatant was removed and the beads were washed with HNN buffer followed by four times washing with 100 mM ammoniumbicarbonate to remove all detergent and protease inhibitors. Further sample processing was carried out as described in detail previously (Gómez-Santos *et al.*, 2019). In short, enriched proteins were eluted by adding 1 µg trypsin (Promega) and incubation for 30 min at 30°C, and further incubated overnight in the presence of 5 mM Tris(2-carboxyethyl)phosphin (TCEP). Following, acetylation using 10 mM iodoacetamide for 30 min at 25°C in the dark the peptides were desalted using C18 solid phase extraction.

LC-MS analysis of the peptide samples were carried out on a Q-Exactive Plus instrument connected to an Ultimate 3000 RSLC nano and a nanospray flex ion source (all Thermo Scientific). Peptide separation was performed on a C18 reverse phase HPLC column (75 µm x 42 cm; 2,4 µm, Dr. Maisch). The peptides were loaded onto a PepMap 100 precolumn (Thermo Scientific) and eluted by a linear ACN gradient from 6-35% solvent B over 30 minutes (solvent A: 0.15% formic acid; solvent B: 99.85% ACN in 0.15% formic acid) with a 300 nl/min flow rate. The spray voltage was set to 2.5 kV, and the temperature of the heated capillary was set to 300°C. Survey full-scan MS spectra (m/z = 375-1500) were acquired in the Orbitrap with a resolution of 70,000 (at m/z 200) after accumulation a maximum of 3×10^6 ions in the Orbitrap. Up to 10 most intense ions were subjected to fragmentation using high collision dissociation (HCD) at 27%

normalized collision energy. Fragment spectra were acquired at 17,500 resolution. The ion accumulation time was set to 50 ms for both MS survey and MS/MS scans. The charged state screening modus was enabled to exclude unassigned and singly charged ions. The dynamic exclusion duration was set to 30 sec.

Label-free quantification (LFQ) of the samples was performed using MaxQuant (Version 1.6.10.43) (Cox and Mann, 2008). For Andromeda database searches implemented in the MaxQuant environment, a *M. xanthus* Uniprot protein databases (downloaded in 10/2016) was used. The search criteria were set as follows: full tryptic specificity was required (cleavage after lysine or arginine residues); two missed cleavages were allowed; carbamidomethylation (C) was set as fixed modification; oxidation (M) and deamidation (N, Q) as variable modification. MaxQuant was operated in default settings without the “Match-between-run” options.

For protein quantification, iBAQ values (intensity-based absolute quantification) were calculated within MaxQuant (Schwanhäusser *et al.*, 2011). Calculated iBAQ values were normalized to iBAQ-protein sum of all detected proteins. Student t-Test were performed within Perseus (https://www.nature.com/articles/nmeth.3901) with following paramters (FDR: 0.01, s0: 0.5).

4.6 Bioinformatic analyses

Genes and protein sequences of *M. xanthus* and were obtained from KEGG (https://www.kegg.jp/). Protein homologs were identified using the reciprocal best BlastP hit method of KEGG SSDB. Alignments and phylogenies were constructed using MEGA-X (Kumar *et al.*, 2018). Similarity and identity between proteins were analyzed with EMBOSS Needle (https://www.ebi.ac.uk/Tools/psa/emboss_needle/). Functional domains were predicted with HMMER (https://www.ebi.ac.uk/Tools/hmmer/). Protein structures were predicted using AlphaFold (Jumper *et al.*, 2021) and visualized using PyMOL (Schrödinger LLC).

5 References

Ajit Tamadaddi, C. & Sahi, C. 2016. J domain independent functions of J proteins. *Cell Stress Chaperones,* **21,** 563-70.

Åkerlund, T., Nordström, K. & Bernander, R. 1995. Analysis of cell size and DNA content in exponentially growing and stationary-phase batch cultures of *Escherichia coli*. *J Bacteriol,* **177,** 6791-7.

Alm, R. A., Bodero, A. J., Free, P. D. & Mattick, J. S. 1996. Identification of a novel gene, *pilZ*, essential for type 4 fimbrial biogenesis in *Pseudomonas aeruginosa*. *J Bacteriol,* **178,** 46-53.

Almblad, H., Randall, T. E., Liu, F., Leblanc, K., Groves, R. A., Kittichotirat, W., Winsor, G. L., Fournier, N., Au, E., Groizeleau, J., Rich, J. D., Lou, Y., Granton, E., Jennings, L. K., Singletary, L. A., Winstone, T. M. L., Good, N. M., Bumgarner, R. E., Hynes, M. F., Singh, M., Stietz, M. S., Brinkman, F. S. L., Kumar, A., Brassinga, A. K. C., Parsek, M. R., Tseng, B. S., Lewis, I. A., Yipp, B. G., MacCallum, J. L. & Harrison, J. J. 2021. Bacterial cyclic diguanylate signaling networks sense temperature. *Nature Communications,* **12,** 1986.

Amikam, D. & Galperin, M. Y. 2006. PilZ domain is part of the bacterial c-di-GMP binding protein. *Bioinformatics,* **22,** 3-6.

An, S. Q., Caly, D. L., McCarthy, Y., Murdoch, S. L., Ward, J., Febrer, M., Dow, J. M. & Ryan, R. P. 2014. Novel cyclic di-GMP effectors of the YajQ protein family control bacterial virulence. *PLoS Pathog,* **10,** e1004429.

Anand, D., Schumacher, D. & Søgaard-Andersen, L. 2020. SMC and the bactofilin/PadC scaffold have distinct yet redundant functions in chromosome segregation and organization in *Myxococcus xanthus*. *Mol Microbiol,* **114,** 839-856.

Arai, K., Yasuda, S. & Kornberg, A. 1981. Mechanism of dnaB protein action. I. Crystallization and properties of dnaB protein, an essential replication protein in *Escherichia coli*. *Journal of Biological Chemistry,* **256,** 5247-5252.

Atkinson, G. C., Tenson, T. & Hauryliuk, V. 2011. The RelA/SpoT homolog (RSH) superfamily: distribution and functional evolution of ppGpp synthetases and hydrolases across the tree of life. *PLoS One,* **6,** e23479.

Badrinarayanan, A., Le, T. B. & Laub, M. T. 2015. Bacterial chromosome organization and segregation. *Annu Rev Cell Dev Biol,* **31,** 171-99.

Barrows, J. M. & Goley, E. D. 2021. FtsZ dynamics in bacterial division: What, how, and why? *Curr Opin Cell Biol,* **68,** 163-172.

Bascos, N. A. D. & Landry, S. J. 2019. A History of Molecular Chaperone Structures in the Protein Data Bank. *Int J Mol Sci,* **20**.

Benach, J., Swaminathan, S. S., Tamayo, R., Handelman, S. K., Folta-Stogniew, E., Ramos, J. E., Forouhar, F., Neely, H., Seetharaman, J. & Camilli, A. 2007. The structural basis of cyclic diguanylate signal transduction by PilZ domains. *The EMBO journal,* **26,** 5153-5166.

Bergeler, S. & Frey, E. 2018. Regulation of Pom cluster dynamics in *Myxococcus xanthus*. *PLoS Comput Biol,* **14,** e1006358.

Bernard, P. & Couturier, M. 1992. Cell killing by the F plasmid CcdB protein involves poisoning of DNA-topoisomerase II complexes. *J Mol Biol,* **226,** 735-45.

Bhattacharya, K., Weidenauer, L., Luengo, T. M., Pieters, E. C., Echeverría, P. C., Bernasconi, L., Wider, D., Sadian, Y., Koopman, M. B., Villemin, M., Bauer, C., Rüdiger, S. G. D., Quadroni, M. & Picard, D. 2020. The Hsp70-Hsp90 co-chaperone Hop/Stip1 shifts the proteostatic balance from folding towards degradation. *Nat Commun,* **11,** 5975.

Böhm, K., Giacomelli, G., Schmidt, A., Imhof, A., Koszul, R., Marbouty, M. & Bramkamp, M. 2020. Chromosome organization by a conserved condensin-ParB system in the actinobacterium *Corynebacterium glutamicum*. *Nat Commun,* **11,** 1485.

Bokal, A. J., Ross, W., Gaal, T., Johnson, R. C. & Gourse, R. L. 1997. Molecular anatomy of a transcription activation patch: FIS-RNA polymerase interactions at the *Escherichia coli rrnB* P1 promoter. *Embo j,* **16,** 154-62.

Bordes, P., Cirinesi, A. M., Ummels, R., Sala, A., Sakr, S., Bitter, W. & Genevaux, P. 2011. SecB-like chaperone controls a toxin-antitoxin stress-responsive system in *Mycobacterium tuberculosis*. *Proc Natl Acad Sci U S A,* **108,** 8438-43.

Bordes, P., Sala, A. J., Ayala, S., Texier, P., Slama, N., Cirinesi, A.-M., Guillet, V., Mourey, L. & Genevaux, P. 2016. Chaperone addiction of toxin–antitoxin systems. *Nature Communications,* **7,** 13339.

Boyd, C. D. & O'Toole, G. A. 2012. Second messenger regulation of biofilm formation: breakthroughs in understanding c-di-GMP effector systems. *Annu Rev Cell Dev Biol,* **28,** 439-62.

Bracher, A. & Verghese, J. 2015. The nucleotide exchange factors of Hsp70 molecular chaperones. *Frontiers in Molecular Biosciences,* **2**.

Brehmer, D., Rüdiger, S., Gässler, C. S., Klostermeier, D., Packschies, L., Reinstein, J., Mayer, M. P. & Bukau, B. 2001. Tuning of chaperone activity of Hsp70 proteins by modulation of nucleotide exchange. *Nat Struct Biol,* **8,** 427-32.

Bukau, B. & Walker, G. C. 1989. Delta dnaK52 mutants of *Escherichia coli* have defects in chromosome segregation and plasmid maintenance at normal growth temperatures. *J Bacteriol,* **171,** 6030-8.

Bulyha, I., Schmidt, C., Lenz, P., Jakovljevic, V., Höne, A., Maier, B., Hoppert, M. & Søgaard-Andersen, L. 2009. Regulation of the type IV pili molecular machine by dynamic localization of two motor proteins. *Mol Microbiol,* **74,** 691-706.

Bush, M. J., Tschowri, N., Schlimpert, S., Flärdh, K. & Buttner, M. J. 2015. c-di-GMP signalling and the regulation of developmental transitions in streptomycetes. *Nature Reviews Microbiology,* **13,** 749-760.

Chin, K.-H., Lee, Y.-C., Tu, Z.-L., Chen, C.-H., Tseng, Y.-H., Yang, J.-M., Ryan, R. P., McCarthy, Y., Dow, J. M., Wang, A. H. J. & Chou, S.-H. 2010. The cAMP Receptor-Like Protein CLP Is a Novel c-di-GMP Receptor Linking Cell–Cell Signaling to Virulence Gene Expression in *Xanthomonas campestris*. *Journal of Molecular Biology,* **396,** 646-662.

Chin, K. H., Kuo, W. T., Yu, Y. J., Liao, Y. T., Yang, M. T. & Chou, S. H. 2012. Structural polymorphism of c-di-GMP bound to an EAL domain and in complex with a type II PilZ-domain protein. *Acta Crystallogr D Biol Crystallogr,* **68,** 1380-92.

Chodavarapu, S. & Kaguni, J. M. 2016. Replication Initiation in Bacteria. *Enzymes,* **39,** 1-30.

Chou, S. H. & Galperin, M. Y. 2016. Diversity of Cyclic Di-GMP-Binding Proteins and Mechanisms. *J Bacteriol,* **198,** 32-46.

Clerico, E. M., Tilitsky, J. M., Meng, W. & Gierasch, L. M. 2015. How hsp70 molecular machines interact with their substrates to mediate diverse physiological functions. *J Mol Biol,* **427,** 1575-88.

Conner, J. G., Zamorano-Sánchez, D., Park, J. H., Sondermann, H. & Yildiz, F. H. 2017. The ins and outs of cyclic di-GMP signaling in Vibrio cholerae. *Current opinion in microbiology,* **36,** 20-29.

Conway de Macario, E., Yohda, M., Macario, A. J. L. & Robb, F. T. 2019. Bridging human chaperonopathies and microbial chaperonins. *Commun Biol,* **2,** 103.

Corrigan, R. M. & Gründling, A. 2013. Cyclic di-AMP: another second messenger enters the fray. *Nature Reviews Microbiology,* **11,** 513-524.

Cox, J. & Mann, M. 2008. MaxQuant enables high peptide identification rates, individualized p.p.b.-range mass accuracies and proteome-wide protein quantification. *Nature Biotechnology,* **26,** 1367-1372.

da Silva, A. C., Simão, R. C., Susin, M. F., Baldini, R. L., Avedissian, M. & Gomes, S. L. 2003. Downregulation of the heat shock response is independent of DnaK and sigma32 levels in *Caulobacter crescentus*. *Mol Microbiol,* **49,** 541-53.

Dahlstrom, K. M. & O'Toole, G. A. 2017. A Symphony of Cyclases: Specificity in Diguanylate Cyclase Signaling. *Annu Rev Microbiol,* **71,** 179-195.

Dame, R. T., Rashid, F. M. & Grainger, D. C. 2020. Chromosome organization in bacteria: mechanistic insights into genome structure and function. *Nat Rev Genet,* **21,** 227-242.

Dillon, S. C. & Dorman, C. J. 2010. Bacterial nucleoid-associated proteins, nucleoid structure and gene expression. *Nature Reviews Microbiology,* **8,** 185-195.

Dorman, C. J., Schumacher, M. A., Bush, M. J., Brennan, R. G. & Buttner, M. J. 2020. When is a transcription factor a NAP? *Curr Opin Microbiol,* **55,** 26-33.

Engelberg-Kulka, H., Amitai, S., Kolodkin-Gal, I. & Hazan, R. 2006. Bacterial programmed cell death and multicellular behavior in bacteria. *PLoS Genet,* **2,** e135.

Fahmi, T., Port, G. C. & Cho, K. H. 2017. c-di-AMP: An Essential Molecule in the Signaling Pathways that Regulate the Viability and Virulence of Gram-Positive Bacteria. *Genes (Basel),* **8**.

Fauvet, B., Finka, A., Castanié-Cornet, M. P., Cirinesi, A. M., Genevaux, P., Quadroni, M. & Goloubinoff, P. 2021. Bacterial Hsp90 Facilitates the Degradation of Aggregation-Prone Hsp70-Hsp40 Substrates. *Front Mol Biosci,* **8,** 653073.

Fernández-Coll, L., Maciag-Dorszynska, M., Tailor, K., Vadia, S., Levin, P. A., Szalewska-Palasz, A. & Cashel, M. 2020. The Absence of (p)ppGpp Renders Initiation of *Escherichia coli* Chromosomal DNA Synthesis Independent of Growth Rates. *mBio,* **11**.

Galperin, M. Y. & Chou, S. H. 2020. Structural Conservation and Diversity of PilZ-Related Domains. *J Bacteriol,* **202**.

Gamer, J., Multhaup, G., Tomoyasu, T., McCarty, J. S., Rüdiger, S., Schönfeld, H. J., Schirra, C., Bujard, H. & Bukau, B. 1996. A cycle of binding and release of the DnaK, DnaJ and GrpE chaperones regulates activity of the *Escherichia coli* heat shock transcription factor sigma32. *Embo j,* **15,** 607-17.

Gelinas, A. D., Toth, J., Bethoney, K. A., Langsetmo, K., Stafford, W. F. & Harrison, C. J. 2003. Thermodynamic linkage in the GrpE nucleotide exchange factor, a molecular thermosensor. *Biochemistry,* **42,** 9050-9.

Gelinas, A. D., Toth, J., Bethoney, K. A., Stafford, W. F. & Harrison, C. J. 2004. Mutational analysis of the energetics of the GrpE.DnaK binding interface: equilibrium association constants by sedimentation velocity analytical ultracentrifugation. *J Mol Biol,* **339,** 447-58.

Genevaux, P., Georgopoulos, C. & Kelley, W. L. 2007. The Hsp70 chaperone machines of Escherichia coli: a paradigm for the repartition of chaperone functions. *Mol Microbiol,* **66,** 840-57.

Gomelsky, M. 2011. cAMP, c-di-GMP, c-di-AMP and now cGMP: bacteria use them all! *Mol Microbiol,* **79,** 562-5.

Gómez-Santos, N., Glatter, T., Koebnik, R., Świątek-Połatyńska, M. A. & Søgaard-Andersen, L. 2019. A TonB-dependent transporter is required for secretion of protease PopC across the bacterial outer membrane. *Nat Commun,* **10,** 1360.

Görke, B. & Stülke, J. 2008. Carbon catabolite repression in bacteria: many ways to make the most out of nutrients. *Nature Reviews Microbiology,* **6,** 613-624.

Grainger, D. C., Hurd, D., Harrison, M., Holdstock, J. & Busby, S. J. 2005. Studies of the distribution of *Escherichia coli* cAMP-receptor protein and RNA polymerase along the E. coli chromosome. *Proc Natl Acad Sci U S A,* **102,** 17693-8.

Guo, M. S., Haakonsen, D. L., Zeng, W., Schumacher, M. A. & Laub, M. T. 2018. A Bacterial Chromosome Structuring Protein Binds Overtwisted DNA to Stimulate Type II Topoisomerases and Enable DNA Replication. *Cell,* **175,** 583-597.e23.

Habazettl, J., Allan, M. G., Jenal, U. & Grzesiek, S. 2011. Solution structure of the PilZ domain protein PA4608 complex with cyclic di-GMP identifies charge clustering as molecular readout. *Journal of biological chemistry,* **286,** 14304-14314.

Han, S., Shen, D., Wang, Y.-C., Chou, S.-H., Gomelsky, M., Gao, Y.-G. & Qian, G. 2020. A YajQ-LysR-like, cyclic di-GMP-dependent system regulating biosynthesis of an antifungal antibiotic in a crop-protecting bacterium, *Lysobacter enzymogenes*. *Molecular Plant Pathology,* **21,** 218-229.

Hariharan, V. N., Yadav, R., Thakur, C., Singh, A., Gopinathan, R., Singh, D. P., Sankhe, G., Malhotra, V., Chandra, N., Bhatt, A. & Saini, D. K. 2021. Cyclic di-GMP sensing histidine kinase PdtaS controls mycobacterial adaptation to carbon sources. *Faseb j,* **35,** e21475.

Harms, A., Treuner-Lange, A., Schumacher, D. & Søgaard-Andersen, L. 2013. Tracking of chromosome and replisome dynamics in *Myxococcus xanthus* reveals a novel chromosome arrangement. *PLoS Genet,* **9,** e1003802.

Harris, B. Z., Kaiser, D. & Singer, M. 1998. The guanosine nucleotide (p)ppGpp initiates development and A-factor production in *Myxococcus xanthus*. *Genes Dev,* **12,** 1022-35.

Harrison, C. J., Hayer-Hartl, M., Di Liberto, M., Hartl, F. & Kuriyan, J. 1997. Crystal structure of the nucleotide exchange factor GrpE bound to the ATPase domain of the molecular chaperone DnaK. *Science,* **276,** 431-5.

Hartl, F. U., Bracher, A. & Hayer-Hartl, M. 2011. Molecular chaperones in protein folding and proteostasis. *Nature,* **475,** 324-332.

Haslbeck, M. & Vierling, E. 2015. A first line of stress defense: small heat shock proteins and their function in protein homeostasis. *J Mol Biol,* **427,** 1537-48.

Haslbeck, M., Weinkauf, S. & Buchner, J. 2019. Small heat shock proteins: Simplicity meets complexity. *Journal of Biological Chemistry,* **294,** 2121-2132.

Hazan, R., Sat, B. & Engelberg-Kulka, H. 2004. *Escherichia coli* mazEF-mediated cell death is triggered by various stressful conditions. *J Bacteriol,* **186,** 3663-9.

He, J., Yin, W., Galperin, M. Y. & Chou, S.-H. 2020. Cyclic di-AMP, a second messenger of primary importance: tertiary structures and binding mechanisms. *Nucleic Acids Research,* **48,** 2807-2829.

Hengge, R. 2009. Principles of c-di-GMP signalling in bacteria. *Nature Reviews Microbiology,* **7,** 263-273.

Hengge, R. 2016. Trigger phosphodiesterases as a novel class of c-di-GMP effector proteins. *Philos Trans R Soc Lond B Biol Sci,* **371**.

Hengge, R. 2021a. Crosstalking second messengers. *Nat Microbiol,* **6,** 9-10.

Hengge, R. 2021b. High-Specificity Local and Global c-di-GMP Signaling. *Trends Microbiol*.

Hesterkamp, T. & Bukau, B. 1998. Role of the DnaK and HscA homologs of Hsp70 chaperones in protein folding in *E. coli*. *Embo j,* **17,** 4818-28.

Hickman, J. W. & Harwood, C. S. 2008. Identification of FleQ from *Pseudomonas aeruginosa* as a c-di-GMP-responsive transcription factor. *Mol Microbiol,* **69,** 376-89.

Hobley, L., Fung, R. K., Lambert, C., Harris, M. A., Dabhi, J. M., King, S. S., Basford, S. M., Uchida, K., Till, R., Ahmad, R., Aizawa, S., Gomelsky, M. & Sockett, R. E. 2012. Discrete cyclic di-GMP-dependent control of bacterial predation versus axenic growth in *Bdellovibrio bacteriovorus*. *PLoS Pathog,* **8,** e1002493.

Hołówka, J. & Zakrzewska-Czerwińska, J. 2020. Nucleoid Associated Proteins: The Small Organizers That Help to Cope With Stress. *Front Microbiol,* **11,** 590.

Hou, Y. J., Yang, W. S., Hong, Y., Zhang, Y., Wang, D. C. & Li, D. F. 2020. Structural insights into the mechanism of c-di-GMP-bound YcgR regulating flagellar motility in *Escherichia coli*. *J Biol Chem,* **295,** 808-821.

Imamoglu, R., Balchin, D., Hayer-Hartl, M. & Hartl, F. U. 2020. Bacterial Hsp70 resolves misfolded states and accelerates productive folding of a multi-domain protein. *Nat Commun,* **11,** 365.

Iniesta, A. A. 2014. ParABS system in chromosome partitioning in the bacterium *Myxococcus xanthus*. *PloS one,* **9,** e86897.

Iniesta, A. A., García-Heras, F., Abellón-Ruiz, J., Gallego-García, A. & Elías-Arnanz, M. 2012. Two systems for conditional gene expression in *Myxococcus xanthus* inducible by isopropyl-β-D-thiogalactopyranoside or vanillate. *J Bacteriol,* **194,** 5875-85.

Irving, S. E., Choudhury, N. R. & Corrigan, R. M. 2021. The stringent response and physiological roles of (pp)pGpp in bacteria. *Nature Reviews Microbiology,* **19,** 256-271.

Jakobsen, J. S., Jelsbak, L., Jelsbak, L., Welch, R. D., Cummings, C., Goldman, B., Stark, E., Slater, S. & Kaiser, D. 2004. Sigma54 enhancer binding proteins and *Myxococcus xanthus* fruiting body development. *J Bacteriol,* **186,** 4361-8.

Jakovljevic, V., Leonardy, S., Hoppert, M. & Søgaard-Andersen, L. 2008. PilB and PilT are ATPases acting antagonistically in type IV pilus function in *Myxococcus xanthus*. *J Bacteriol,* **190,** 2411-21.

Jalal, A. S. B. & Le, T. B. K. 2020. Bacterial chromosome segregation by the ParABS system. *Open Biol,* **10,** 200097.

Janssen, G. R., Wireman, J. W. & Dworkin, M. 1977. Effect of temperature on the growth of *Myxococcus xanthus*. *Journal of bacteriology,* **130,** 561-562.

Jenal, U., Reinders, A. & Lori, C. 2017. Cyclic di-GMP: second messenger extraordinaire. *Nat Rev Microbiol,* **15,** 271-284.

Jiang, Y., Rossi, P. & Kalodimos, C. G. 2019. Structural basis for client recognition and activity of Hsp40 chaperones. *Science,* **365,** 1313-1319.

Jonas, K., Liu, J., Chien, P. & Laub, M. T. 2013. Proteotoxic stress induces a cell-cycle arrest by stimulating Lon to degrade the replication initiator DnaA. *Cell,* **154,** 623-36.

Julien, B., Kaiser, A. D. & Garza, A. 2000. Spatial control of cell differentiation in *Myxococcus xanthus*. *Proc Natl Acad Sci U S A,* **97,** 9098-103.

Jumper, J., Evans, R., Pritzel, A., Green, T., Figurnov, M., Ronneberger, O., Tunyasuvunakool, K., Bates, R., Žídek, A., Potapenko, A., Bridgland, A., Meyer, C., Kohl, S. A. A., Ballard, A. J., Cowie, A., Romera-Paredes, B., Nikolov, S., Jain, R., Adler, J., Back, T., Petersen, S., Reiman, D., Clancy, E., Zielinski, M., Steinegger, M., Pacholska, M., Berghammer, T., Bodenstein, S., Silver, D., Vinyals, O., Senior, A. W., Kavukcuoglu, K., Kohli, P. & Hassabis, D. 2021. Highly accurate protein structure prediction with AlphaFold. *Nature,* **596,** 583-589.

Junkermeier, E. H. & Hengge, R. 2021. A Novel Locally c-di-GMP-Controlled Exopolysaccharide Synthase Required for Bacteriophage N4 Infection of *Escherichia coli*. *mBio,* **12,** e0324921.

Jurėnas, D., Fraikin, N., Goormaghtigh, F. & Van Melderen, L. 2022. Biology and evolution of bacterial toxin–antitoxin systems. *Nature Reviews Microbiology,* **20,** 335-350.

Kaczmarczyk, A., Hempel, A. M., von Arx, C., Böhm, R., Dubey, B. N., Nesper, J., Schirmer, T., Hiller, S. & Jenal, U. 2020. Precise timing of transcription by c-di-GMP coordinates cell cycle and morphogenesis in *Caulobacter*. *Nature Communications,* **11,** 816.

Kaiser, D., Manoil, C. & Dworkin, M. 1979. Myxobacteria: cell interactions, genetics, and development. *Annu Rev Microbiol,* **33,** 595-639.

Kampinga, H. H., Andreasson, C., Barducci, A., Cheetham, M. E., Cyr, D., Emanuelsson, C., Genevaux, P., Gestwicki, J. E., Goloubinoff, P., Huerta-Cepas, J., Kirstein, J., Liberek, K., Mayer, M. P., Nagata, K., Nillegoda, N. B., Pulido, P., Ramos, C., De Los Rios, P., Rospert, S., Rosenzweig, R., Sahi, C., Taipale, M., Tomiczek, B., Ushioda, R., Young, J. C., Zimmermann, R., Zylicz, A., Zylicz, M., Craig, E. A. & Marszalek, J. 2019. Function, evolution, and structure of J-domain proteins. *Cell Stress Chaperones,* **24,** 7-15.

Kampinga, H. H. & Craig, E. A. 2010. The HSP70 chaperone machinery: J proteins as drivers of functional specificity. *Nat Rev Mol Cell Biol,* **11,** 579-92.

Kapuscinski, J. 1995. DAPI: a DNA-specific fluorescent probe. *Biotech Histochem,* **70,** 220-33.

Kazmierczak, B. I., Lebron, M. B. & Murray, T. S. 2006. Analysis of FimX, a phosphodiesterase that governs twitching motility in *Pseudomonas aeruginosa*. *Mol Microbiol,* **60,** 1026-43.

Kim, Y.-I., Levchenko, I., Fraczkowska, K., Woodruff, R. V., Sauer, R. T. & Baker, T. A. 2001. Molecular determinants of complex formation between Clp/Hsp100 ATPases and the ClpP peptidase. *Nature Structural Biology,* **8,** 230-233.

Kimura, Y., Nakato, H., Ishibashi, K. & Kobayashi, S. 2005. A *Myxococcus xanthus* CbpB containing two cAMP-binding domains is involved in temperature and osmotic tolerances. *FEMS Microbiology Letters,* **244,** 75-83.

Kityk, R., Kopp, J. & Mayer, M. P. 2018. Molecular Mechanism of J-Domain-Triggered ATP Hydrolysis by Hsp70 Chaperones. *Mol Cell,* **69,** 227-237.e4.

Kluck, C. J., Patzelt, H., Genevaux, P., Brehmer, D., Rist, W., Schneider-Mergener, J., Bukau, B. & Mayer, M. P. 2002. Structure-function analysis of HscC, the *Escherichia coli* member of a novel subfamily of specialized Hsp70 chaperones. *J Biol Chem,* **277,** 41060-9.

Konovalova, A., Petters, T. & Søgaard-Andersen, L. 2010. Extracellular biology of *Myxococcus xanthus*. *FEMS Microbiol Rev,* **34,** 89-106.

Krasteva, P. V., Giglio, K. M. & Sondermann, H. 2012. Sensing the messenger: the diverse ways that bacteria signal through c-di-GMP. *Protein Sci,* **21,** 929-48.

Kroos, L. 2017. Highly Signal-Responsive Gene Regulatory Network Governing *Myxococcus* Development. *Trends Genet,* **33,** 3-15.

Kumar, S., Stecher, G., Li, M., Knyaz, C. & Tamura, K. 2018. MEGA X: Molecular Evolutionary Genetics Analysis across Computing Platforms. *Molecular biology and evolution,* **35,** 1547-1549.

Kuzmich, S., Blumenkamp, P., Meier, D., Szadkowski, D., Goesmann, A., Becker, A. & Søgaard-Andersen, L. 2022. CRP-Like Transcriptional Regulator MrpC Curbs c-di-GMP and 3',3'-cGAMP Nucleotide Levels during Development in *Myxococcus xanthus*. *mBio***,** e0004422.

Kuzmich, S., Skotnicka, D., Szadkowski, D., Klos, P., Pérez-Burgos, M., Schander, E., Schumacher, D. & Søgaard-Andersen, L. 2021. Three PilZ Domain Proteins, PlpA, PixA, and PixB, Have Distinct Functions in Regulation of Motility and Development in *Myxococcus xanthus*. *J Bacteriol,* **203,** e0012621.

Laemmli, U. K. 1970. Cleavage of structural proteins during the assembly of the head of bacteriophage T4. *Nature,* **227,** 680-5.

Lancero, H., Caberoy, N. B., Castaneda, S., Li, Y., Lu, A., Dutton, D., Duan, X. Y., Kaplan, H. B., Shi, W. & Garza, A. G. 2004. Characterization of a *Myxococcus xanthus* mutant that is defective for adventurous motility and social motility. *Microbiology (Reading),* **150,** 4085-93.

Laufen, T., Mayer, M. P., Beisel, C., Klostermeier, D., Mogk, A., Reinstein, J. & Bukau, B. 1999. Mechanism of regulation of Hsp70 chaperones by DnaJ cochaperones. *Proceedings of the National Academy of Sciences,* **96,** 5452-5457.

LeBowitz, J. H. & McMacken, R. 1986. The *Escherichia coli* dnaB replication protein is a DNA helicase. *Journal of Biological Chemistry,* **261,** 4738-4748.

Lin, L., Osorio Valeriano, M., Harms, A., Søgaard-Andersen, L. & Thanbichler, M. 2017. Bactofilin-mediated organization of the ParABS chromosome segregation system in *Myxococcus xanthus*. *Nat Commun,* **8,** 1817.

Lin, Z. & Rye, H. S. 2006. GroEL-mediated protein folding: making the impossible, possible. *Crit Rev Biochem Mol Biol,* **41,** 211-39.

Little, R. H., Grenga, L., Saalbach, G., Howat, A. M., Pfeilmeier, S., Trampari, E. & Malone, J. G. 2016. Adaptive Remodeling of the Bacterial Proteome by Specific Ribosomal Modification Regulates *Pseudomonas* Infection and Niche Colonisation. *PLoS Genet,* **12,** e1005837.

Liu, K., Bittner, A. N. & Wang, J. D. 2015. Diversity in (p)ppGpp metabolism and effectors. *Curr Opin Microbiol,* **24,** 72-9.

Lori, C., Ozaki, S., Steiner, S., Böhm, R., Abel, S., Dubey, B. N., Schirmer, T., Hiller, S. & Jenal, U. 2015. Cyclic di-GMP acts as a cell cycle oscillator to drive chromosome replication. *Nature,* **523,** 236-9.

Mayer, M. P. 2021. The Hsp70-Chaperone Machines in Bacteria. *Front Mol Biosci,* **8,** 694012.

Mayer, M. P. & Gierasch, L. M. 2019. Recent advances in the structural and mechanistic aspects of Hsp70 molecular chaperones. *J Biol Chem,* **294,** 2085-2097.

McDonough, K. A. & Rodriguez, A. 2011. The myriad roles of cyclic AMP in microbial pathogens: from signal to sword. *Nat Rev Microbiol,* **10,** 27-38.

Merighi, M., Lee, V. T., Hyodo, M., Hayakawa, Y. & Lory, S. 2007. The second messenger bis-(3′-5′)-cyclic-GMP and its PilZ domain-containing receptor Alg44 are required for alginate biosynthesis in *Pseudomonas aeruginosa*. *Molecular microbiology,* **65,** 876-895.

Mills, E., Pultz, I. S., Kulasekara, H. D. & Miller, S. I. 2011. The bacterial second messenger c-di-GMP: mechanisms of signalling. *Cellular microbiology,* **13,** 1122-1129.

Moak, P. L., Black, W. P., Wallace, R. A., Li, Z. & Yang, Z. 2015. The Hsp70-like StkA functions between T4P and Dif signaling proteins as a negative regulator of exopolysaccharide in *Myxococcus xanthus*. *PeerJ,* **3,** e747.

Mogk, A., Kummer, E. & Bukau, B. 2015. Cooperation of Hsp70 and Hsp100 chaperone machines in protein disaggregation. *Frontiers in Molecular Biosciences,* **2**.

Muñoz-Dorado, J., Inouye, S. & Inouye, M. 1991. A gene encoding a protein serine/threonine kinase is required for normal development of *M. xanthus*, a gram-negative bacterium. *Cell,* **67,** 995-1006.

Muñoz-Dorado, J., Marcos-Torres, F. J., García-Bravo, E., Moraleda-Muñoz, A. & Pérez, J. 2016. Myxobacteria: Moving, Killing, Feeding, and Surviving Together. *Front Microbiol,* **7,** 781.

Navarro, M. V., De, N., Bae, N., Wang, Q. & Sondermann, H. 2009. Structural analysis of the GGDEF-EAL domain-containing c-di-GMP receptor FimX. *Structure,* **17,** 1104-16.

Newell, P. D., Monds, R. D. & O'Toole, G. A. 2009. LapD is a bis-(3',5')-cyclic dimeric GMP-binding protein that regulates surface attachment by *Pseudomonas fluorescens* Pf0-1. *Proc Natl Acad Sci U S A,* **106,** 3461-6.

Newton, A. C., Bootman, M. D. & Scott, J. D. 2016. Second Messengers. *Cold Spring Harb Perspect Biol,* **8**.

Nolivos, S. & Sherratt, D. 2014. The bacterial chromosome: architecture and action of bacterial SMC and SMC-like complexes. *FEMS Microbiol Rev,* **38,** 380-92.

O'Connor, K. A. & Zusman, D. R. 1991. Development in *Myxococcus xanthus* involves differentiation into two cell types, peripheral rods and spores. *Journal of bacteriology,* **173,** 3318-3333.

Odermatt, N. T., Sala, C., Benjak, A. & Cole, S. T. 2018. Essential Nucleoid Associated Protein mIHF (Rv1388) Controls Virulence and Housekeeping Genes in *Mycobacterium tuberculosis*. *Scientific Reports,* **8,** 14214.

Oren, A. & Garrity, G. M. 2021. Valid publication of the names of forty-two phyla of prokaryotes. *International Journal of Systematic and Evolutionary Microbiology,* **71**.

Orr, M. W., Donaldson, G. P., Severin, G. B., Wang, J., Sintim, H. O., Waters, C. M. & Lee, V. T. 2015. Oligoribonuclease is the primary degradative enzyme for pGpG in *Pseudomonas aeruginosa* that is required for cyclic-di-GMP turnover. *Proceedings of the National Academy of Sciences,* **112,** E5048-E5057.

Osorio-Valeriano, M., Altegoer, F., Das, C. K., Steinchen, W., Panis, G., Connolley, L., Giacomelli, G., Feddersen, H., Corrales-Guerrero, L., Giammarinaro, P. I., Hanßmann, J., Bramkamp, M., Viollier, P. H., Murray, S., Schäfer, L. V., Bange, G. & Thanbichler, M. 2021. The CTPase activity of ParB determines the size and dynamics of prokaryotic DNA partition complexes. *Mol Cell,* **81,** 3992-4007.e10.

Osorio-Valeriano, M., Altegoer, F., Steinchen, W., Urban, S., Liu, Y., Bange, G. & Thanbichler, M. 2019. ParB-type DNA Segregation Proteins Are CTP-Dependent Molecular Switches. *Cell,* **179,** 1512-1524.e15.

Overgaard, M., Wegener-Feldbrügge, S. & Søgaard-Andersen, L. 2006. The orphan response regulator DigR is required for synthesis of extracellular matrix fibrils in *Myxococcus xanthus*. *J Bacteriol,* **188,** 4384-94.

Ozaki, S., Schalch-Moser, A., Zumthor, L., Manfredi, P., Ebbensgaard, A., Schirmer, T. & Jenal, U. 2014. Activation and polar sequestration of PopA, a c-di-GMP effector protein involved in *Caulobacter crescentus* cell cycle control. *Molecular Microbiology,* **94,** 580-594.

Paintdakhi, A., Parry, B., Campos, M., Irnov, I., Elf, J., Surovtsev, I. & Jacobs-Wagner, C. 2016. Oufti: an integrated software package for high-accuracy, high-throughput quantitative microscopy analysis. *Mol Microbiol,* **99,** 767-77.

Pan, Z., Zhang, Z., Zhuo, L., Wan, T. Y. & Li, Y. Z. 2021. Bioinformatic and Functional Characterization of Hsp70s in *Myxococcus xanthus*. *mSphere,* **6**.

Paul, K., Nieto, V., Carlquist, W. C., Blair, D. F. & Harshey, R. M. 2010. The c-di-GMP binding protein YcgR controls flagellar motor direction and speed to affect chemotaxis by a "backstop brake" mechanism. *Mol Cell,* **38,** 128-39.

Pérez-Burgos, M. & Søgaard-Andersen, L. 2020. Regulation by Cyclic di-GMP in *Myxococcus xanthus*. *In:* CHOU, S.-H., GUILIANI, N., LEE, V. T. & RÖMLING, U. (eds.) *Microbial Cyclic Di-Nucleotide Signaling.* Cham: Springer International Publishing.

Pesavento, C. & Hengge, R. 2009. Bacterial nucleotide-based second messengers. *Current Opinion in Microbiology,* **12,** 170-176.

Petters, T., Zhang, X., Nesper, J., Treuner-Lange, A., Gomez-Santos, N., Hoppert, M., Jenal, U. & Søgaard-Andersen, L. 2012. The orphan histidine protein kinase SgmT is a c-di-GMP receptor and regulates composition of the extracellular matrix together with the orphan DNA binding response regulator DigR in *Myxococcus xanthus*. *Molecular microbiology,* **84,** 147-165.

Plumley, B. A., Martin, K. H., Borlee, G. I., Marlenee, N. L., Burtnick, M. N., Brett, P. J., AuCoin, D. P., Bowen, R. A., Schweizer, H. P. & Borlee, B. R. 2017. Thermoregulation of Biofilm Formation in *Burkholderia pseudomallei* Is Disrupted by Mutation of a Putative Diguanylate Cyclase. *J Bacteriol,* **199**.

Pogue, C. B., Zhou, T. & Nan, B. 2018. PlpA, a PilZ-like protein, regulates directed motility of the bacterium *Myxococcus xanthus*. *Molecular microbiology,* **107,** 214-228.

Pratt, J. T., Tamayo, R., Tischler, A. D. & Camilli, A. 2007. PilZ domain proteins bind cyclic diguanylate and regulate diverse processes in *Vibrio cholerae*. *J Biol Chem,* **282,** 12860-70.

Ptacin, J. L., Lee, S. F., Garner, E. C., Toro, E., Eckart, M., Comolli, L. R., Moerner, W. & Shapiro, L. 2010. A spindle-like apparatus guides bacterial chromosome segregation. *Nature cell biology,* **12,** 791-798.

Ricci, D. P., Melfi, M. D., Lasker, K., Dill, D. L., McAdams, H. H. & Shapiro, L. 2016. Cell cycle progression in *Caulobacter* requires a nucleoid-associated protein with high AT sequence recognition. *Proc Natl Acad Sci U S A,* **113,** E5952-e5961.

Richter, A. M., Possling, A., Malysheva, N., Yousef, K. P., Herbst, S., von Kleist, M. & Hengge, R. 2020. Local c-di-GMP Signaling in the Control of Synthesis of the *E. coli* Biofilm Exopolysaccharide pEtN-Cellulose. *Journal of Molecular Biology,* **432,** 4576-4595.

Richter, K., Haslbeck, M. & Buchner, J. 2010. The Heat Shock Response: Life on the Verge of Death. *Molecular Cell,* **40,** 253-266.

Römling, U., Galperin, M. Y. & Gomelsky, M. 2013. Cyclic di-GMP: the first 25 years of a universal bacterial second messenger. *Microbiol. Mol. Biol. Rev.,* **77,** 1-52.

Rosario, C. J. & Singer, M. 2007. The *Myxococcus xanthus* developmental program can be delayed by inhibition of DNA replication. *J Bacteriol,* **189,** 8793-800.

Rosenbluh, A., Nir, R., Sahar, E. & Rosenberg, E. 1989. Cell-density-dependent lysis and sporulation of *Myxococcus xanthus* in agarose microbeads. *J Bacteriol,* **171,** 4923-9.

Ryjenkov, D. A., Simm, R., Romling, U. & Gomelsky, M. 2006. The PilZ domain is a receptor for the second messenger c-di-GMP: the PilZ domain protein YcgR controls motility in enterobacteria. *J Biol Chem,* **281,** 30310-4.

Schäper, S., Steinchen, W., Krol, E., Altegoer, F., Skotnicka, D., Søgaard-Andersen, L., Bange, G. & Becker, A. 2017. AraC-like transcriptional activator CuxR binds c-di-GMP by a PilZ-like mechanism to regulate extracellular polysaccharide production. *Proc Natl Acad Sci U S A,* **114,** E4822-e4831.

Schirmer, T. 2016. C-di-GMP Synthesis: Structural Aspects of Evolution, Catalysis and Regulation. *Journal of Molecular Biology,* **428,** 3683-3701.

Schmittgen, T. D. & Livak, K. J. 2008. Analyzing real-time PCR data by the comparative C(T) method. *Nat Protoc,* **3,** 1101-8.

Schramm, F. D., Schroeder, K. & Jonas, K. 2019. Protein aggregation in bacteria. *FEMS Microbiology Reviews,* **44,** 54-72.

Schroeder, K. & Jonas, K. 2021. The Protein Quality Control Network in *Caulobacter crescentus*. *Frontiers in Molecular Biosciences,* **8**.

Schumacher, D., Bergeler, S., Harms, A., Vonck, J., Huneke-Vogt, S., Frey, E. & Søgaard-Andersen, L. 2017. The PomXYZ Proteins Self-Organize on the Bacterial Nucleoid to Stimulate Cell Division. *Dev Cell,* **41,** 299-314.e13.

Schumacher, D., Harms, A., Bergeler, S., Frey, E. & Søgaard-Andersen, L. 2021. PomX, a ParA/MinD ATPase activating protein, is a triple regulator of cell division in *Myxococcus xanthus*. *Elife,* **10**.

Schumacher, D. & Søgaard-Andersen, L. 2017. Regulation of Cell Polarity in Motility and Cell Division in *Myxococcus xanthus*. *Annu Rev Microbiol,* **71,** 61-78.

Schumacher, R. J., Hansen, W. J., Freeman, B. C., Alnemri, E., Litwack, G. & Toft, D. O. 1996. Cooperative action of Hsp70, Hsp90, and DnaJ proteins in protein renaturation. *Biochemistry,* **35,** 14889-98.

Schwanhäusser, B., Busse, D., Li, N., Dittmar, G., Schuchhardt, J., Wolf, J., Chen, W. & Selbach, M. 2011. Global quantification of mammalian gene expression control. *Nature,* **473,** 337-342.

Sell, S. M., Eisen, C., Ang, D., Zylicz, M. & Georgopoulos, C. 1990. Isolation and characterization of *dnaJ* null mutants of *Escherichia coli*. *J Bacteriol,* **172,** 4827-35.

Shi, W., Zhou, Y., Wild, J., Adler, J. & Gross, C. A. 1992. DnaK, DnaJ, and GrpE are required for flagellum synthesis in *Escherichia coli*. *J Bacteriol,* **174,** 6256-63.

Shi, X., Wegener-Feldbrügge, S., Huntley, S., Hamann, N., Hedderich, R. & Søgaard-Andersen, L. 2008. Bioinformatics and experimental analysis of proteins of two-component systems in *Myxococcus xanthus*. *J Bacteriol,* **190,** 613-24.

Singer, M. & Kaiser, D. 1995. Ectopic production of guanosine penta- and tetraphosphate can initiate early developmental gene expression in *Myxococcus xanthus*. *Genes Dev,* **9,** 1633-44.

Singh, A., Izac, J. R., Schuler, E. J. A., Patel, D. T., Davies, C. & Marconi, R. T. 2021a. High-resolution crystal structure of the *Borreliella burgdorferi* PlzA protein in complex with c-di-GMP: new insights into the interaction of c-di-GMP with the novel xPilZ domain. *Pathog Dis,* **79**.

Singh, G., Yadav, M., Ghosh, C. & Rathore, J. S. 2021b. Bacterial toxin-antitoxin modules: classification, functions, and association with persistence. *Curr Res Microb Sci,* **2,** 100047.

Skotnicka, D., Petters, T., Heering, J., Hoppert, M., Kaever, V. & Søgaard-Andersen, L. 2016a. Cyclic Di-GMP Regulates Type IV Pilus-Dependent Motility in *Myxococcus xanthus*. *J Bacteriol,* **198,** 77-90.

Skotnicka, D., Smaldone, G. T., Petters, T., Trampari, E., Liang, J., Kaever, V., Malone, J. G., Singer, M. & Søgaard-Andersen, L. 2016b. A Minimal Threshold of c-di-GMP Is Essential for Fruiting Body Formation and Sporulation in *Myxococcus xanthus*. *PLoS Genet,* **12,** e1006080.

Skotnicka, D., Steinchen, W., Szadkowski, D., Cadby, I. T., Lovering, A. L., Bange, G. & Søgaard-Andersen, L. 2020. CdbA is a DNA-binding protein and c-di-GMP receptor important for nucleoid organization and segregation in *Myxococcus xanthus*. *Nat Commun,* **11,** 1791.

Sondermann, H., Shikuma, N. J. & Yildiz, F. H. 2012. You've come a long way: c-di-GMP signaling. *Current opinion in microbiology,* **15,** 140-146.

Spangler, C., Böhm, A., Jenal, U., Seifert, R. & Kaever, V. 2010. A liquid chromatography-coupled tandem mass spectrometry method for quantitation of cyclic di-guanosine monophosphate. *Journal of microbiological methods,* **81,** 226-231.

Srivastava, D., Harris, R. C. & Waters, C. M. 2011. Integration of cyclic di-GMP and quorum sensing in the control of *vpsT* and *aphA* in *Vibrio cholerae*. *J Bacteriol,* **193,** 6331-41.

Srivatsan, A. & Wang, J. D. 2008. Control of bacterial transcription, translation and replication by (p)ppGpp. *Current Opinion in Microbiology,* **11,** 100-105.

Steinchen, W. & Bange, G. 2016. The magic dance of the alarmones (p)ppGpp. *Molecular Microbiology,* **101,** 531-544.

Stülke, J. & Krüger, L. 2020. Cyclic di-AMP Signaling in Bacteria. *Annu Rev Microbiol,* **74,** 159-179.

Susin, M. F., Baldini, R. L., Gueiros-Filho, F. & Gomes, S. L. 2006a. GroES/GroEL and DnaK/DnaJ Have Distinct Roles in Stress Responses and during Cell Cycle Progression in *Caulobacter crescentus*. *Journal of Bacteriology,* **188,** 8044-8053.

Susin, M. F., Baldini, R. L., Gueiros-Filho, F. & Gomes, S. L. 2006b. GroES/GroEL and DnaK/DnaJ have distinct roles in stress responses and during cell cycle progression in *Caulobacter crescentus*. *J Bacteriol,* **188,** 8044-53.

Tamayo, R., Pratt, J. T. & Camilli, A. 2007. Roles of cyclic diguanylate in the regulation of bacterial pathogenesis. *Annu Rev Microbiol,* **61,** 131-48.

Tomoyasu, T., Ogura, T., Tatsuta, T. & Bukau, B. 1998. Levels of DnaK and DnaJ provide tight control of heat shock gene expression and protein repair in *Escherichia coli*. *Molecular Microbiology,* **30,** 567-581.

Townsley, L. & Yildiz, F. H. 2015. Temperature affects c-di-GMP signalling and biofilm formation in *Vibrio cholerae*. *Environ Microbiol,* **17,** 4290-305.

Trampari, E., Stevenson, C. E., Little, R. H., Wilhelm, T., Lawson, D. M. & Malone, J. G. 2015. Bacterial rotary export ATPases are allosterically regulated by the nucleotide second messenger cyclic-di-GMP. *J Biol Chem,* **290,** 24470-83.

Treuner-Lange, A., Aguiluz, K., van der Does, C., Gómez-Santos, N., Harms, A., Schumacher, D., Lenz, P., Hoppert, M., Kahnt, J., Muñoz-Dorado, J. & Søgaard-Andersen, L. 2013. PomZ, a ParA-like protein, regulates Z-ring formation and cell division in *Myxococcus xanthus*. *Mol Microbiol,* **87,** 235-53.

Treuner-Lange, A. & Søgaard-Andersen, L. 2020. Überlebenskünstler mit sozialen und kommunikativen Fähigkeiten. *BIOspektrum,* **26,** 28-31.

Tschowri, N., Schumacher, M. A., Schlimpert, S., Chinnam, N. B., Findlay, K. C., Brennan, R. G. & Buttner, M. J. 2014. Tetrameric c-di-GMP mediates effective transcription factor dimerization to control *Streptomyces* development. *Cell,* **158,** 1136-1147.

Tyanova, S., Temu, T., Sinitcyn, P., Carlson, A., Hein, M. Y., Geiger, T., Mann, M. & Cox, J. 2016. The Perseus computational platform for comprehensive analysis of (prote)omics data. *Nat Methods,* **13,** 731-40.

Tzeng, L. & Singer, M. 2005. DNA replication during sporulation in *Myxococcus xanthus* fruiting bodies. *Proc Natl Acad Sci U S A,* **102,** 14428-33.

Unterholzner, S. J., Poppenberger, B. & Rozhon, W. 2013. Toxin-antitoxin systems: Biology, identification, and application. *Mob Genet Elements,* **3,** e26219.

Vickery, L. E. & Cupp-Vickery, J. R. 2007. Molecular chaperones HscA/Ssq1 and HscB/Jac1 and their roles in iron-sulfur protein maturation. *Crit Rev Biochem Mol Biol,* **42,** 95-111.

Voth, W. & Jakob, U. 2017. Stress-Activated Chaperones: A First Line of Defense. *Trends Biochem Sci,* **42,** 899-913.

Wang, Y.-C., Chin, K.-H., Tu, Z.-L., He, J., Jones, C. J., Sanchez, D. Z., Yildiz, F. H., Galperin, M. Y. & Chou, S.-H. 2016. Nucleotide binding by the widespread high-affinity cyclic di-GMP receptor MshEN domain. *Nat Commun,* **7,** 1-12.

Weimer, R. M., Creighton, C., Stassinopoulos, A., Youderian, P. & Hartzell, P. L. 1998. A chaperone in the HSP70 family controls production of extracellular fibrils in *Myxococcus xanthus*. *J Bacteriol,* **180,** 5357-68.

Wickner, S., Nguyen, T. L. & Genest, O. 2021. The Bacterial Hsp90 Chaperone: Cellular Functions and Mechanism of Action. *Annu Rev Microbiol,* **75,** 719-739.

Wright, T. A., Jiang, L., Park, J. J., Anderson, W. A., Chen, G., Hallberg, Z. F., Nan, B. & Hammond, M. C. 2020. Second messengers and divergent HD-GYP phosphodiesterases regulate 3',3'-cGAMP signaling. *Mol Microbiol,* **113,** 222-236.

Wu, S. S. & Kaiser, D. 1995. Genetic and functional evidence that Type IV pili are required for social gliding motility in *Myxococcus xanthus*. *Mol Microbiol,* **18,** 547-58.

Wu, S. S. & Kaiser, D. 1997. Regulation of expression of the *pilA* gene in *Myxococcus xanthus*. *Journal of Bacteriology,* **179,** 7748-7758.

Xiao, J. & Goley, E. D. 2016. Redefining the roles of the FtsZ-ring in bacterial cytokinesis. *Current opinion in microbiology,* **34,** 90-96.

Yatskevich, S., Rhodes, J. & Nasmyth, K. 2019. Organization of Chromosomal DNA by SMC Complexes. *Annu Rev Genet,* **53,** 445-482.

Zhang, Y., Zhang, J., Hara, H., Kato, I. & Inouye, M. 2005. Insights into the mRNA cleavage mechanism by MazF, an mRNA interferase. *J Biol Chem,* **280,** 3143-50.

Zietkiewicz, S., Krzewska, J. & Liberek, K. 2004. Successive and synergistic action of the Hsp70 and Hsp100 chaperones in protein disaggregation. *J Biol Chem,* **279,** 44376-83.

Zuiderweg, E. R., Bertelsen, E. B., Rousaki, A., Mayer, M. P., Gestwicki, J. E. & Ahmad, A. 2013. Allostery in the Hsp70 chaperone proteins. *Top Curr Chem,* **328,** 99-153.

Zusman, D. R., Scott, A. E., Yang, Z. & Kirby, J. R. 2007. Chemosensory pathways, motility and development in *Myxococcus xanthus. Nature Reviews Microbiology,* **5,** 862-872.

Acknowledgements

So this is it, huh? It is such a weird feeling to be writing all of this together, finishing up the work of four years and closing this chapter of my life - but here we are, a pandemic and a war/energy crisis later. As a first-generation doctoral student in my family, this rollercoaster of a ride was definitely not easy, and so many people were at my side during the highs and lows that I want to acknowledge.

First and foremost, I want to thank Prof. Dr. Lotte Søgaard-Andersen for accepting me into her group; I grew a lot not only as a scientist, but also as a person since I started working in your group. I want to thank Prof. Dr. Martin Thanbichler, Prof. Dr. Hans-Ulrich Mösch and Prof. Dr. Victor Sourjik for being members of my thesis committee.

I want to express my gratitude for Dr. Dorota Skotnicka, for the direct supervision at the start of this journey and for starting the CdbA/CdbS project. Thank you for all the discussions, your patience and your kindness!

Dear Timo, thank you for the nice collaboration and all the conversations on the A2 floor.

Danke an Susanne für all deine Mühen und Anstrengungen, das Laborleben am Laufen zu halten. Liebe Yvonne, ohne dich wäre die Laborarbeit um einiges anstrengender und langweiliger gewesen. Danke, dass du uns täglich so viel Arbeit abgenommen hast und ich bin sehr froh, dich in meinem *inneren Zirkel* zu haben! Danke an Andrea für all die Hilfe, Unterstützung und Unterhaltungen in den letzten Jahren, meine Arbeit wäre ohne dich so nicht möglich gewesen. Genauso hilfreich und unterstützend war Steffi, vielen Dank für all die kniffligen Klonierungen und unsere gemeinsame Auszeit beim Mensa Mobil und beim Mittagessen!

It is common knowledge that I would not have survived without my dearest Miss Müller. Dear Franzi, you were my tower of strength over the last few years, we have so many amazing memories together and I love you (*lol*, *planctonically*), even if our combined music playlists are truly awful. Thank you for all your opinions, advices and for proofreading this thesis. I think I can never thank you enough for the handprint you left on my heart. *UK, hun?*

To my dear Jana, you are the kindest soul on the planet and I lovingly remember our joint time in Lab 3. Who could have known that *Temptation Island* would be the start of a great friendship filled with *a lot* of Sushi nights! Dear Memduha, you are one of the strongest people I know and I respect you a lot for all the things you have accomplished so far. To Michel, thank you for all the open conversations and fun times, especially your witty jokes in and outside the coffee breaks.

Thank you so much to Dominik for all the help, advices and the laughs. I am deeply grateful for the proof reading of this thesis. However, I still do not forgive you for doubting me with the PBS recipe, and my body is still recovering from the countless rounds of Glühwein at the Christmas market.

María, I aspire your attention to detail and your brain power, even when your head often wasn't that good. Thank you for all your scientific critics and all the proof readings. And Marco, thank you for always being so helpful with even the little things. My dear Luís, I deeply enjoyed our afternoon/evening talks, whether about science, Lady Gaga's dogs or *tango argentino*.

To Philipp, it was a pleasure to witness your development from Bachelor to Master student to Doctoral Researcher. Thank you for all the (even if quiet) laughs in Lab 3. To Ozan, thanks for all the calm moments in the lab, I will never forget your face after we went on the Blue Fire rollercoaster together. To Johannes, I wish I had your dedication and determination to do research without procrastinating. But I am still wondering: *Can it ever be too big?*

Thank you Anke for helpful discussions and advices, I am very proud to have (somewhat) taught you how to boil agar safely in the microwave. Dobro, without your help I probably would still be struggling with the Köhler illumination at the TIRF. Thanks for the countless times when I needed your help!

David, you started as my Bachelor student with hardly any practical experience due to the pandemic. I am so proud of your development and the great story you put together in those ten months that we had together! My dear Milena, your presence was always a joy, I hope our paths will cross again! *Hygge*!

Thanks to the entire AG Diepold for being great lab neighbours on A2. To Coco and Francesca, I am so glad we became friends. Thanks for all the science talks, all the bus rides, and most importantly all the schnitzels, ramen & beers. My dear Evgenii, I think it was destiny that

(and especially *how*) we met. I loved every of our dinner dates filled with gossip flavor, you are a great friend! Dear Philipp, thanks for the many social events inside, outside or on top of the institute. To Franziska, thanks for all the open conversations about science and life. Thank you also to my fellow Doctoral Researcher representatives.

To my *mango goat apes* and *rich rich girlz* Josephine and Maite. Thank you for all the amazing memories in- and outside Marburg. I still cannot believe our trip to Neuschwanstein Castle actually happened. I also want to thank all the Müllers, I am still proud of the potatoes we grew in your garden. I also want to thank Clyde & Hannybal for all the emotional cat support.

Even though we were very far apart in different countries during this period of our lifes, Domml has been a gigantic rock for me. I cherished all our hours-long phone calls about life, academia or the fangirlings about the *gaga lady*. What a crazy time we had in those two weeks during the Chromatica Ball Tour, I loved every second with you. *Same DNA!*

To my friends back home: Julia & Julian, Julia & Nick, Bine & Stefan, Hanna & Tobi (& Emil), Caro. Thanks for inviting me for all the breakfasts, coffees, and dinners every time I was back in Bavaria and for giving me an escape from the doctoral research reality. I also want to thank Raphaela, Janna and Issy. A big shout out also to Dr. Nazzareno Dominelli, Heidi, Lisa, Lukas and Julia, who have been there since the start of my uni days.

I want to thank Babara for igniting my passion for research. Thanks to Ralf, who has been a big supporter of my academic journey through all those years. Finally, thank you to Susanne for giving me a chance to fly.

Zu guter Letzt danke ich meiner gesamten Familie. Ihr wisst bestimmt immer noch nicht, was ich die letzten paar Jahre eigentlich gearbeitet habe, aber ihr wart immer für mich da, wenn ich eine Auszeit gebraucht habe. Danke für all die Gespräche, das großartige Essen, all die Kartenspiele und natürlich das gute bayrische Bier!

Curriculum vitae

Removed from electronic version for data protection

List of publications

Eckstein, S., Brehm, J., **Seidel, M.**, Lechtenfeld, M. & Heermann, R. (2021).
Two novel XRE-like transcriptional regulators control phenotypic heterogeneity in *Photorhabdus luminescens* cell populations.
BMC Microbiology 21, 63. https://doi.org/10.1186/s12866-021-02116-2

Seidel, M., Skotnicka, D., Glatter, T. & Søgaard-Andersen, L. (2023)
During heat stress in *Myxococcus xanthus*, the CdbS PilZ domain protein, in concert with two PilZ-DnaK chaperones, perturbs chromosome organization and accelerates cell death.
PLOS Genetics 19(6): e1010819. https://doi.org/10.1371/journal.pgen.1010819

Erklärung

Ich versichere, dass ich meine Dissertation mit dem Titel:

Characterization of CdbS, a PilZ domain protein involved in chromosome organization and segregation during heat shock stress in *Myxococcus xanthus*

selbstständig ohne unerlaubte Hilfe angefertigt und keine anderen als die in der Arbeit angegebenen Hilfsmittel verwendet und mich dabei keiner anderen als der von mir ausdrücklich bezeichneten Quellen und Hilfsmittel bedient habe

Diese Dissertation wurde in der jetzigen oder einer ähnlichen Form noch bei keiner anderen Hochschule eingereicht und hat noch keinen sonstigen Prüfungszwecken gedient.

Marburg, den ____ . ____ . _____ _____

Michael Seidel

Einverständniserklärung

Hiermit erkläre ich mich einverstanden, dass die vorliegende Dissertation mit dem Titel

Characterization of CdbS, a PilZ domain protein involved in chromosome organization and segregation during heat shock stress in Myxococcus xanthus

in Bibliotheken zugänglich gemacht wird.

Dazu gehört, dass sie von der Bibliothek der Einrichtung, in der meine Dissertation angefertigt wurde,

- zur Benutzung in ihren Räumen bereitgehalten wird;
- in konventionellen und maschinenlesbaren Katalogen, Verzeichnissen und Datenbanken verzeichnet wird;
- im Rahmen der urheberrechtlichen Bestimmungen für Kopierzwecke benutzt werden kann.

Marburg, den ____ . ____ . _____ _____

Michael Seidel